EXPERIMENTAL AND NUMERICAL VIBRATION ANALYSIS OF THE GUN CONTROL UNIT COLUMN WITH ISOLATOR

İZOLATÖRLÜ SİLAH KONTROL ÜNİTESİ TUTAMAĞININ DENEYSEL VE NÜMERİK TİTREŞİM ANALİZİ

TAYFUN DOĞRAR

ASSOC. PROF. DR. BARIŞ SABUNCUOĞLU

Supervisor

Submitted to

Graduate School of Science and Engineering of Hacettepe University

as a Partial Fulfillment to the Requirements

for the Award of the Degree of Master of Science

in Mechanical Engineering

2020

To my father…

ABSTRACT

EXPERIMENTAL AND NUMERICAL VIBRATION ANALYSIS OF THE GUN CONTROL UNIT COLUMN WITH ISOLATOR

Tayfun DOĞRAR

Master's Thesis, Department of Mechanical Engineering

Supervisor: Assoc. Prof. Dr. Barış SABUNCUOĞLU

September 2020, 120 pages

A remote-controlled weapon system can be integrated into the naval and ground platforms. The weapon system and its sub-units are exposed to the vibration that comes from the platform on which the weapon system is fitted. The weapon system and its sub-units are expected to withstand vibration-related failure throughout its life. Therefore, the fatigue analysis is carried out for the weapon system during the design process.

The system is used in the tracked military vehicle. Hence, the tracked vehicle vibration test procedure is applied to the control column by using the shaker. The random vibration test procedure is presented in the document of the AECTP 400 Mechanical Environment Test. As a result of the test, the control column was broken from part of the base. This thesis is aimed to obtain a control column that will preserve its structural integrity after vibration test and to develop a finite element model of the weapon control unit validated with experimental modal analysis results.

In the first part of the thesis, initially, the original structure is modeled by the finite element method, and the fatigue analysis is performed under the tracked vehicle random vibration test profile. Then the analysis is performed with a vibration isolator, which is

assembled under the damaged part of the control column. The result of the analysis shows that the isolator prevents the damage occurring in the control column. Afterward, a prototype of the control column with the isolator is manufactured, and the accelerated track vehicle random vibration is applied to the prototype by using the shaker. The shaker test's result proves that the isolator prevents the damage.

In addition, the sine sweep vibration test is applied to the gun control unit, and one of the resonance frequency of the control column is determined. The obtained resonance frequency is different from the one which is calculated by finite element analysis, from which it can be deduced that the finite element model of the gun control unit is inaccurate. For this reason, the finite element analysis is needed to be validated.

In the second part of the thesis, an accurate finite element model of the gun control unit is developed. At first, experimental modal analysis is performed. The impact hammer method, which is one of the experimental modal analysis techniques, is used. As a result, natural frequencies, corresponding mode shapes, and damping ratios are determined. The experimental modal analysis result is used to create a reference model. In addition, the elasticity modulus of the neoprene is determined with the help of the tensile test. Then the finite element model is updated according to the test results, and the finite element model is validated.

Keywords: Experimental Modal Analysis, Fatigue Analysis, Finite Element Analysis, Neoprene, Random Vibration, Shaker Test, Tensile Test

ÖZET

İZOLATÖRLÜ SİLAH KONTROL ÜNİTESİ TUTAMAĞININ DENEYSEL VE NÜMERİK TİTREŞİM ANALİZİ

Tayfun DOĞRAR

Yüksek Lisans, Makina Mühendisliği Bölümü

Tez Danışmanı: Doç. Dr. Barış SABUNCUOĞLU

Eylül 2020, 120 sayfa

Uzaktan Komutalı Silah Sistemleri kara, deniz, hava platformları gibi birçok araca entegre edilebilmektedir. Silah sistemi ve alt birimleri yerleştirildikleri platformdan kaynaklı olarak titreşimlere maruz kalmaktadır. Silah sistemi ve bileşenlerinin, kendisine etkiyen titreşimlere karşı platformun kullanım ömrü boyunca dayanıklı olması beklenmektedir. Bu sebeple, silah sistemi ve bileşenlerinin tasarım aşamasında yorulma analizleri gerçekleştirilmektedir.

Silah kontrol ünitesi, silah sisteminin bir alt bileşenidir ve biri sabit diğeri hareketli olmak üzere iki adet kontrol tutamağından oluşmaktadır. Bu çalışmada, titreşim testlerinde hasar gören sabit tutamak yapısı ile ilgilenilmektedir. Uzaktan komutalı silah sisteminin paletli araçlarda kullanılması planlanmaktadır. Bu sebeple, sarsıcı aracılığıyla silah kontrol ünitesine paletli araç rastsal titreşim testi prosedürü uygulanmıştır. Test prosedürü "AECTP 400 Mechanical Environmental Test" standardında sunulmaktadır. Test sırasında, kontrol tutamağı taban kısmından kırılmıştır. Bu çalışmanın amacı, kontrol tutamağında oluşan yorulma hasarının önlenmesi ve paletli araç titreşimine karşı kullanım ömrü boyunca yapısal bütünlüğünü koruyacak bir kontrol tutamağı elde etmektedir.

Tezin ilk kısmında, bir sönümleyici tasalanmış ve bu sönümleyici kontrol tutamağı yapısında kırılan parçanın alt kısmına yerleştirilmiştir. Tezin bu kısmında yapı, sonlu

elemanlar metodu kullanılarak modellenmiş ve standartta belirtilen prosedüre göre paletli araç titreşim yükü altında göre yapının yorulma analizleri gerçekleştirilmiştir. Analizlerin sonucunda, sönümleyici yapının kontrol tutamağında oluşan yorulma hasarını önlediği görülmüştür. Daha sonra prototipi üretilen kontrol tutamağının, paletli araç rastsal titreşim yükü altında titreşim testleri gerçekleştirilmiştir. Titreşim testleri sonucunda sönümleyici yapının kontrol tutamağındaki oluşan hasarı önlediği kanıtlanmıştır.

Sarsıcı tabla üzerinde gerçekleşen rastsal titreşim testleri dışında, yapıya Y ekseni yönünde sinüs taraması titreşimi uygulanmış ve kontrol tutamağının rezonans frekanslarından biri elde edilmiştir. Y ekseni salınımı moduna ait doğal frekans değerinin, sonlu elemanlar analizinde elde edilen doğal frekans değerinden oldukça farklı olduğu görülmüştür. Bu sonuç üzerine, yapının sonlu elemanlar analiz modelinin doğru olmadığı anlaşılmış ve doğrulanması gerektiği ihtiyacı ortaya çıkmıştır.

Tezin ikinci kısmında, güvenilir bir sonlu elemanlar modeli geliştirilmiştir. Çalışmanın başında, silah kontrol ünitesinin deneysel modal analizleri gerçekleştirilmiştir. Testler, deneysel modal analiz tekniklerinden biri olan darbe çekici yöntemiyle gerçekleştirilmiştir. Testler sonucunda kontrol tutamağının doğal frekansları, mod şekilleri ve modların sönüm oranları bulunmuştur. Deneysel modal analiz sonuçları, sonlu elemanlar modeli için referans model olarak kullanılmıştır. Ayrıca tezin bu kısmında, neoprene malzemesinin çekme testleri gerçekleştirilmiş ve malzemenin farklı deformasyon hızlarında elastik modülü elde edilmiştir. Son olarak, deneysel modal analiz ve malzeme testlerinde elde edilen çıktılar kullanılarak sonlu elemanlar modeli güncellenmiş ve güncellenen analiz modelinin sonuçları, titreşim testi sonuçlarıyla doğrulanmıştır.

Anahtar Kelimeler: Çekme Testi, Deneysel Modal Analiz, Neopren, Rastsal Titreşim Testi, Sonlu Elemanlar Metodu, Yorulma Analizi

ACKNOWLEDGMENTS

TABLE OF CONTENTS

LIST OF FIGURES

LIST OF TABLES

SYMBOLS AND ABBREVIATION

Symbols

e_max	Percentage of the maximum difference in natural frequencies between the analysis and the experiment
e1	Percentage of difference in natural frequency of the first mode between the analysis and the experiment
e2	Percentage of difference in natural frequency of the first mode between the analysis and the experiment
f1	Natural frequency corresponding to first mode
f2	Natural frequency corresponding to second mode
D1	Outer diameter of the isolator
D2	Inner diameter of the isolator
$H1$	Height of the cylindrical part of the isolator
$H2$	Height of the conical part of the isolator
[K]	Stiffness Matrix
[M]	Mass Matrix
ω_i	Natural frequencies
$\emptyset_i$	Mode Shapes
N_1	number of stress cycles required to produce a fatigue failure
N_2	reference number of stress cycles at S-N curve
S_1	1-sigma RMS Stress
S_2	stress to fail at reference point N_1
b	slope of fatigue line with stress concentration
n_i	the actual number of fatigue cycles
N_i	the number of fatigue cycles to produce fatigue failure

Abbreviation

ACC	Accelerometer
Config	Configuration
DC	Direct Current
DIR	Direction
DUT	Device Under Test
FE	Finite Element
FEA	Finite Element Analysis
FEM	Finite Element Method
FFT	Fast Fourier Transform
FRF	Frequency Response Function
Imag	Imaginary
PSD	Power Spectral Density
RCWS	Remote-controlled weapon systems
RMS	Root Mean Square

1. INTRODUCTION

Remote-controlled weapon systems (RCWS) have been developed to meet the needs of modern armies. These high-tech systems can be controlled remotely and can be used as target tracking in day and night. RCWS can easily be integrated into various platforms such as the naval, air, land platforms, and fixed platform. RCWS systems consist of many sub-units, one of which is the gun control unit. The gun control unit, as shown in Figure 1-1, enables the crew to control the turret remotely. The gun control unit consists of a fixed control column and a moving control column that pivots on a base. In the scope of this thesis, the fatigue failure occurring in the fixed control column integrated into the tracked vehicle platform is discussed.

Figure 1-1: The gun control unit and the monitor [1]

1.1 Definition of Study

The gun control unit has been used in wheeled vehicle platforms for a long time. The control column was designed to meet the vibration requirements of the military standard for wheeled vehicle platforms. However, tests performed in the Environmental Test Laboratory at the facility of ASELSAN A.Ş showed that the control column was damaged under the load of the vibration test profile presented in the military standard for tracked vehicles. It was revealed that the fatigue life of the current control column is not enough to be used in the tracked vehicle platforms. The damaged control column is shown in Figure 1-2.

Figure 1-2: The control column damaged by accelerated tracked vehicle vibration testing

The gun control unit should meet the tracked vehicle vibration requirements presented in military standards for use on the tracked vehicle platforms. The fatigue life of the control column body should be increased in order to satisfy the vibration requirement for a tracked vehicle. Therefore, the design of the structure has been changed by adding an isolator to the control column structure.

Before the physical prototype production of the new design, finite element methods are utilized to see the effect of isolator structure on the control column's fatigue strength. Thanks to finite element analysis (FEM), complex and irregular shaped control column bodies are easily modeled, and fatigue damage ratios occurring on the structure under tracked vehicle vibration loading conditions are calculated quickly.

After the prototype of the control column with the isolator is produced, accelerated vibration tests of the control column are performed on the shaker table, and a control column design model compatible with the vibration requirements of the tracked vehicle is obtained.

In addition, sine sweep vibration is applied to the gun control unit. As a result of this test, the resonance frequency of the control column is obtained. Although the accelerated vibration test results validate random vibration results of the initial FEM, the resonance frequency of the control column obtained in the sine sweep test is quite different from the finite element model (FEM) results. Hence, it can be deduced that the FEM is not constructed accurately. From this point on, efforts are made to develop a correct FEM.

To this end, experimental modal analysis is carried out to obtain the dynamical parameters of the control column structure in detail. Then, the tensile testing of the isolator material is conducted to obtain the elasticity modulus of it. Finally, FEM is calibrated according to the experimental modal analysis results by changing the material parameters and boundary conditions. Thereby, an accurate FEM correlated with the test result is achieved.

1.2 Aim and Objectives of the Thesis

In this thesis, two different problems are discussed. As stated in the definition of the study, the control column body is damaged by tracked vehicle vibration. The motivation of the thesis is to prevent damage to the control column structure. The first aim is to obtain a control column that will maintain its structural integrity after the vibration test presented in the section "Material in turret bustle rack or installed in turret" of the AECTP 400 Mechanical Environmental Test Standard. For this purpose, a control column with an isolator is designed to reduce the vibration transmitted from the platform to the control column body. Before the control column with isolator is produced and tested, finite element analyses are used to see the effect of the isolator structure on fatigue damage of the structure. Based on the results of the FEM, the control column with the isolator is manufactured. Then, the vibration test defined in the AECTP 400 Mechanical Environmental Test Standard is performed for the control column with the isolator. As a result, the gun control unit passed the vibration tests successfully.

The second aim of this study is to develop a FEM correlated with experimental modal analysis results. Although a successful design is achieved with the initial FEM, in the sine sweep test, the resonance frequency of the control column with the isolator is found to be different from the finite element results. Moreover, the dynamics of the structure are analyzed in detail with experimental modal analysis, and as a result, it is understood that the FEM is not constructed accurately. Therefore, material parameters and boundary conditions of the FEM were updated to achieve correlated results with experimental modal analysis.

Additional objectives of the study are as follows:

- Understanding of the effect of the bolt pretension on the natural frequencies of control column;

- Determination of the elasticity modulus of the neoprene at different strain rates;

- Understanding the effect of types of isolator connection on the natural frequencies of the control column.

1.3 Research Methodology

In the scope of the thesis, two different problems are studied. The problems and solution approaches studied in this thesis are presented schematically in Figure 1-3. The first problem is the damage in the control column during the vibration test. The study started with the aim of preventing fatigue damage of a control column. First of all, the FEM of the control column is constructed, and the fatigue analysis of the original structure is performed. As a result of the analysis, fatigue failure is revealed. In order to prevent this failure, the control column is updated with the addition of an isolator, and finite element analysis (FEA) is performed. The analysis results show that the isolator prevents the damage. Afterward, a prototype of the control column with the isolator is manufactured, and the accelerated track vehicle vibration is applied to the prototype during the shaker test. The test result proves that the isolator prevents the damage due to the random vibration.

Afterward, sine sweep vibration is applied to the control column to obtain the resonance frequency of the structure. When the resonance frequency obtained from this test is compared with FE results, a great discrepancy is observed. From this point on, efforts are given to minimize the discrepancy and to develop accurate FEM. At first, the dynamical behavior of the structure is obtained in detail with experimental modal analysis methods. Then, the elastic module of the isolator's material is determined by performing tensile tests. According to the results of the experimental modal analysis and material test, the FEM of the control column is updated, and the model is calibrated. In the last part of the study, the effect of model parameters are discussed, and conclusions obtained from this study are presented.
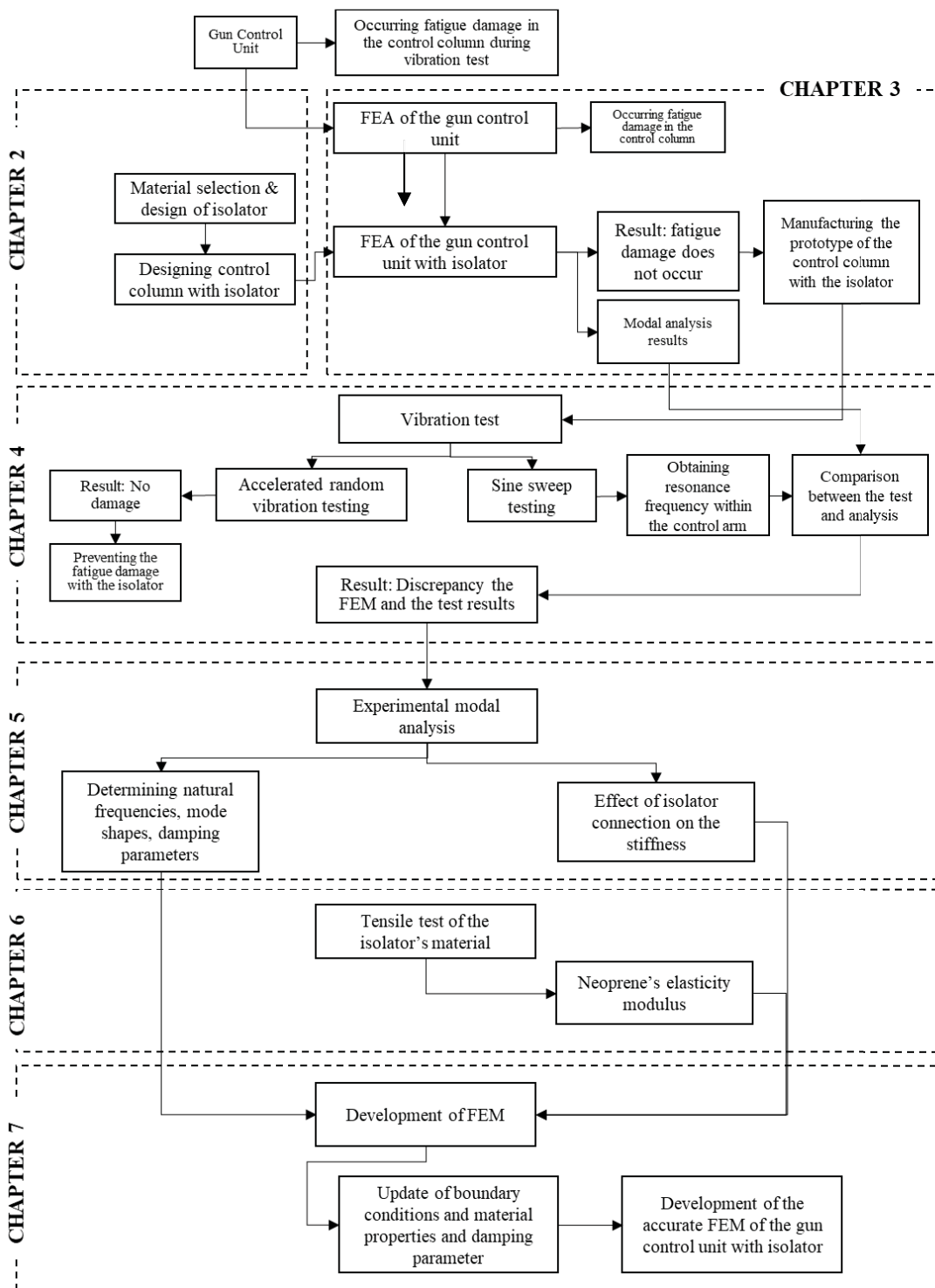
Figure 1-3: Methodology of the Study

1.4 Outline of Study

This study consists of eight chapters. The summary of the chapters are as follows:

Chapter 2, Design of Control Column with the Isolator: The motivation of the use of elastomer isolator is mentioned. The mechanical design of the isolator and material selection for the isolator is presented. The installation of the isolator to the control column is described.

Chapter 3, FEA of the Control Column: The FEM of the initial control column and control column with isolator is built. Modal analysis and random vibration analysis are performed. As a result of these analyses, natural frequencies, their mode shapes, and fatigue damages within the control column body are calculated.

Chapter 4, Vibration Tests: Firstly, the accelerated tracked vehicle vibration is applied to the prototype of the control column with an isolator, and the fatigue strength of the structure is examined. Secondly, the resonances within the control column body are determined by performing the sine sweep test.

Chapter 5, Experimental Modal Analysis: The experimental modal analysis is performed by making use of the impact hammer test method. As a result of the analysis, the natural frequencies, mode shapes, and damping ratios are determined. Experiments are carried out in two different configurations so as to examine the effect of the isolator connection on the natural frequencies of the structure.

Chapter 6, Determination of Neoprene Material Properties: Tensile tests of neoprene material used for the isolator are performed, and the elastic modulus of neoprene is determined. By conducting tests at different crosshead speeds, the effect of the test speed on the elastic modulus of the neoprene is examined.

Chapter 7, The Finite Element Model Updating: In this chapter, a FEM is developed that is compatible with the results of experimental modal analysis. Outcomes of the experimental modal analysis and the material test are utilized to update the FEM of the control column. In addition, the effects of different types of isolator connections on the natural frequencies of the control are examined, and the connection type of the isolator is updated in the FEM. Finally, the FEM is calibrated with the help of the parametric analyses according to experimental modal analysis results, which leads to achieving an accurate FEM of the control column with the isolator.

2. DESIGN OF THE CONTROL COLUMN WITH THE ISOLATOR

2.1 Introduction

The suitability of the gun control unit for use in tracked vehicle platforms was tested. During the tests, the fixed control column in the gun control unit was broken. It was concluded that gun control column does not have sufficient fatigue strength for use in tracked vehicle platforms.

This study starts with the aim of enabling the gun control unit to be used in the tracked vehicle platforms without occurring fatigue damage. In order to prevent fatigue damage in the control column structure, stresses on the structure resulted from tracked vehicle vibration should be reduced. In this chapter, the mechanical design changes are made to achieve a control column that can maintain structural integrity throughout the life of a tracked vehicle platform are described.

The motivation of using an isolator to prevent fatigue damage is explained; the selection of material for the isolator and the mechanical design of the isolator are stated. Finally, the isolator is installed in the control column structure.

2.2 The Motivation of the Design

In this chapter, it is aimed to increase the fatigue life of the control column and make it usable in tracked vehicle platforms. As the vibration requirements are predetermined by the standards, the design of the control column should be changed. There are two approaches in this case. The first one is changing the overall design of the control column, and the second one is installing an additional absorbent structure that reduces the vibration transmitted to the column.

The control column is produced in large quantities. For this reason, the main body of the column has been manufactured using the aluminum die casting process to keep the manufacturing cost per item low. In contrast, the die casting process has the disadvantage of the high initial cost caused by the casting mold. If the overall design of the control column is changed, the new casting mold would have to be remanufactured. As it is uneconomical, it is decided that adding an isolator would be more appropriate.

2.3 Isolator Design

In order to reduce the damaging effects of vibration, an absorbent structure which is called an "isolator," is installed under the control column. In this section, the material selection, mechanical design, and the mounting of the isolator are described.

2.3.1 Determination of the Material for the Isolator

The material to be used as an isolator should have certain properties. First, and the most important is that it should have a good damping performance as damping plays an important role in decreasing the response at the resonance frequency. The higher the damping ratio provides, the lesser the amount of transmissibility at the resonance frequency. An elastomer material which has a higher degree of damping helps reduce transmissibility at the resonance. The transmissibility curves of an elastomer relative to steel spring are presented in Figure 2-1 [2, 3].
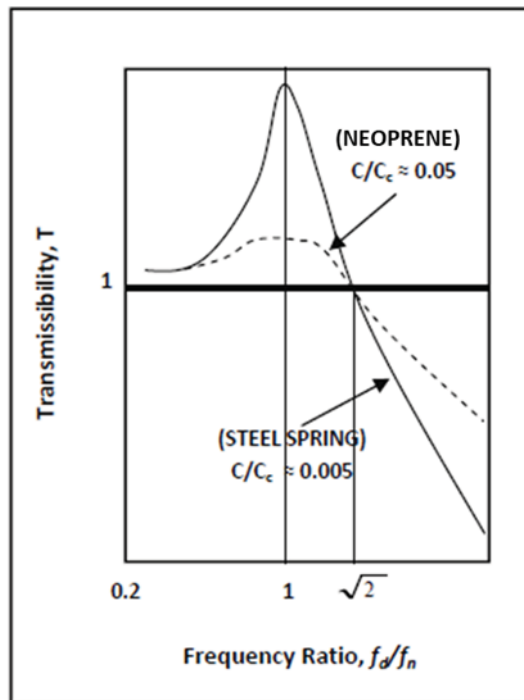
Figure 2-1: Typical transmissibility curves for highly and lightly damped systems.

Second, the isolator should be small as there is not enough space to accommodate a large isolator such as friction damped springs or air damping, etc.. Other required properties are low density to prevent extra additional mass, easy to be installed, manufacturability, and accessibility in the industry so that it can be supplied in large numbers at a low cost.

Consequently, it is decided to use an elastomer as the absorber material since it meets the required conditions. Installing elastomer in the control column structure will cause flexibility throughout the structure. During the use of the control column structure, too much flexibility should be avoided. For this reason, neoprene material with a higher young modulus than other elastomers is chosen for the absorber material (Table 2-1) [4].

Table 2-1: Comparison of the Elastomers [5]

Elastomer	Damping Ratio	Young Modulus (MPa)
Natural Rubber	0.05	1.65
Neoprene	0.06	1.87
Butyl	0.35	1.10
Butadiene Rubber	0.05	1.55

2.3.2 Mechanical Design of the Isolator

Elastomers show a good vibration isolation performance under the different types of loading, such as tension, compression, shear, etc. according to their shapes. Conical elastomers are commonly used in order to isolate vibration in both axial and radial directions as they have similar stiffness characteristics in all directions [6]. In our case, the column is subjected to vibration load in all three axial directions. Hence, conical geometry is used in the design of the elastomer isolator. The solid model of the vibration isolator is shown in Figure 2-2. The technical drawing of the isolator is presented in Figure 2-3.
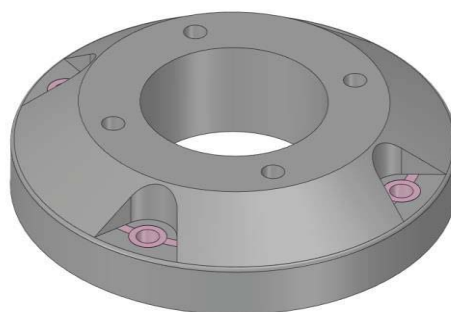
Figure 2-2: The design of the isolator
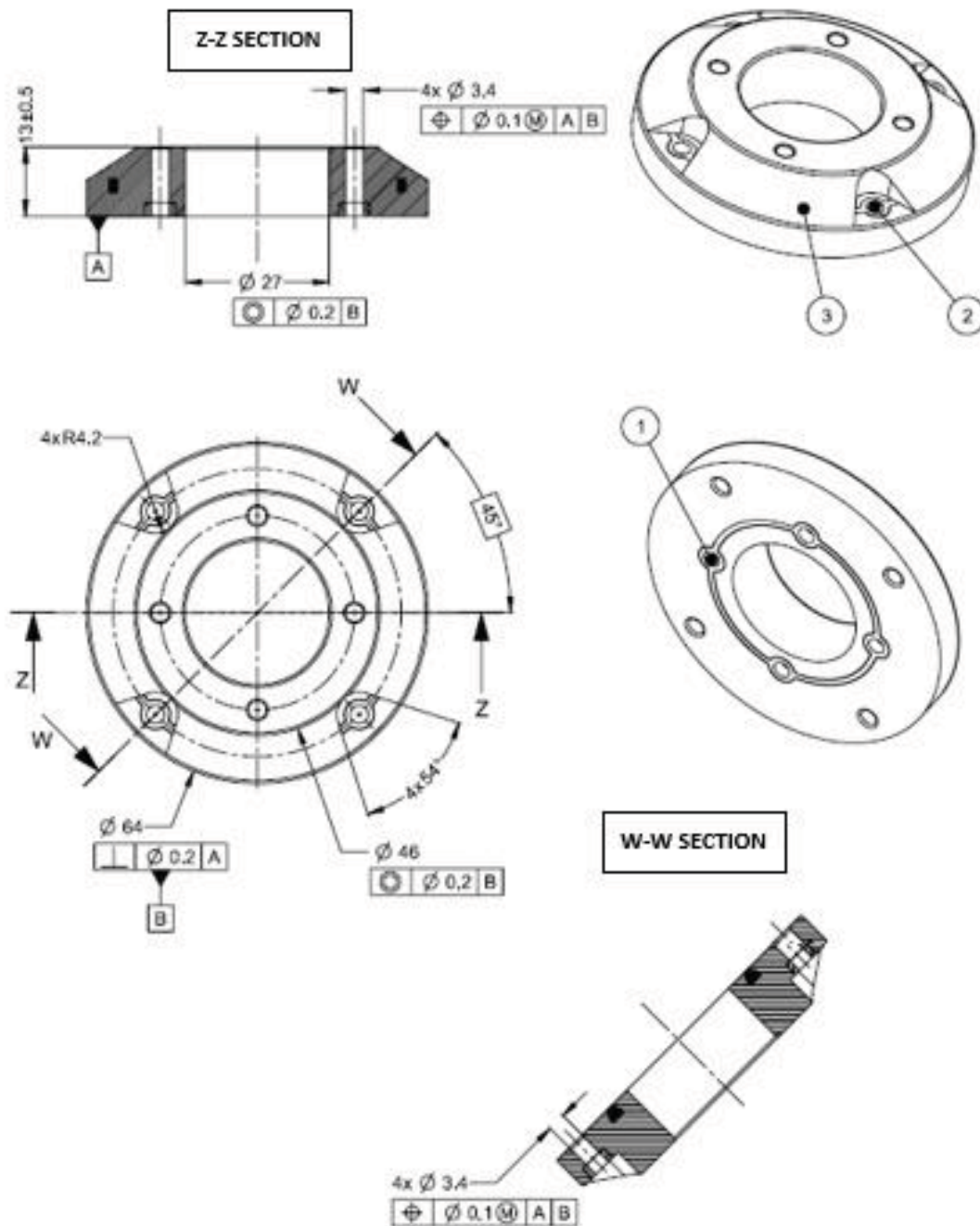
Figure 2-3: Technical drawing of the Isolator

2.3.3 Installation of Isolator in the Control Column Structure

The Elastomer Isolator is connected to the conical base with four threaded bolts. Apart from these bolts, it is attached to the holder with four threaded bolts. It is important to reiterate that the isolator is not attached to the holder and conical base with the same bolts.

Thus, the transmission of vibration to the column via threaded bolts is prevented. The installation of the isolator on the control column is presented in Figure 2-4.

a)   b)
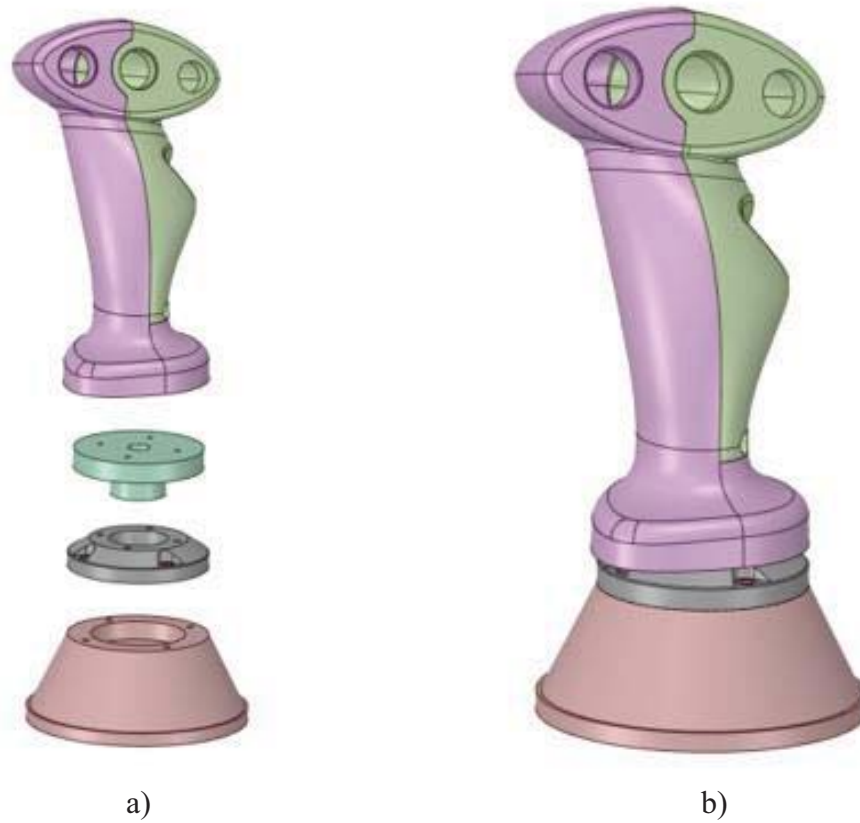
Figure 2-4: Installation of the isolator: a) Exploded view; b) assembly view

Two ring type of metal inserts were embedded in the elastomer so that the isolator can be bolted properly. They provide that the bolt head press on the more rigid and the larger surface. The metal inserts and their assembly are shown in Figure 2-5.
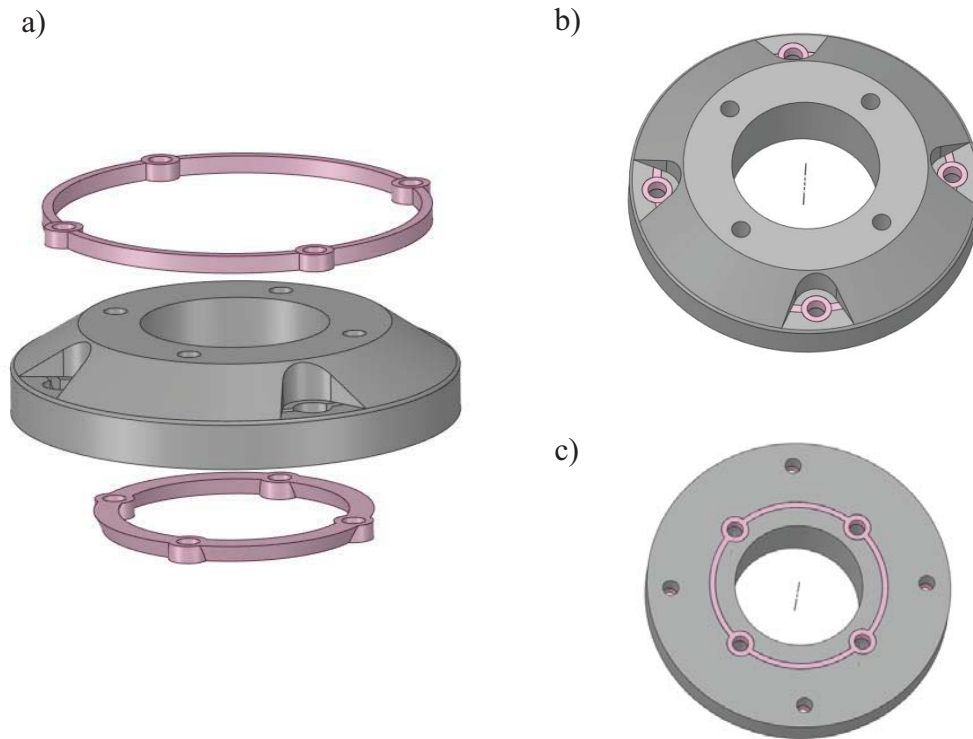
Figure 2-5: Metal inserts embedded in elastomer isolator: a) Exploded view; b) top view; c) bottom view

2.4 Conclusion

In this chapter, a neoprene isolator was designed for vibration isolation. The isolator is added to the control column structure to increase the fatigue life of the control column against the tracked vehicle vibration. In the next chapter, the fatigue life of the control column with or without isolator will be analyzed with the finite element method, and the advantages of the isolator usage are demonstrated.

3. FINITE ELEMENT ANALYSIS OF THE CONTROL COLUMN

3.1 Introduction

As mentioned previously, the control column (without isolator) was damaged during the accelerated tracked vehicle vibration test. Before improving the design of the damaged gun control unit, it is modeled by using the FE methods, and the vibration test of the gun control unit is simulated with the FEA.

With the FEA of the gun control unit, the control column is demonstrated to be damaged as in the vibration test results. Then, as explained in Chapter 2, the control column with an isolator is designed to prevent fatigue damage in the control column structure. Hence, the geometry in the FEM of the gun control unit is changed by adding the isolator, and FEA is solved. In the results of the analysis, the effects of the isolator added to the control column on the natural frequencies and fatigue strength of the control column are examined in detail.

With the FE method, it is aimed to predict the effect of the isolator on fatigue damage in the control column and to prevent fatigue failure by minimizing the need for prototypes.

In this chapter, the FEMs of the gun control unit with and without the isolator is developed. With the FEA, the natural frequencies and their mode shapes are calculated for both models. Besides, the fatigue strength of the control column with and without the isolator under the tracked vehicle vibration is determined. Finally, the analysis results of the gun control unit with and without the isolator are compared, and the effects of the isolator on the results are evaluated.

3.2 The FEA of the Control Column Without Isolator

In this section, the FEM of the gun control unit, which is damaged during the vibration test, was built in ANSYS Workbench v19.0 software. Then the results of the modal analysis and random vibration analysis are obtained. These results are compared with vibration test results.

3.2.1 The Methodology

First of all, the design model is imported from CAD Software, and then the model was idealized for FEA by doing necessary simplifications. All components of the gun control unit are included in the model. The contacts between the parts and boundary conditions are defined. The properties of materials used in the gun control unit are defined in the analysis model. After the analysis model is constructed, the modal analysis is performed primarily in order to determine the dynamic characteristics of the structure. In the modal analysis, natural frequencies and mode shapes are calculated from equation 1.

$$([K] - \omega_i^2[M])\{\emptyset_i\} = 0 \qquad (1)$$

The modal analyses are carried out with the following assumptions [7]:

- Stiffness and mass matrix are constant.

- Mode shapes are relative values, not absolute.

- Linear elastic material behavior is assumed.

- Damping is not included.

- No excitation of the structure is assumed.

- Small deflection theory is used, and no nonlinearities are included.

After obtaining the natural frequencies, mode shapes, and mode participation factors of the structures in modal analysis, random vibration analysis is conducted using the mode superposition method [8]. The aim of the random vibration analysis is to determine some statistical properties of structural response, such as the standard deviation of displacement, force, or stress. A tracked vehicle traveling on the road creates random vibration on the vehicle. Random vibration contains all frequencies at the same time. The amplitudes at these frequencies vary randomly with time. Therefore, we need a statistical process in order to characterize random excitation. It can be described statistically in terms of a Power Spectral Density (PSD) plot. The total frequency range is divided into bins. The excitation is squared, and the average is calculated for each bin. It is called the mean square. Consequently, the average squared amplitudes are divided by the bin bandwidth, and the random vibration can be expressed as $(units\ RMS)^2/Hz$. For this vibration analysis, the acceleration input is used as the input PSD whose units is G^2/Hz.

The response function obtained in the modal analysis is multiplied by the input PSD, so that response PSDs at each frequency is calculated. Since it is required in the average response of the system, it is taken integral of the response PSD curve in order to obtain the mean square response. The square root of the mean square gives the RMS, which means the average or one sigma deviation. The RMS value (sigma value) for the entire frequency range is calculated for every node in every free direction [9]. Consequently, 1-sigma response acceleration, displacement, and velocity for every node in every direction are obtained.

The RMS responses give the average response. According to Gaussian distribution, 1-sigma accounts for ~68.27 % of the total response. While the 1-sigma is multiplied by 2 and 3, 2-sigma and 3-sigma responses are obtained. 2-sigma responses account for ~95.45 %, whereas 3-sigma responses account for ~95.45 % of the total responses.

In the random vibration analysis, 1-sigma, 2-sigma, and 3-sigma stresses are obtained for fatigue analysis. Finally, the fatigue life of the structure was predicted by combining the stresses with cumulative damage theory and three interval method proposed by Steinberg [10, 11]. The first step is to determine the number of stress cycles needed to produce a fatigue failure for 1-sigma, 2-sigma, and 3-sigma stresses. They can be obtained from equation 2.

$$N_1 = N_2 \left(\frac{S_2}{S_1}\right)^b \tag{2}$$

The second step is to determine the actual number of fatigue cycles (n_i) accumulated during the service time of vibration for the 1-sigma, 2-sigma, 3-sigma values. Finally, Miner's fatigue damage cycle ratio is calculated by equation 3 [12].

$$R = \sum_{i=1}^{i=3} \frac{n_i}{N_i} \tag{3}$$

3.2.2   The Preparation of the Analysis Geometry

The CAD model has a lot of features, such as small edges, double edges, and very small faces, etc. These details make generating mesh nearly impossible. Thus, the geometry

should be simplified to idealize for the FEA. The CAD model of the control column structure is presented in Figure 3-1. The CAD model is imported into ANSYS SpaceClaim software. By making the necessary simplifications, the model is made suitable for analysis. The analysis model is shown in Figure 3-2. The assembly of the weapon control unit consists of 14 different components. The components of the weapon control unit are presented in Figure 3-3.
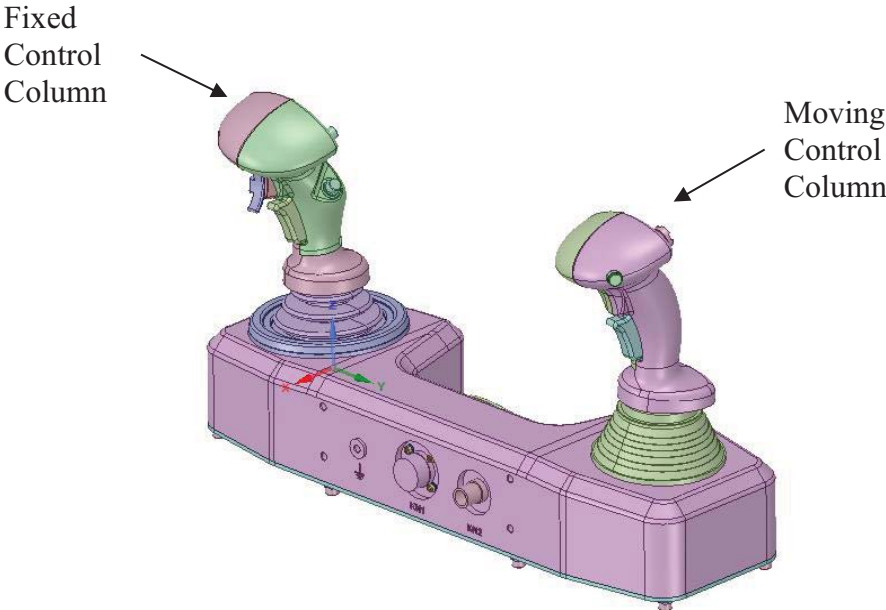
Figure 3-1: The CAD model of the gun control unit

Figure 3-2: The analysis geometry – Gun Control Unit

1	Button 1
2	Control Column-Left Body
3	Trigger Holder
4	Trigger Switch
5	Control Column Holder
6	Button 2
7	Button 3
8	Button 4
9	Trigger
10	Control Column-Right Body
11	Spacer
12	Conical Base
13	Case
14	Fixture
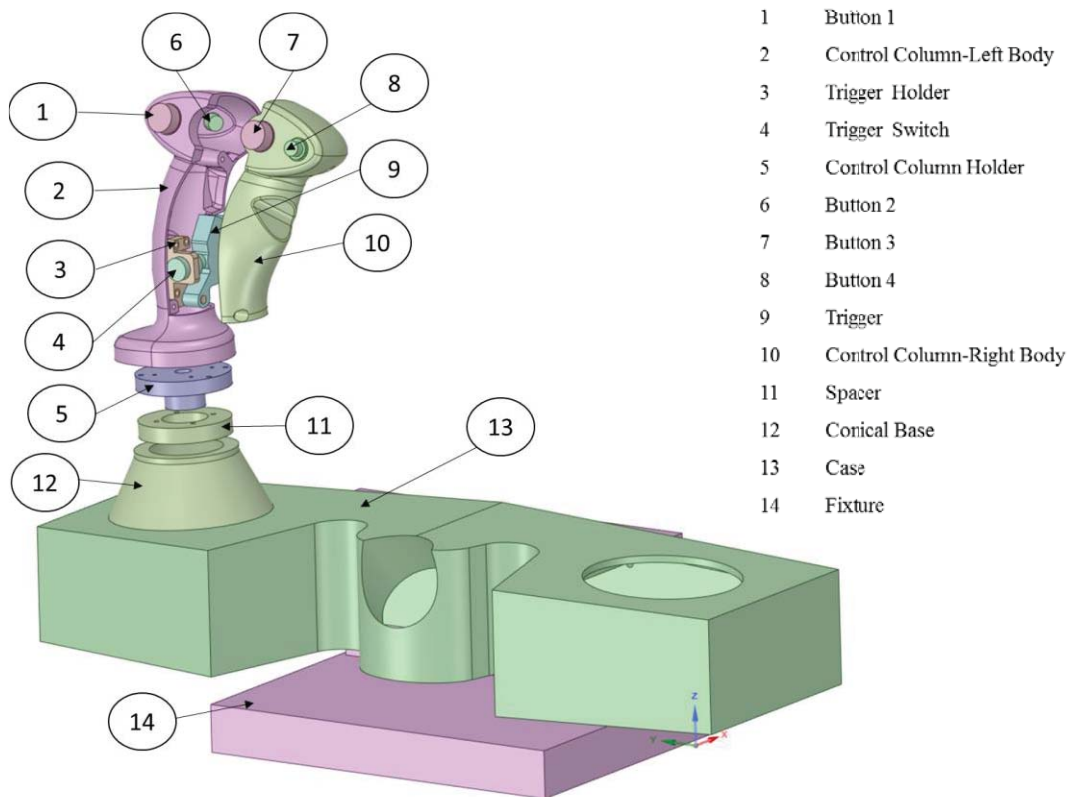
Figure 3-3: Components of the weapon control unit

Besides, the operating column (the other column in the unit) is not included in the geometry as a solid model. The other column is not concerned in this study since it is not damaged in the vibration test. So, it is modeled as a point mass that has the mass, the center of gravity, and inertial effects of the moving control column. The point mass is connected to the associated face, the behavior of which is deformable. The face and the location of the reference coordinate system are shown in Figure 3-4. The mass and inertia of the point mass are presented in Table 3-1.
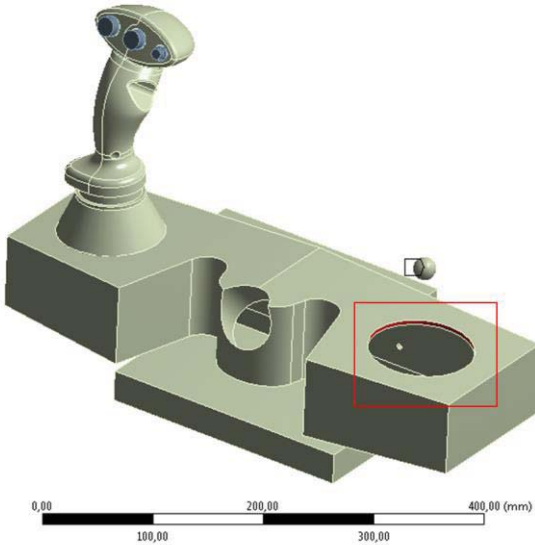
Figure 3-4: Point mass definition of the second control column

Table 3-1: The mass and inertia of the point mass

Part	Mass (kg)	Inertia (kg. mm^2)			Center of Gravity (mm)		
		X	Y	Z	X	Y	Z
Moving Control Column	0.45	4085.6	778.34	4085.6	79.6	75.25	161.94

3.2.3 Machine Elements

The components of the weapon control unit are connected with bolts. In this model, all connection bolts are modeled by using the beam element. The surface of the washer is selected as a contact face, whereas the threaded face is chosen as the target face in beam element modeling. Bolted connections are presented between Figure 3-5 and Figure 3-10.
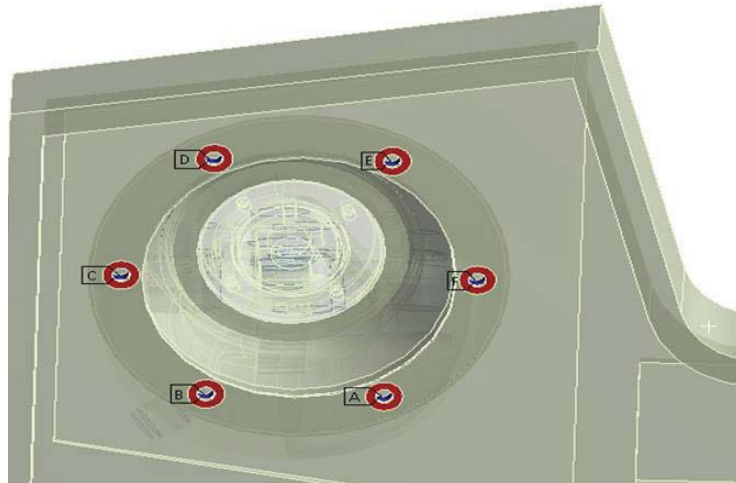
Figure 3-5: The bolted connection between the console and the base of the control column.
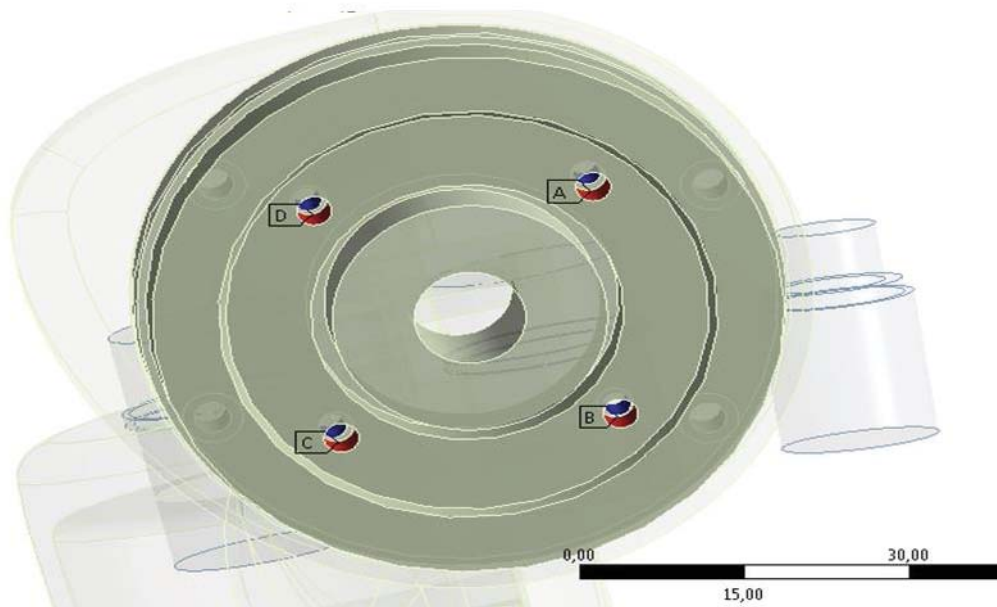
Figure 3-6: The bolted connection between the spacer and the holder
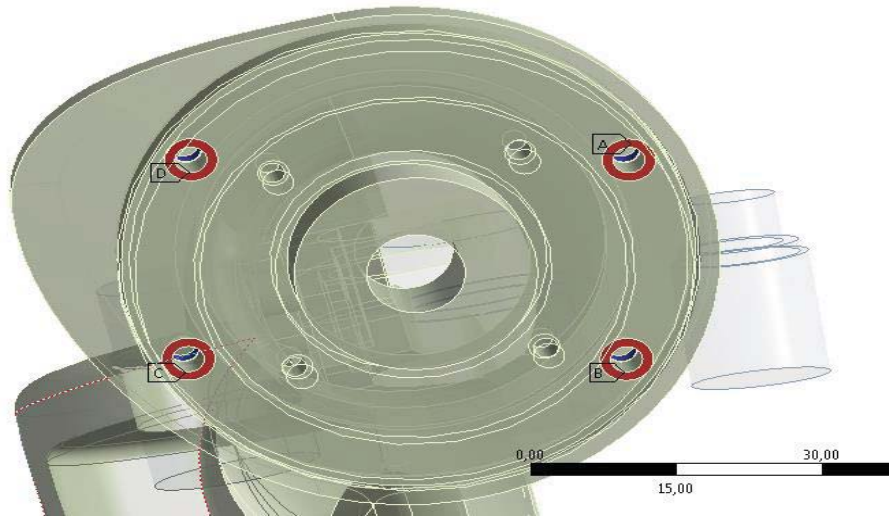
Figure 3-7: The bolted connection between the left body of the column and the holder

a)

b)
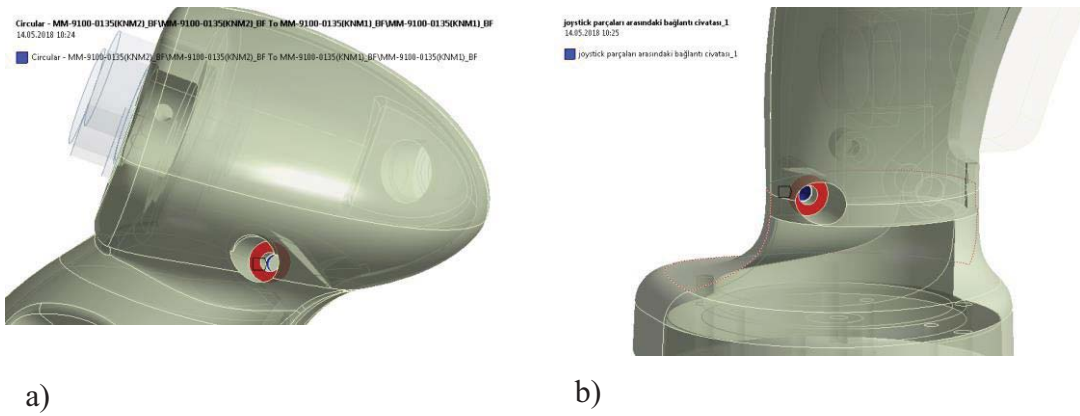
Figure 3-8: The bolted connection between the left and right body of the column: a) the upper connection bolt; b) the lower connection bolt
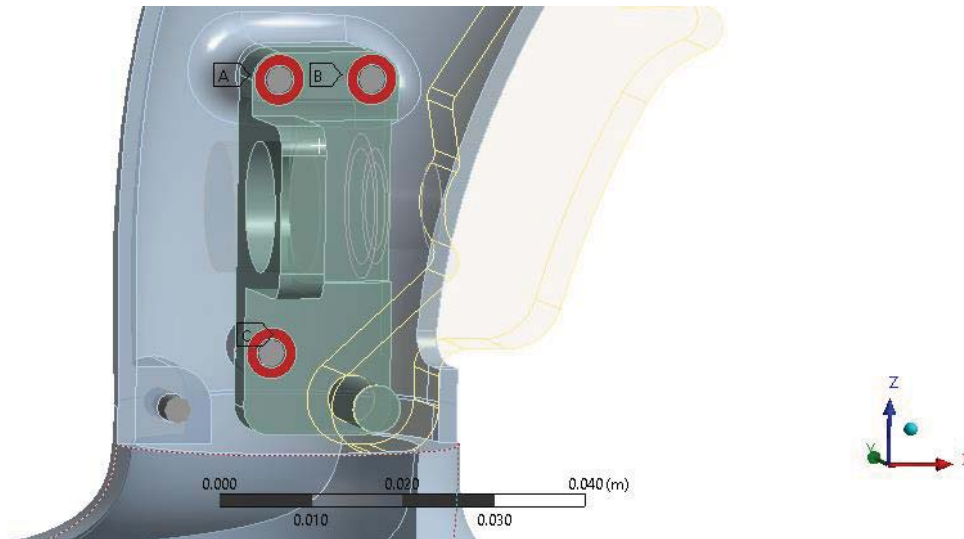
Figure 3-9: The bolted connection between the trigger holder and the left body of the column
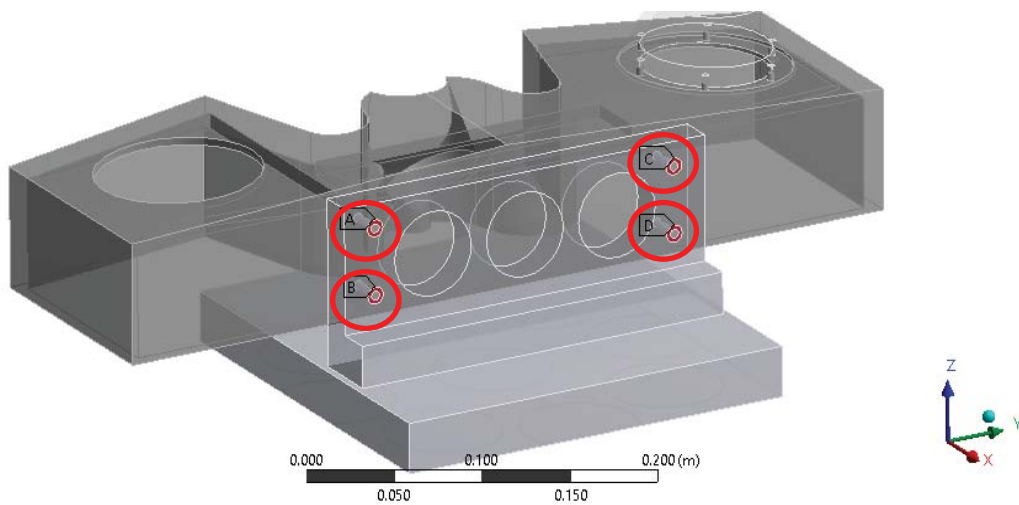
Figure 3-10: The bolted connection between the test fixture and the case of the control unit

In the analysis model, the revolute joint is used in the connection of the trigger and trigger holder. The revolute joints provide the single-axis rotation function to the trigger mechanism. Also, the trigger is connected to the trigger button with a spring mechanism. The surfaces used for connection of the revolute joint and the spring element in the trigger mechanism are shown in Figure 3-11 and Figure 3-12, respectively.
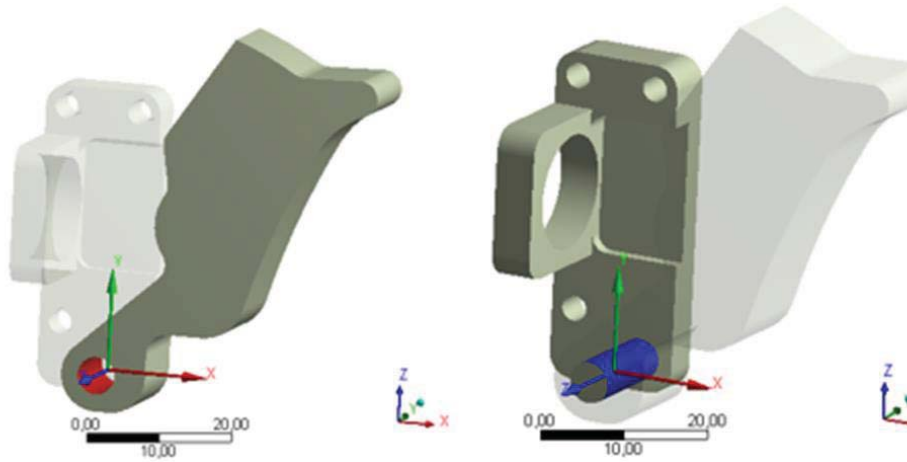
Figure 3-11: The surfaces to which the revolute joint is defined
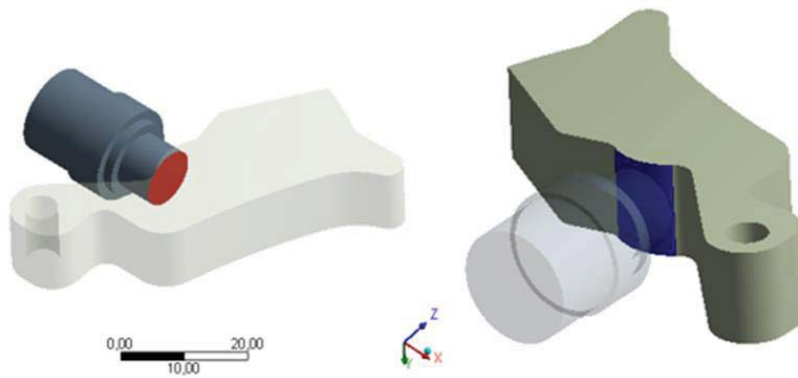
Figure 3-12: The surfaces to which the spring element is defined

3.2.4 Mesh Generation

The types of the element of "Tet10" are used in the FEM in order to meshing. The gun control handle meshes with an element size of 0.75 mm. In total, 478167 mesh elements and 732730 nodes are used to solve the analysis model. The generated mesh and its element quality distribution are shown in Figure 3-13 and Figure 3-14, respectively.
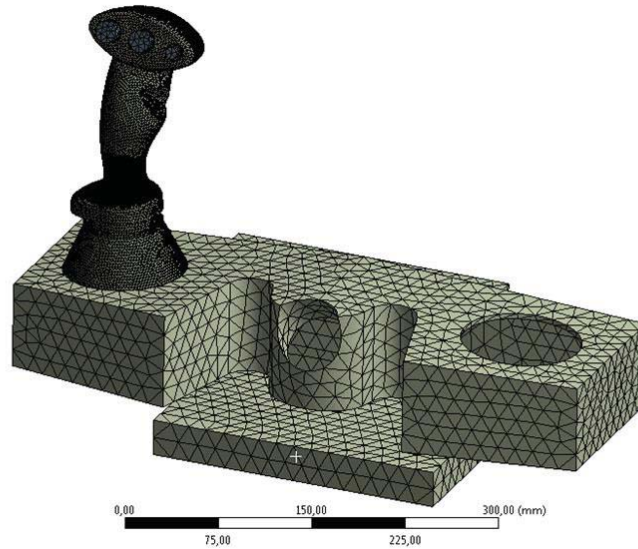
Figure 3-13: The generated mesh
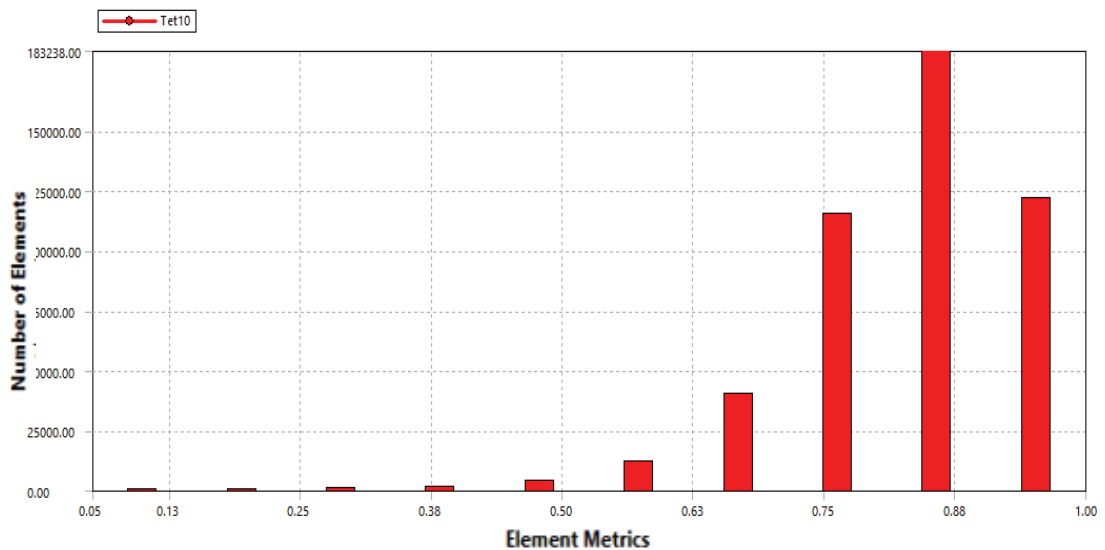
Figure 3-14: The mesh quality

3.2.5   Boundary Conditions and Contacts

The fixture is attached to the table of the electrodynamic shaker with bolts. Bolts and the table of the shaker are not included in the analysis model as a solid model. The fixed support boundary condition is applied to the base of the text fixture. The fixed support condition is shown in Figure 3-15. The switches on the control column are connected to the control column by using the "bonded contact" algorithm. The connections of switches are shown in Figure 3-16.
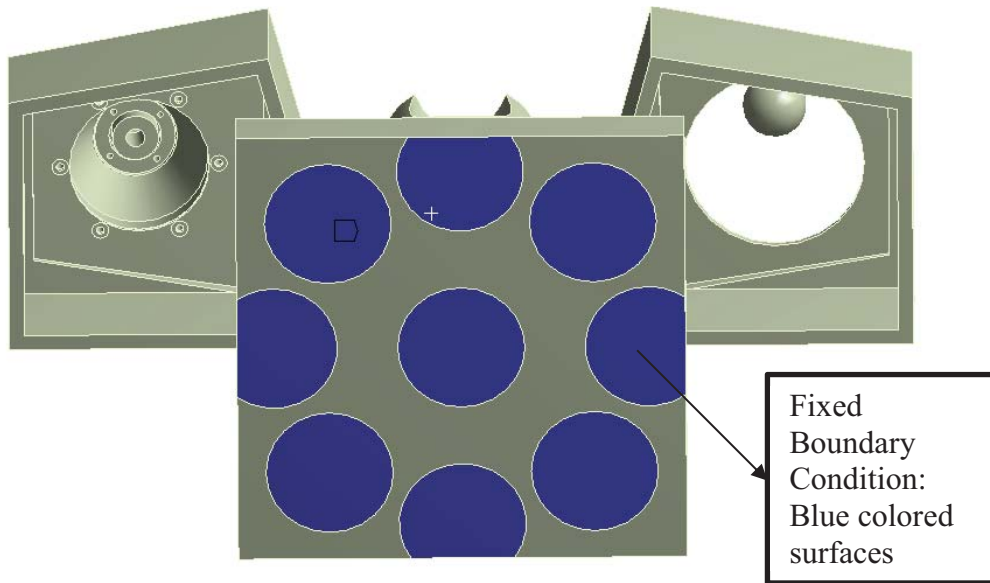
Figure 3-15: The pressure cone surface on which the test fixture is fixed
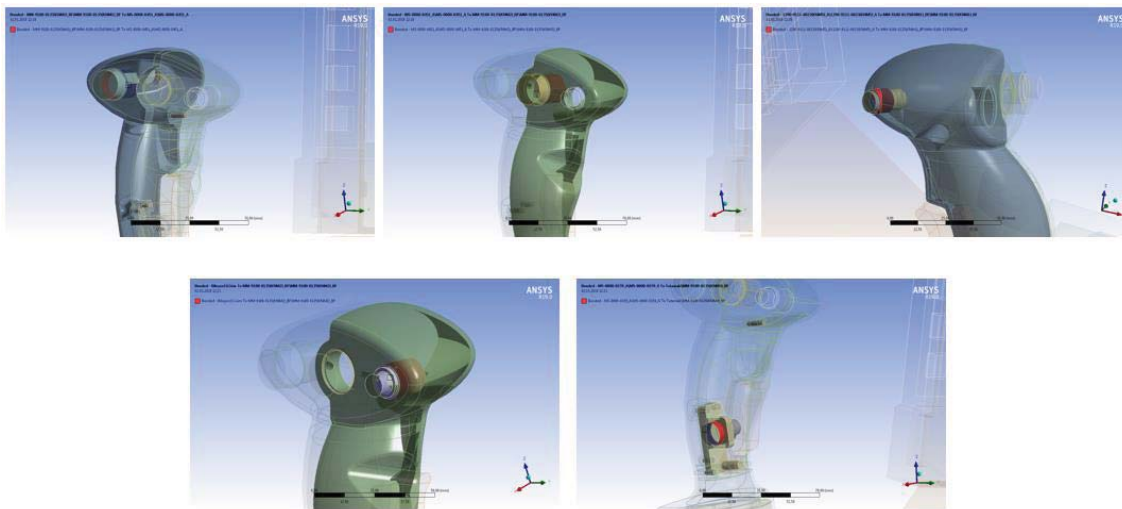
Figure 3-16: Button connections

3.2.6 Analysis Settings

Modal analysis and random vibration analysis in three axes are performed in order to obtain the fatigue damage of the structure. The results obtained in the modal analysis is used in random vibration analysis as inputs. The method is called the mode superposition. The frequency range of the modes extracted in modal analysis plays an important role in random vibration analysis. In order to obtain accurate results in random vibration analysis, the modal frequency range should be 1.5 times greater than the random load

range [13]. As the frequency range of the tracked vehicle vibration load is 5-2000 Hz, modes are extracted up to 3000 Hz in the modal analysis. The modal analysis setting is presented in Figure 3-17.

Options	
Max Modes to Find	100
Limit Search to Range	Yes
Range Minimum	0. Hz
Range Maximum	3000. Hz
Solver Controls	
Damped	No
Solver Type	Program Controlled
Rotordynamics Controls	
Coriolis Effect	Off
Campbell Diagram	Off
Advanced	
Contact Split (DMP)	Off
Output Controls	
Stress	Yes
Surface Stress	No
Back Stress	No
Strain	Yes
Contact Data	Yes
Nodal Forces	Constrained Nodes
Volume and Energy	Yes
Euler Angles	Yes
Calculate Reactions	Yes
Store Modal Results	Program Controlled
General Miscellaneous	No
Result File Compression	Program Controlled

Figure 3-17: The modal analysis settings

The structural damping value has to be defined in order to calculate the response PSD. It is observed at the previous studies of a similar area that the damping ratio is chosen as %5. However, the damping ratio is taken as %2 in this study to stay safe side [14]. The random vibration analysis settings are shown in Figure 3-18.

Options	
Number Of Modes To Use	All
Exclude Insignificant Modes	No
Output Controls	
Keep Modal Results	No
Calculate Velocity	Yes
Calculate Acceleration	Yes
Result File Compression	Program Controlled
Damping Controls	
Constant Damping	Manual
☐ Damping Ratio	2.e-002
Stiffness Coefficient Define By	Direct Input
☐ Stiffness Coefficient	0.
☐ Mass Coefficient	0.

Figure 3-18: The random vibration analysis settings

ANSYS fatigue tool, which is embedded in the random vibration environment, is used for the calculation of fatigue life and damage. Steinberg Method is used to calculate the fatigue strength of the structure [15].

In order to determine the number of fatigue cycles, the exposure duration of the random vibration should be defined in the analysis. According to the standard of AECTP 400, the structure is exposed to the tracked vehicle vibration for 4 hours. The fatigue tool settings are presented in Figure 3-19.

Domain	
Domain Type	Frequency
Options	
Method Selection	Steinberg
Stress Component	Equivalent (von-Mises)
Coordinate System	Solution Coordinate System
Definition	
Exposure Duration	14400 s

Figure 3-19: The fatigue tool settings

3.2.7 Load Conditions

Tracked vehicle vibration profile is defined in the section of "Material in turret bustle rack or installed in turret" of the AECTP 400 Mechanical Environmental Tests [16]. Figure B-2 test profile is presented in Figure 3-20. The gun control unit is tested with this vibration profile on the shaker table. In the random vibration analysis, this profile is also planned to use as input PSD. However, the vibration profile can't be defined in the FEA

model since the Figure B-2 test profile contains narrow band frequency, which is shifted with time in the specified frequency range.

FIGURE B-2   MATERIEL IN TURRET BUSTLE RACK OR INSTALLED IN TURRET
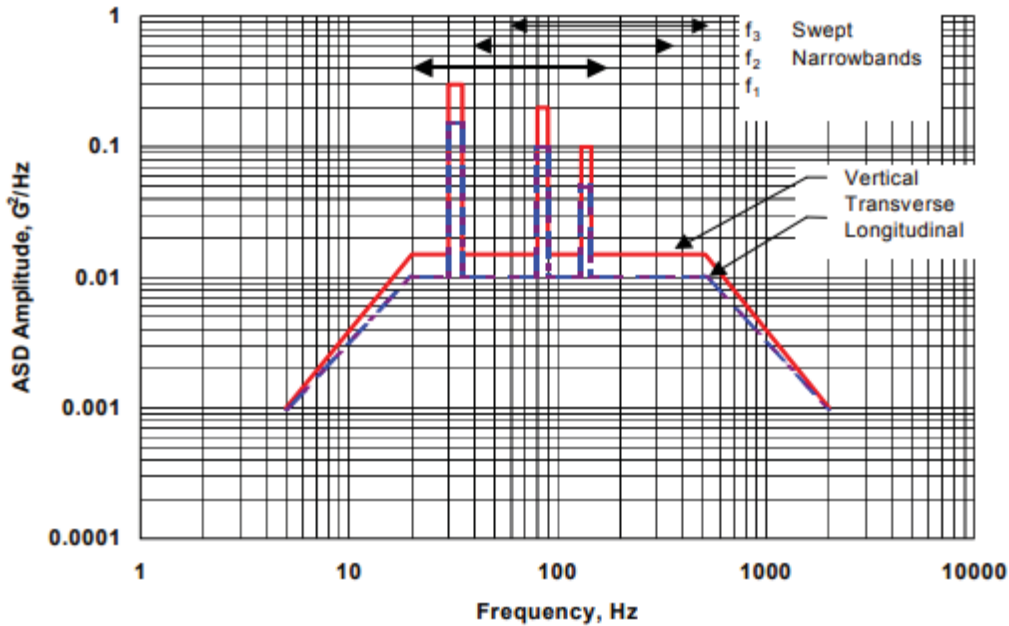
Figure 3-20: AECTP 400 Mechanical Environmental Test Figure B-2 Tracked Vehicle Vibration Test Profile

The equivalent vibration profile that covers the energy of Figure B-2 Test profile is obtained by using the enveloping method, which is presented in the standard of MIL-STD-810G [17]. The equivalent PSD profile is used as the PSD input in the analysis model. The equivalent PSD profiles have 5-2000 Hz of the frequency band as similar to the Figure B-2 test profile. Similarly, the equivalent PSD profile is applied to the structure for 4 hours. Besides, PSD loads are applied to the structure from the surface on which the fixed support is defined. In addition, the equivalent PSD profiles vary with the axis, such as the lateral and the vertical directions. They are shown in Figure 3-21 and Figure 3-22, respectively.
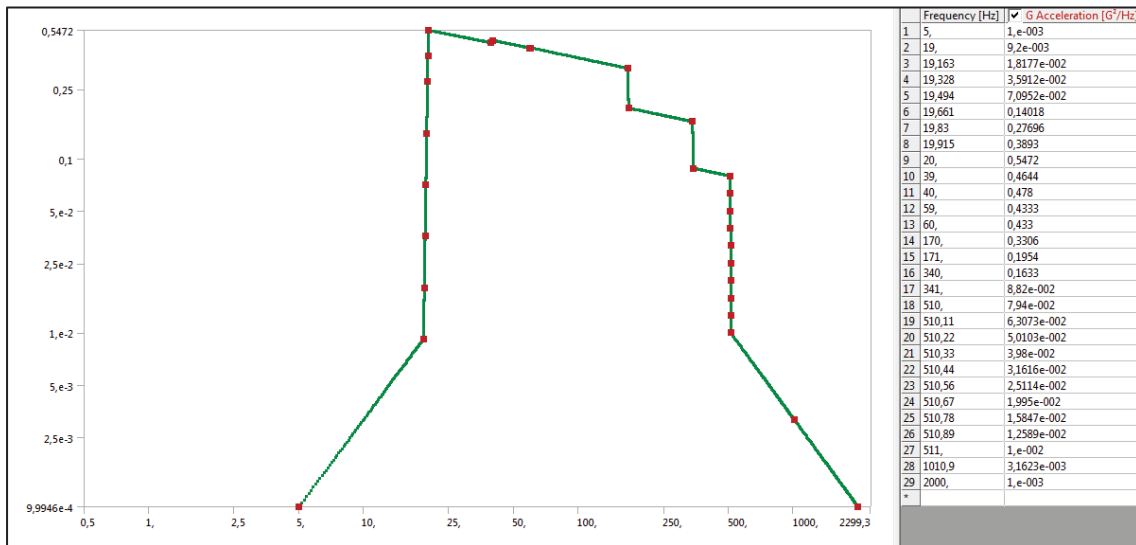
Figure 3-21: AECTP-400 Ed.3 Figure B-4 Lateral & Transverse Axes Vibration Profile
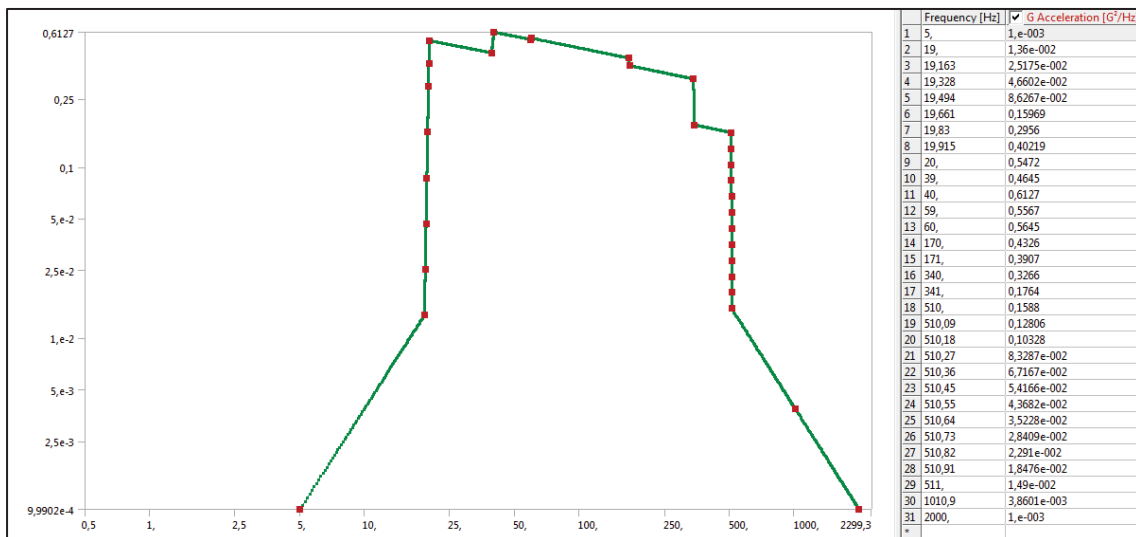
Figure 3-22: AECTP-400 Ed.3 Figure B-4 Vertical Axis Vibration Profile

3.2.8 Materials

The materials that are assigned for the components are listed in Table 3-2, and they are shown in Figure 3-23. Material properties are specified in Table 3-3. The S-N curve, which is defined only for Aluminum material, is used in order to estimate the fatigue life of the structure. It is not set for polyethylene material since the fatigue results of buttons are not concerned.

Table 3-2: Materials of the Components

Number of Components	Component	Material
	Button 1	Polyethylene
2	Control Column Left Body	Aluminum A 413 Die-Cast
3	Trigger Holder	Sheet Aluminum 6061 T6/T62/T651
4	Trigger Switch	Sheet Aluminum 6061 T6/T62/T651
5	Control Column Holder	Sheet Aluminum 6061 T6/T62/T651
6	Button 2	Polyethylene
7	Button 3	Polyethylene
8	Button 4	Polyethylene
9	Trigger	Sheet Aluminum 6061 T6/T62/T651
10	Control Column Right Body	Aluminum A 413 Die-Cast
11	Column Spacer	Sheet Aluminum 6061 T6/T62/T651
12	Conical Base	Sheet Aluminum 6061 T6/T62/T651
13	Case	Sheet Aluminum 6061 T6/T62/T651
14	Fixture	Sheet Aluminum 6061 T6/T62/T651
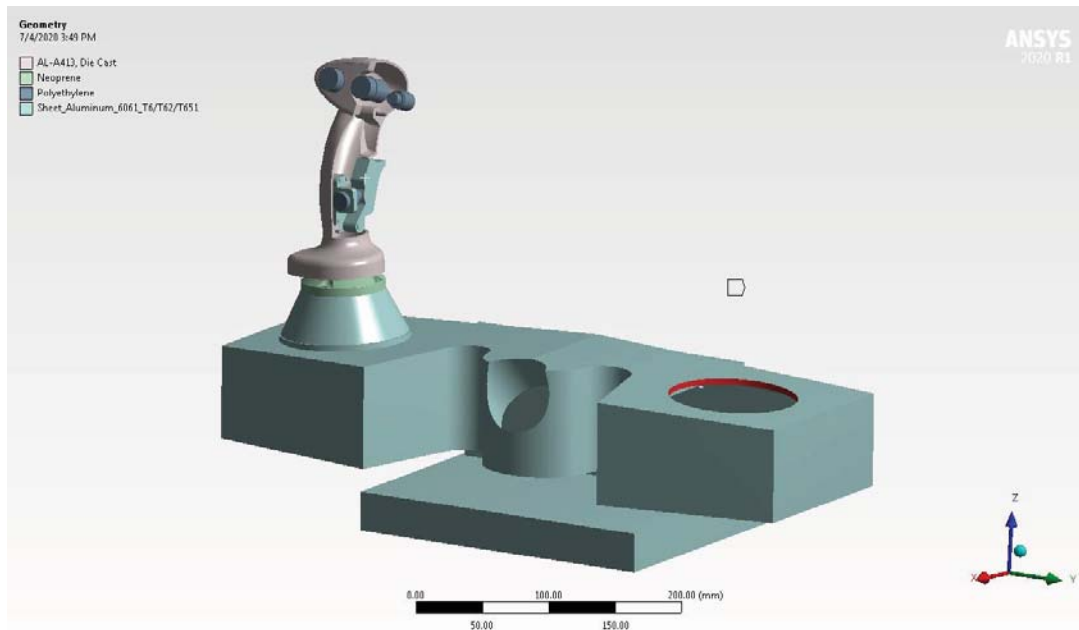
Figure 3-23: Material Assignment

Table 3-3: Material Properties

Materials	ρ	E	v	σ_y	σ_u	S-N Curve	
	(kg/m^3)	(GPa)		(MPa)	(MPa)	Number of Cycles	Stress (MPa)
Aluminum A413 Die Cast	2700	68	0.33	240	319	1E+03	262
						1E+06	138
Sheet Aluminum 6061 T6/T62/T651	2655	71	0.33	130	290	1E+03	175
						1E+06	130
Polyethylene	950	1.1	0.42	250	330	-	

3.2.9 Damage Criteria

In order to analyze the fatigue analysis, the cumulative fatigue damage cycle ratio is calculated according to Miner's Rule [18]. If the damage ratio is greater than the value of 1, then it is estimated that crack formation will occur in the structure. In this case, it can

be estimated that the fatigue life of the structure is not adequate for the tracked vehicle environment. Thus, it is required that the damage ratio should be less than the value of 1 in the fatigue analysis, except the singularity region.

3.2.10 Analysis Results

The modal analysis gives the natural frequencies and their corresponding mode shapes of the structure, whereas fatigue damage ratios are obtained with the random vibration analysis, which is performed at three directions of the axes. In this section, the results of these analyses are presented, respectively.

3.2.10.1   Modal analysis

The weapon gun control unit has the 51 resonance frequencies in the range of 0 – 3000 Hz. The obtained natural frequencies are shown in Figure 3-24. The first six natural frequencies and corresponding mode shapes are represented in Table 3-4.

	Mode	☑ Frequency [Hz]
1	1.	24.497
2	2.	87.293
3	3.	119.97
4	4.	128.18
5	5.	144.36
6	6.	207.45
7	7.	249.33
8	8.	328.19
9	9.	342.63
10	10.	372.97
11	11.	383.77
12	12.	386.54
13	13.	410.51
14	14.	523.27
15	15.	574.43
16	16.	640.
17	17.	682.93
18	18.	730.34
19	19.	827.77
20	20.	917.89
21	21.	1020.
22	22.	1083.6
23	23.	1094.5
24	24.	1130.2
25	25.	1295.8
26	26.	1319.8
27	27.	1382.8
28	28.	1453.
29	29.	1509.2
30	30.	1557.8
31	31.	1665.4
32	32.	1764.3
33	33.	1787.5
34	34.	1853.8
35	35.	1894.
36	36.	2005.
37	37.	2044.4
38	38.	2118.9
39	39.	2222.6
40	40.	2349.3
41	41.	2434.4
42	42.	2466.7
43	43.	2483.8
44	44.	2495.2
45	45.	2611.3
46	46.	2689.
47	47.	2767.8
48	48.	2792.2
49	49.	2863.
50	50.	2901.3
51	51.	2935.

Figure 3-24: Natural frequencies of the gun control unit

Table 3-4: Natural frequencies and mode shapes

Number of Modes	Natural Frequency (Hz)	Mode Shape Definition	Mode Shapes
1*	24.5	Mode of the trigger spring	
2	87.3	Oscillation of the control column in the direction of X-axis (longitudinal) and the bending mode of the gun control unit	
3	120	Oscillation of the control column in the direction of Y-axis (transverse)	
4	128.2	Oscillation of the control column in the direction of the X-Y plane	
5	144.4	Torsional mode of the control column	

6	207.5	Oscillation of gun control unit in the direction of Y-axis	
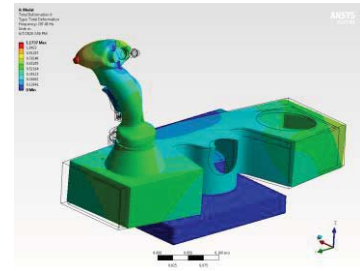
*: The third mode occurred at 25.9 Hz comes from the trigger spring constant (1500 N/m), and it is the local mode of the trigger and does not depend on the dynamic of the control column.

3.2.10.2 Random Vibration and Fatigue Analysis

The gun-control unit is analyzed under a random vibration profile presented for a tracked vehicle. The fatigue strength of structures is examined under the PSD profile. As a result of this study, the fatigue damage ratio is obtained for the control column. The maximum cumulative fatigue damage ratios are represented in Table 3-5. It can be estimated that the crack formation will occur in the region where the fatigue damage ratio is greater than one during the service life of the equipment. As it can be observed in Table 3-5, the damage ratio is greater than one in all direction. It can be evaluated that the control column does not provide strength during its service life in the tracked vehicle vibration environment. Based on the fatigue results, the crack initiation occurs in the left and right body of the control column in the analysis also performed in three directions. Damaged parts in the analyses performed in the direction of X, Y, Z are represented in Figure 3-25, Figure 3-26, and Figure 3-27, respectively.

Table 3-5: The results of the fatigue analysis

Analysis	X-Axis	Y-Axis	Z-Axis
Maximum Damage Ratio	1.89E+02	1.18E+06	2.66E+15
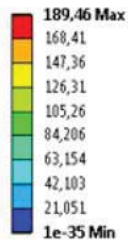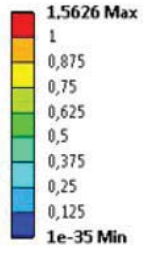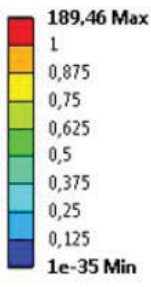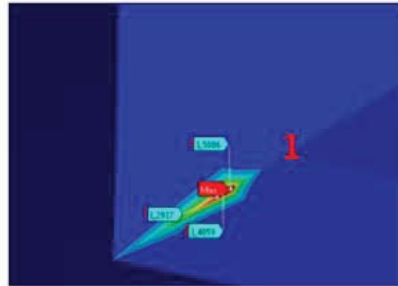
Figure 3-25: X-Axis Damage Ratio: a) Total control column body; b) left body of the control column; c) right body of the control column; d) zoomed view of the region
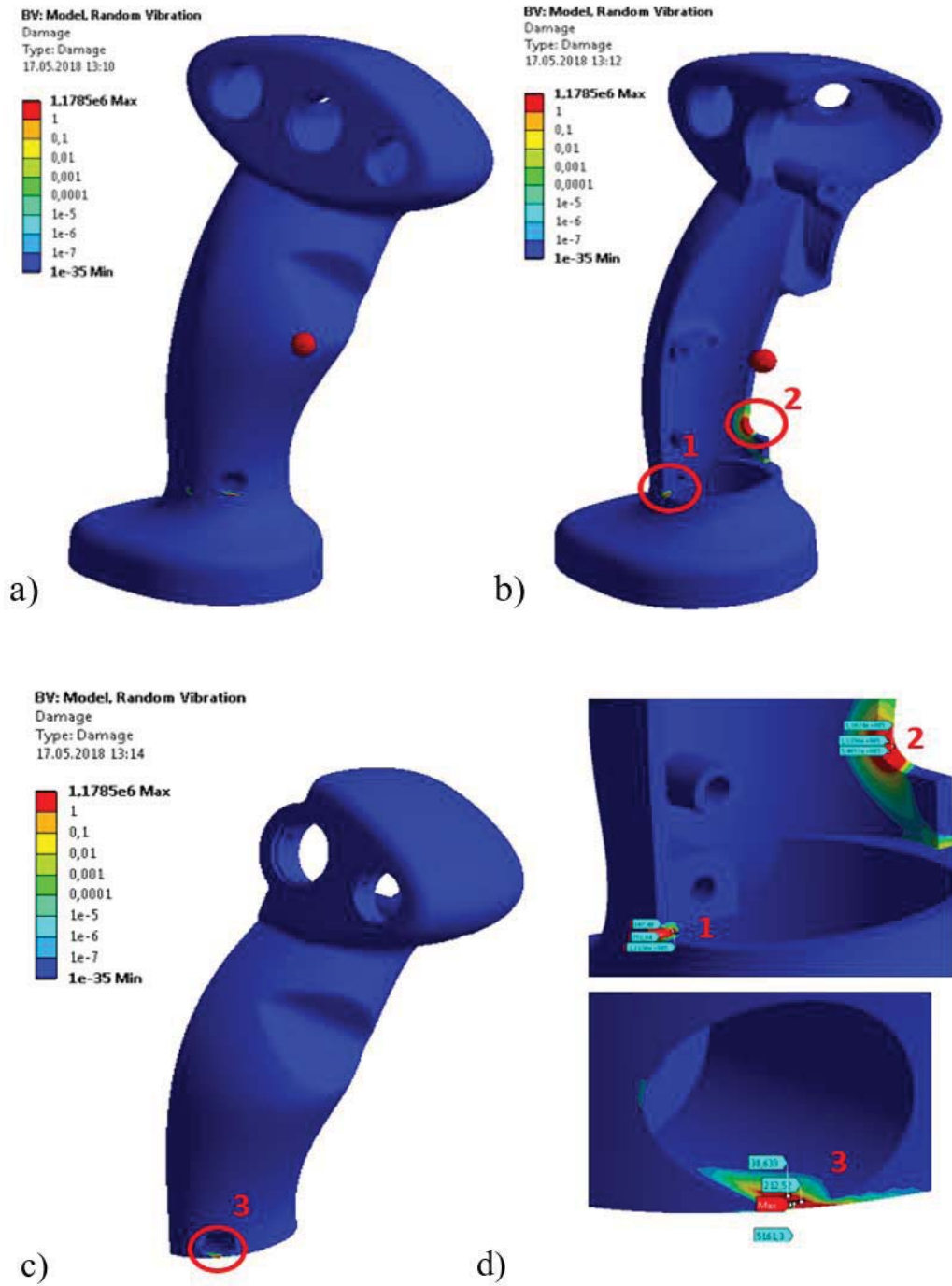
Figure 3-26: Y-Axis Damage Ratio: a) Total control column body; b) left body of the control column; c) right body of the control column; d) zoomed view of the region
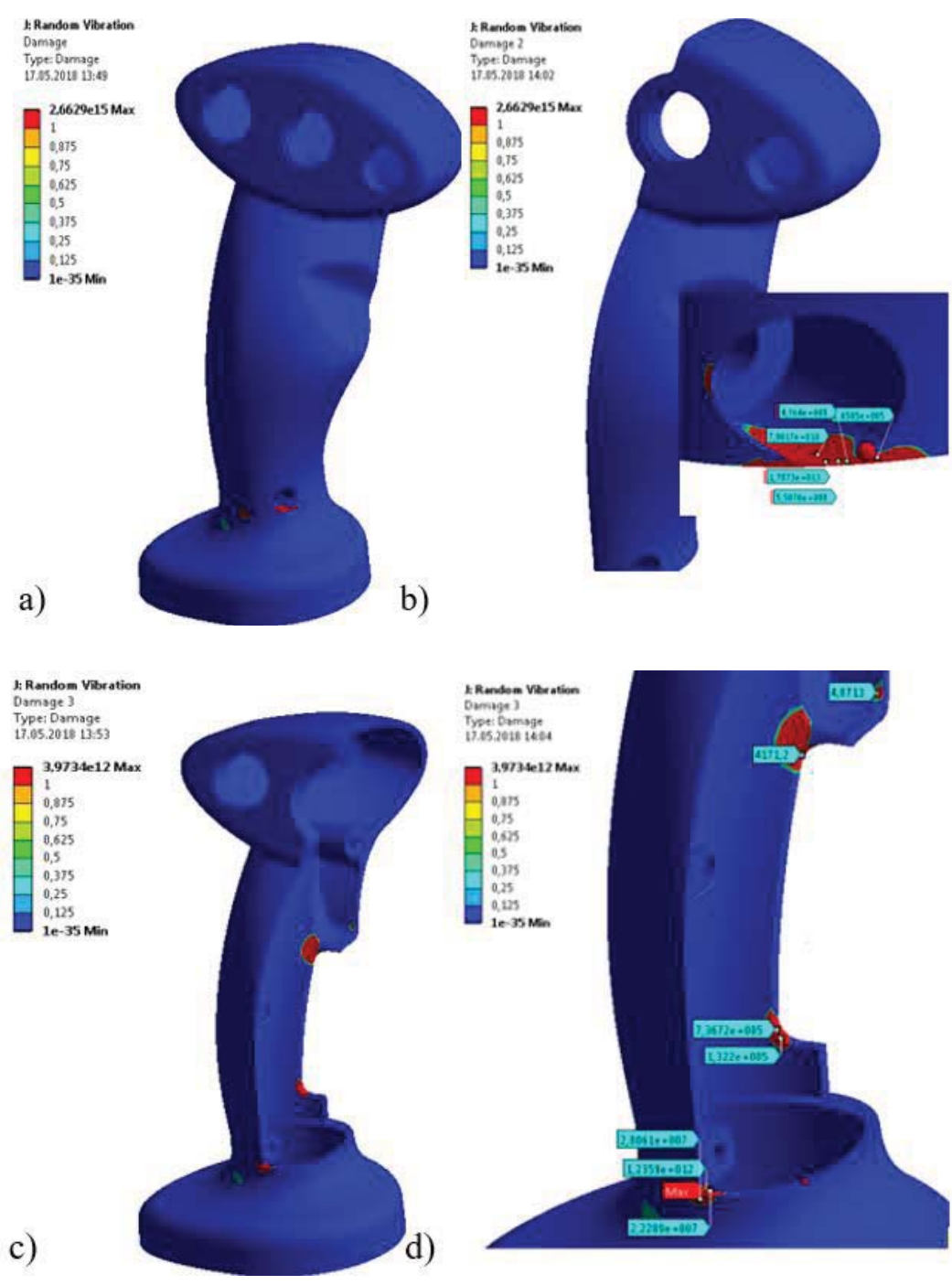
Figure 3-27: Z-Axis Damage Ratio: a) Total control column body; b) left body of the control column; c) right body of the control column; d) zoomed view of the region

Furthermore, Response PSDs are calculated for a node in the damage region to see the effect of the modes of the structure on the damage. The frequency-dependent normal stresses for the selected node were obtained in three axes. Thus, the modes that have the most impact on the damage of the structure are observed.

Firstly, Response PSDs in analyses carried out in the Y-axis direction is calculated. The node selected from stress zones for calculating Response PSD is shown in Figure 3-28 (shown by black arrow). The curves showing normal stresses versus frequency in three axes are presented in Figure 3-29.
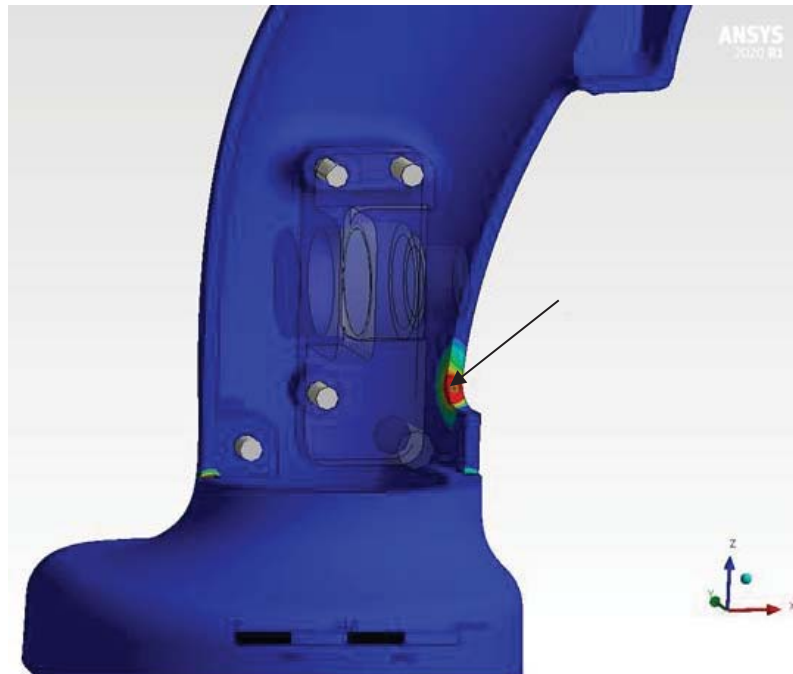
Figure 3-28: Damage region as a result of loading applied on the Y-axis
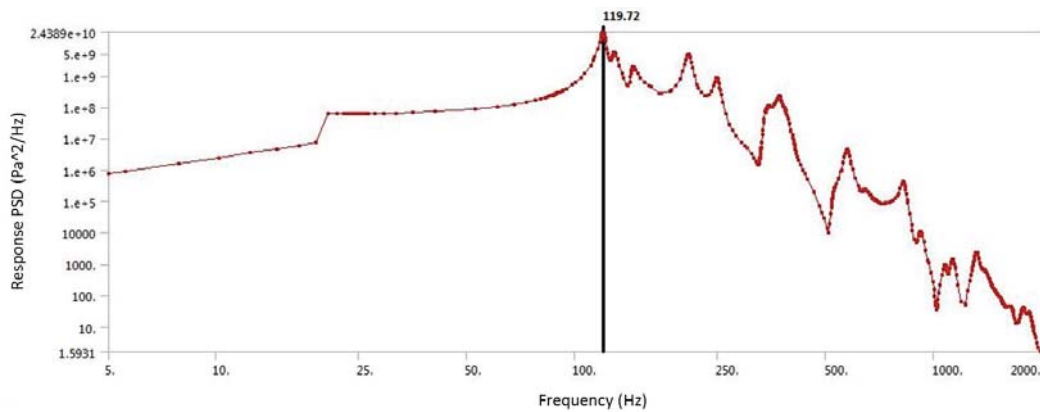
a)
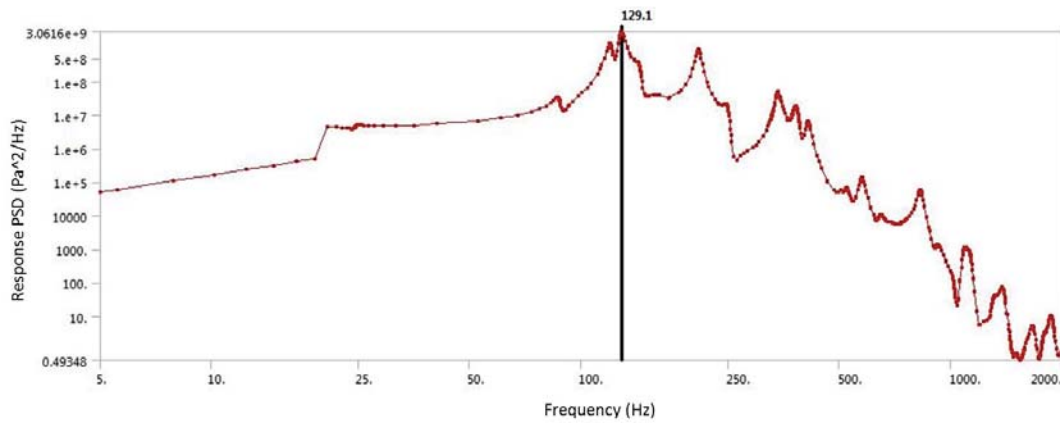
b)
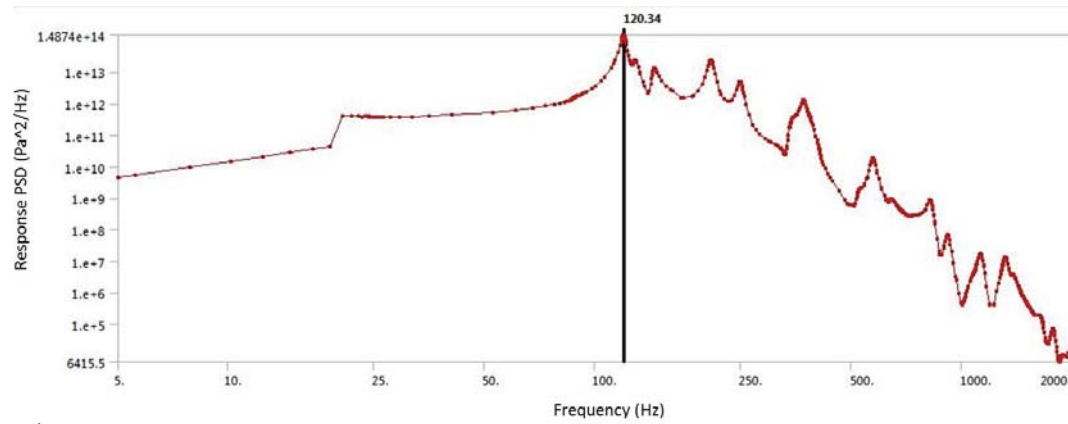
c)

Figure 3-29: Response PSD curves in the direction of X, Y, and Z-axes as a result of loading applied on the Y-axis

Secondly, the Response PSDs curve in analyses performed in the direction of the Z-axis is calculated. The node selected from stress zones (shown by the red arrow) for calculating Response PSD is shown in Figure 3-30. The curves of the normal stresses versus frequency in all three axes are presented in Figure 3-31.
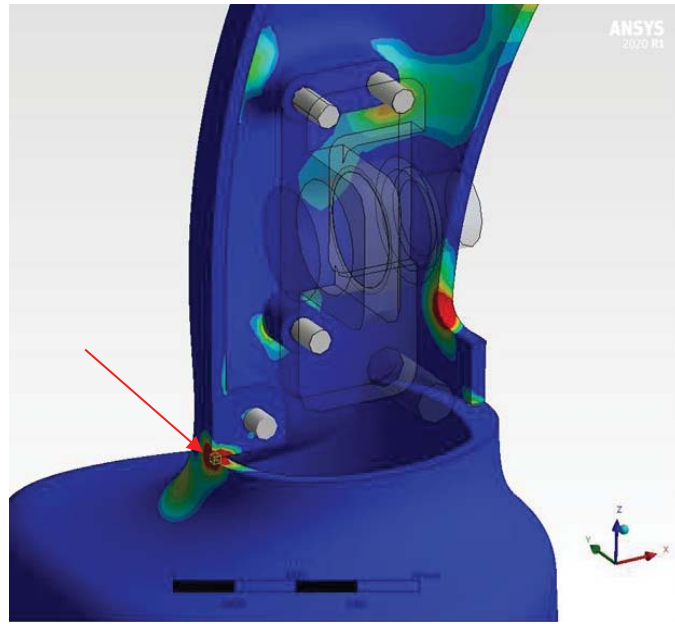
Figure 3-30: Damage region as a result of loading applied on the Z-axis
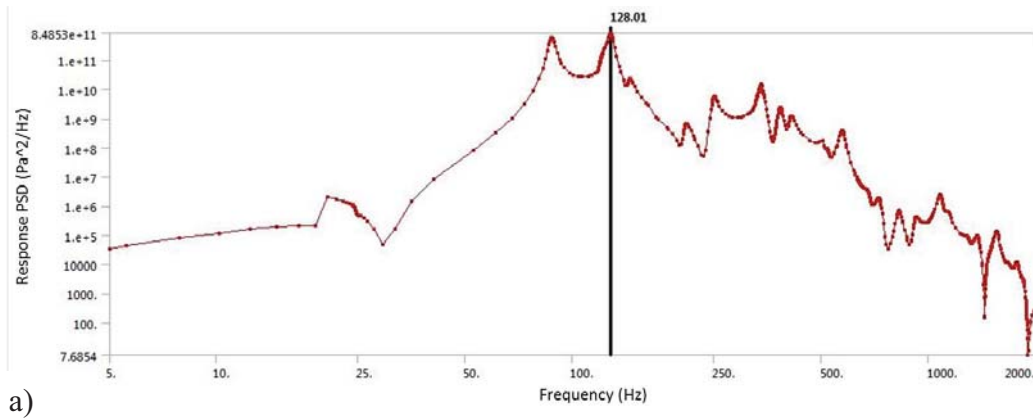
a)
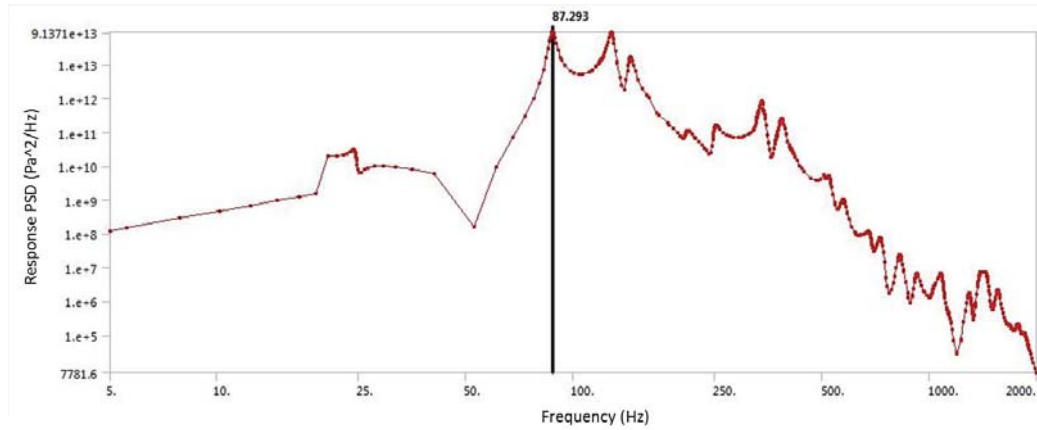
b)
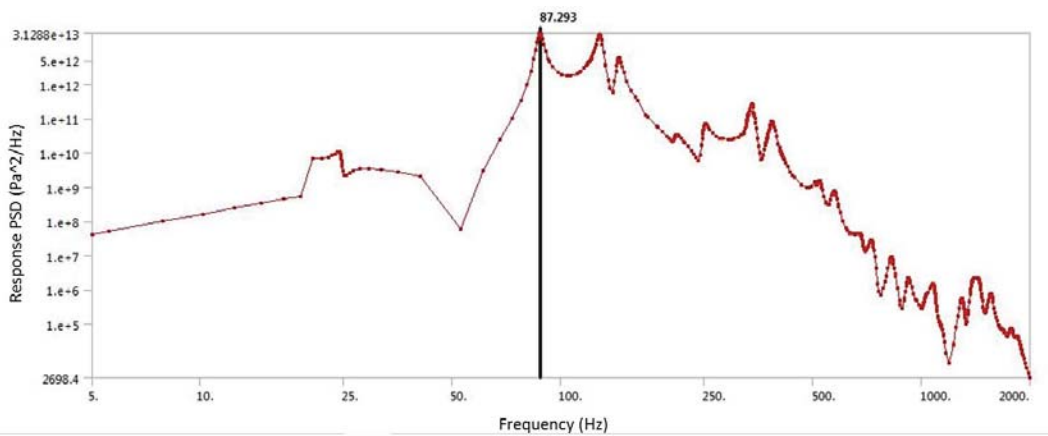
c)

Figure 3-31: Response PSD curves in the direction of X, Y, and Z-axes as a result of loading applied on the Z-axis

As a result of the analyses, the frequencies where the highest normal stresses occur are obtained. When these frequencies are compared with the modal analysis results, it is observed that the frequencies are correlated to the natural frequencies of the control column. These frequencies and corresponding natural frequencies and mode shapes are tabulated in Table 3-6. The table shows that modes with oscillations in the direction of X and Y-axes have high energy and cause damage to the control column structure. For this reason, the natural frequencies at these mode shapes are taken into consideration in further studies.

Table 3-6: Frequencies where the highest normal stresses occur

		The frequency at highest responses (Hz)	Corresponding Natural Frequency (Hz)	Mode Shape
Analysis performed in Y-axis	Normal Stress X-axis	119.7	120	Oscillation of the control column in the direction of Y-axis
	Normal Stress Y-axis	129.1	128.2	Oscillation of the control column in the direction of the X-Y plane
	Normal Stress Z-axis	120.3	120	Oscillation of the control column in the direction of Y-axis
Analysis performed in Z-axis	Normal Stress X-axis	128.1	128.2	Oscillation of the control column in the direction of the X-Y plane
	Normal Stress Y-axis	87.3	87.3	Oscillation of the control column in the direction of X-axis
	Normal Stress Z-axis	87.3	87.3	Oscillation of the control column in the direction of X-axis

3.2.11 Comparison of the Results of Analysis and Vibration Test

The gun control column was failed during the vibration test with a crack formation near to the base. In this section, the simulation of the vibration tests performed on the shaker of the control column was carried out with FEA. As seen in the vibration test, also in the FEA, the base of the control column was found to be damaged under the tracked vehicle vibration loads. Thus, the FEA model of the control column is verified by the vibration test performed on the shaker. As the results of the analysis, the damaged part is obtained, and the vibration test is shown in Figure 3-32.

a)   b)

Figure 3-32: The damaged part: a) Test result; b) FEA result

In order to solve this problem, an absorber structure is added to the design of the control column to isolate the vibration. In the next section, the FEA of the control column to which the isolator added is performed, and the effect of the design change on the fatigue strength of the control column is analyzed.

3.3 The FEA of the Control Column with Isolator

In the previous section, it was revealed that the body of the control column was failed under tracked vehicle random vibration in both the analysis and the test. It was understood that the column body has not enough fatigue strength against the tracked vehicle random vibration. In order to increase the fatigue life of the control column, the isolator is added to the base of the control column body. In this section, the effect of the isolator on the fatigue strength of the control column is examined by the finite element methods.

3.3.1 The Analysis Model

The FEM of the gun control unit built in the previous section is updated with adding the isolator to the geometry. In order to mount the isolator in the control column, some of the components are redesigned, whereas some of them are removed from the assembly. As it can be observed from Figure 3-33, the component referred to as "the spacer" is removed from its location. Instead of the spacer, the isolator is added to this place. Besides, minor design changes are made on the base geometry. The base geometries are shown in Figure 3-34. The other components are defined as described in the previous model. The updated analysis geometry is represented in Figure 3-35.
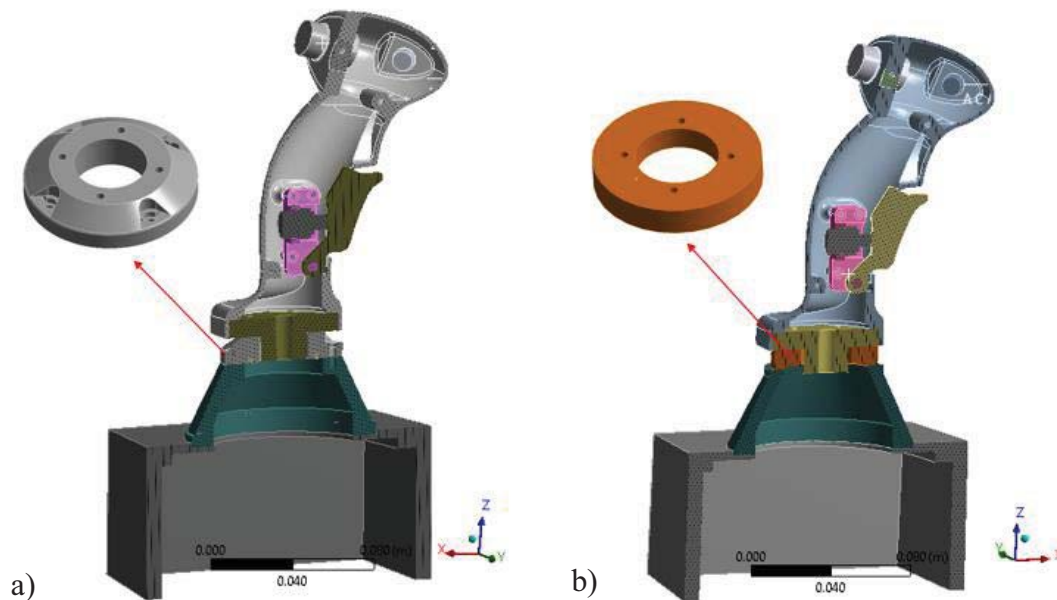
Figure 3-33: The section view of the control column: a) Model with isolator; b) initial model (without isolator)
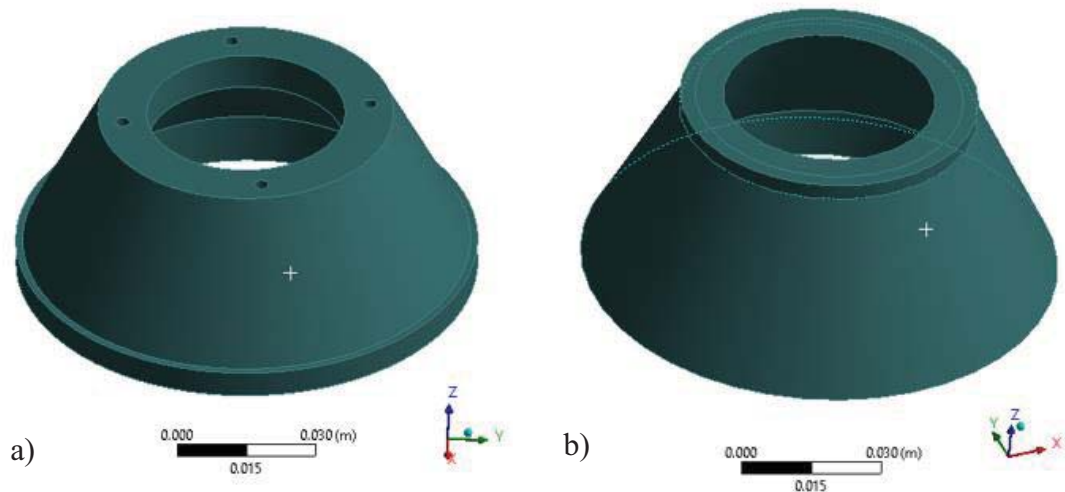
Figure 3-34: The base geometry: a) model with isolator; b) old model
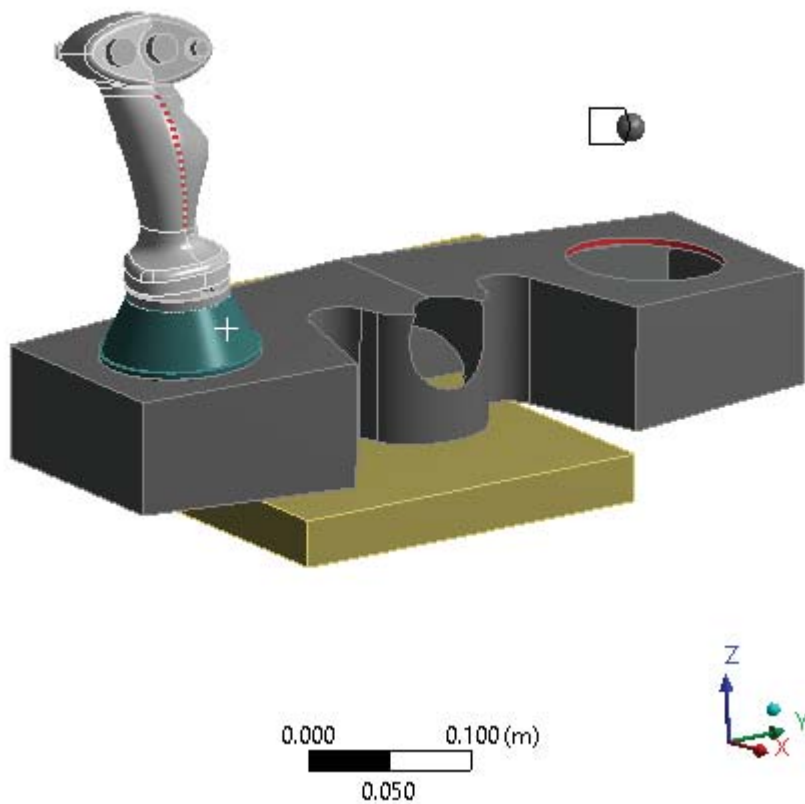
Figure 3-35: The updated analysis geometry

3.3.2   Boundary Conditions and Connections

All contacts and boundary conditions are defined as described in the previous model except for the isolator connections. As described in Chapter 2, the isolator is attached to

its adjacent components with eight different bolts. In the analysis model, the bolts are modeled with beam elements. The connection of the isolator is shown in Figure 3-36.

a)

b)

c)

d)
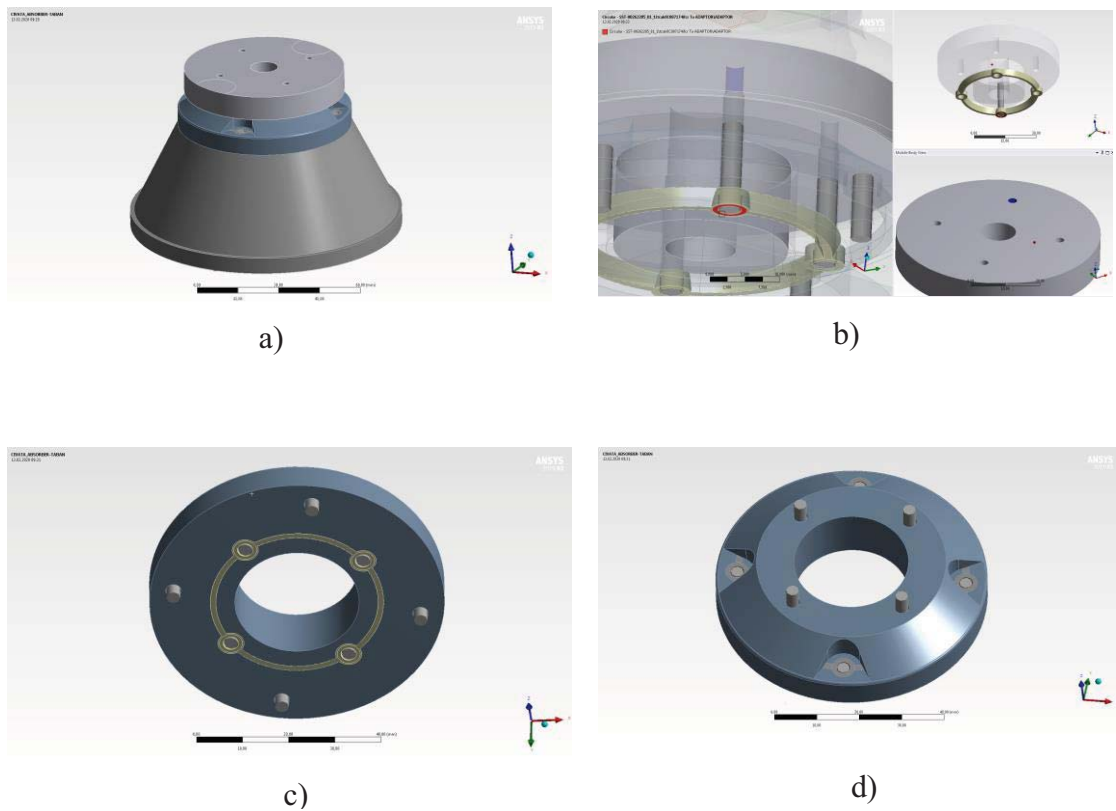
Figure 3-36: The connection of the isolator: a) The assembly view; b) connection faces; c) bottom view; d) top view

3.3.3 Analysis of Setting and Load Conditions

The analyses performed in the previous study are repeated for the model with the isolator under the same loading conditions and analysis settings.

3.3.4 Materials

As mentioned in Chapter 2, the isolator is made of neoprene elastomer. In the analysis model, it is assumed that neoprene exhibits linear behavior. Non-linear elastic property like the hyperelasticity is not defined since it is not subjected to large strains. The elasticity modulus of neoprene is determined from the correlation of its durometer hardness found by A.N Rent [19]. Besides, Aluminum inserts are embedded in the neoprene isolator in order to attach the isolator to its adjacent parts rigidly. The material properties of the isolator structure are shown in Table 3-7.

Table 3-7: Material Properties of the Isolator

Components	Materials	ρ (kg/m^3)	E (GPa)	ν	σ_y (MPa)	σ_u (MPa)
Isolator	Neoprene 60 Shore A	1240	0.00206	0.48	12-24	-
Top and Bottom Inserts	Sheet Aluminum 6061 T6/ T651	2700	68	0.33	240	319

3.3.5   Analysis Results

3.3.5.1 Modal Analysis

One hundred fifty modes of the structure in the frequency range of 0-1090 Hz are extracted in the modal analysis. The mass participation ratios in all directions are listed in Table 3-8. The first three natural frequencies and corresponding mode shapes are represented in Table 3-9.
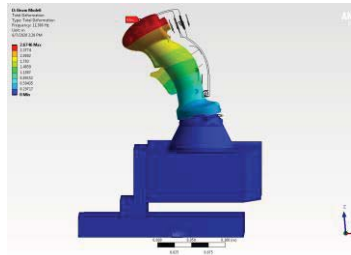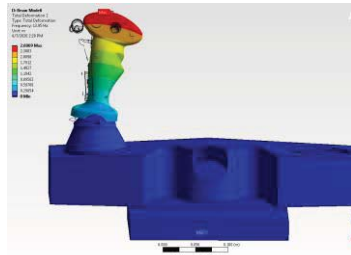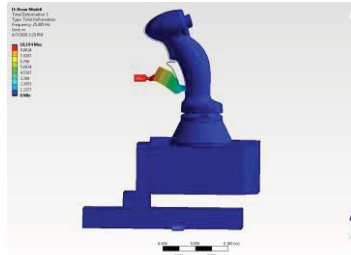
Theoretically, it is known that the modal analysis should be captured at least 80% of mass participation or 1.5 times of frequencies of interest in order to get accurate results in random vibration analysis [9]. The number of modes extracted in the analysis contributes to the cumulative effective mass participation factor of 78% of the system in the direction of the three-axis. Besides, the frequency content of the extracted modes is less than the frequency range of interest. The frequency range and cumulative mass participation ratio obtained in the analysis is not sufficient to meet the requirements. However, since the resonance frequencies causing fatigue damage to the control column were extracted in the modal analysis and energy of the higher resonance frequencies on the damaged body is ignorable, this requirement was neglected, and the analysis results are accepted as valid.

Table 3-8: The Modal Mass Participation Ratio

	X-Axis	Y-Axis	Z-Axis	RotX-Axis	RotY-Axis	RotZ-Axis

Mass Participation Ratio	0.78	0.78	0.78	0.96	0.99	0.84

Table 3-9: Natural Frequencies and Mode Shapes

Number of Modes	Natural Frequency (Hz)	Mode Shape Definition	Mode Shapes
1	11.4	Oscillation of the control column in the direction of X-axis (longitudinal)	
2	14.0	Oscillation of the control column in the direction of Y-axis (transverse)	
3*	25.9	Mode of the trigger spring	

*: The third mode occurred at 25.9 Hz comes from the trigger spring constant (1500 N/m), and it is the local mode of the trigger and does not depend on the dynamic of the control column.

3.3.5.2 Random Vibration and Fatigue Results

After the modal analysis, the random vibration analysis is performed. Random vibration analysis is followed by fatigue analysis. As a result of the FEAs, the fatigue damage ratio that occurs in the control column body can be obtained. According to the cumulative damage ratio, it can be evaluated whether the control column's body will be damaged.

The fatigue damage ratio on the column body under loads of the random vibration applied in the three-axis is represented in Table 3-10. As can be seen in the results, the damage ratios for the column body are less than 1. This means that the control column with the isolator can maintain the structural integrity after vibration exposure, which is defined in the military test standard.

Table 3-10: The cumulative damage ratio on the control column

Analysis	X-Axis	Y-Axis	Z-Axis
Maximum Damage Ratio	2.03e-19	3.46e-9	3.66e-10

3.4 Comparisons of Analysis Results with and without the Isolator

The comparisons of the first three natural frequencies obtained in the modal analyses are presented in Table 3-11. The comparisons show that the natural frequency values corresponding to mode shapes of the control column in the model with isolator are less than the model without the isolator. In the model with the isolator, the aluminum spacer is removed from the model. Instead of the spacer, the neoprene isolator is added to the model since neoprene material has less stiffness than aluminum material, natural frequencies of the control column decrease in the modal analysis.

Table 3-11: Comparison of the first five natural frequencies of the model without isolator and with isolator

Mode Shape Definition	Natural Frequency (Hz)	
	Without Isolator	With Isolator
Trigger Spring Mode	24.5	25.9

Oscillation in X-Axis	87.3	11.4
Oscillation in Y-Axis	120	14.0

The comparison of the cumulative damage ratios obtained by the fatigue analysis is presented in Table 3-12. According to the results, it was evaluated that crack formation occurs in the control column body without isolator, whereas no damage will happen in the control column with the isolator. The results show that the isolator can prevent fatigue damage by reduced the vibration transmitted to the control column body.

Table 3-12: Comparison of the damage ratios of the model with and without isolator

Loading Direction	X-Axis	Y-Axis	Z-Axis
Damage ratio of the model without isolator	1.89E+02	1.18E+06	2.66E+15
Damage ratio of the model with isolator	2.03e-19	3.46e-9	3.66e-10

3.5 Conclusion

This chapter consists of two different finite element analyses. In the first part of this chapter, the gun control unit is modeled by FEM. The control column body is failed in the accelerated tracked vehicle vibration test according to Figure B-2 ("Material in turret bustle rack or installed in turret") test procedure presented in the AECTP 400 Environmental Mechanical Test Standard. Then, the control column is analyzed under tracked vehicle random vibration. In this way, the vibration test is simulated by using FEM. As a result of the analysis, it is evaluated that the control column body is damaged under the tracked vehicle vibration, as it can be observed in the accelerated vibration test. Thus, it can be deduced that the analysis results are consistent with the test results.

In the second part of this chapter, the finite element analysis geometry is updated with the control column with the isolator to prevent damage. Then, the analyses are performed again to calculate the fatigue strength of the control column with the isolator. The fatigue analysis results show that the control column with the isolator is not damaged. Thus, it is

determined that the isolator absorbs vibration and prevents failure in the control column body. The FEA results indicate that the problem can be solved by using the isolator.

In the next chapter, the vibration tests are performed by using the shaker table. The accelerated tracked vehicle vibration and sine sweep vibration are applied to the gun control unit with the isolator.

4. VIBRATION TESTS

4.1 Introduction

Vibration tests are applied to the gun control unit with the electrodynamic shaker. The tests are performed on the vibration test system that is in the Environmental Test Laboratory at the facility of Aselsan A.Ş. In the scope of this chapter, two main concepts of the vibration test are applied: accelerated random vibration and sine sweep.

In the random vibration test, the tracked vehicle vibration environment is simulated in the laboratory, and the weapon gun control unit with the isolator is exposed to tracked vehicle vibration. The test procedure defined in the standard of the AECTP 400 Mechanical Environment Test Standart for tracked vehicles [16] is implemented. As a result of the test, it can be deduced whether the control column withstands the tracked vehicle vibration during its service life or not.

In the second part of this chapter, the gun control unit is subjected to the sine sweep test with the electrodynamic shaker. In the sine sweep test, the shaker excites the DUT (device under test, also called the "gun control unit") at a constant amplitude within a certain frequency range. The frequency of sinusoidal excitation increases from a low frequency to a higher frequency at a constant logarithmic rate. During the test, the time-acceleration data is collected from accelerometers located on the shaker table and the structure. By using the Fast Fourier Transform (FFT)[20] algorithm, time-domain data is transformed into the frequency domain. The data of the acceleration versus frequency is used for identifying the natural resonances of structure.

In the FEA, in Chapter 3, the second resonance frequency was found to be 14.0 Hz, and at this frequency, the control column oscillated in Y-axis. In this Chapter, this natural resonance of the control column is obtained by the sine sweep test. Finally, the natural frequency obtained in the analysis is compared with that obtained by the test to evaluate whether the FEM is valid or not.

4.2 Test and Equipment

The vibration test system consists of an electrodynamic shaker, accelerometers, a controller, and a power amplifier [21].

An electrodynamic shaker converts the electrical energy to mechanical vibrations. It works on the principle of electromagnetism, as described by Maxwell and Fleming.

- A power amplifier multiplies the output of the controller by a fixed gain and feeds it to the electrodynamic shaker.

- A controller with a computer allows the user to enter the test parameters and generates a signal in real-time. In the closed-loop system, the controller updates continuously according to data from the accelerometer on the shaker table and changes the output drive signal to meet the test profile.

- An accelerometer is used to measure and to control applied vibration by sending feedback to the controller.

The test equipment used in the test is listed in Table 4-1. 3 accelerometers are used in the test. They are used to control the signal and measure the vibration level at their location. The schematic of the vibration test is shown in Figure 4-1.

Table 4-1: Test equipment

Equipment	Manufacturer	Model
Electrodynamic shaker	LDS	V895
Control Accelerometer	PCB	353B03
Output Accelerometer 1	PCB	353B03
Output Accelerometer 2	PCB	353B03
Controller	LDS	-
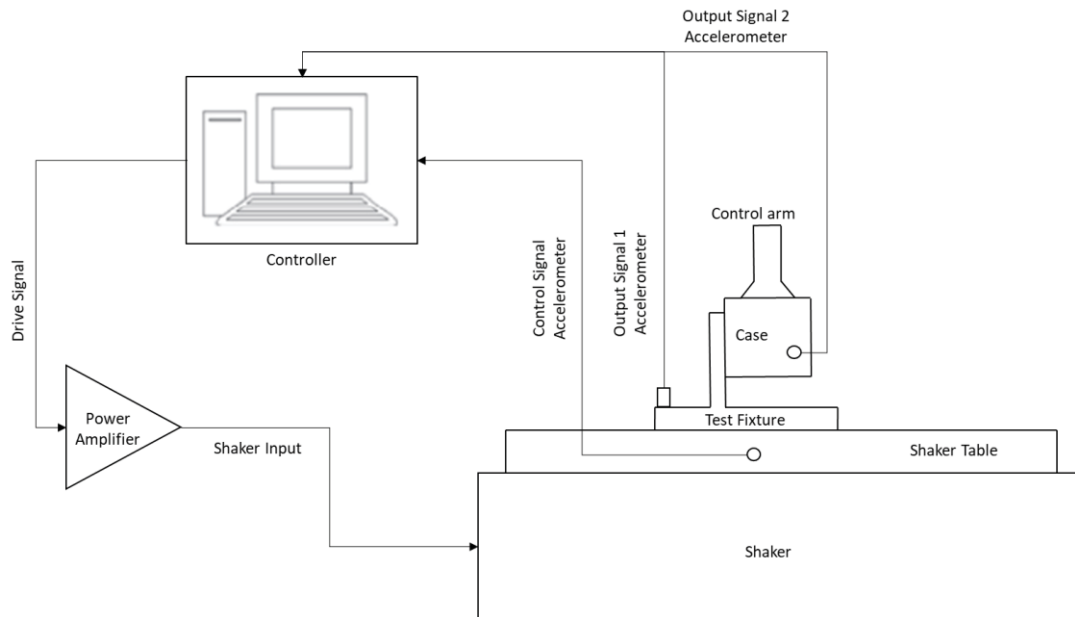
Figure 4-1: Schematic of the vibration test

4.3 DUT (Device Under Test)

The components of DUT are:

- Test fixture,

- Gun control unit (also include moving control column)

The visual of DUT is shown in Figure 4-2. The test fixture is used to hold the DUT and provides proper mounting to the shaker table. The text fixture is attached to the shaker table with nine different bolts.
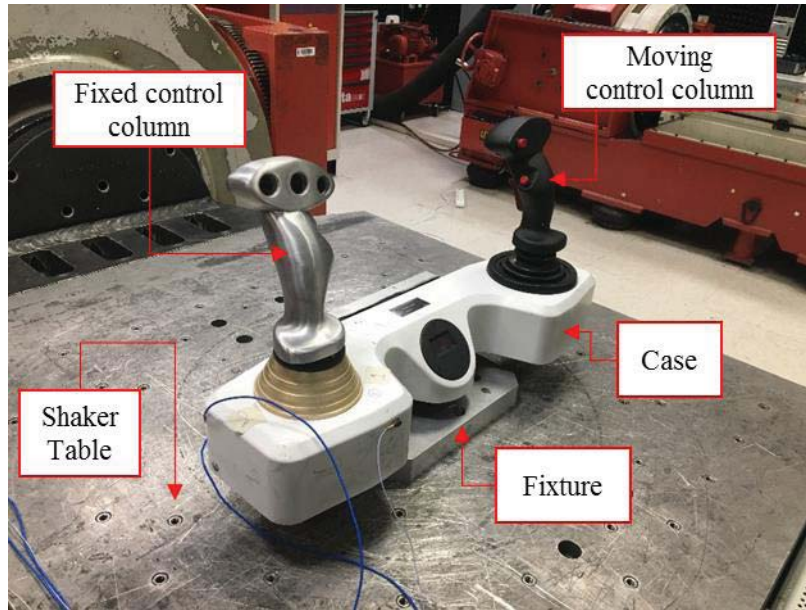
Figure 4-2: Test Sample

4.4 Random Vibration Test

Random vibration testing usually is used to evaluate the durability of a product and to check whether the product works under the conditions that it may be exposed to vibration during its lifecycle. It is hard to define the vibration environment that simulates the real-world scenario in the laboratory since vibration in life scenarios are not repetitive and predictable. However, the vibration environment for the specified product can be defined as the power content at any frequency. This is called the Power Spectral Density (PSD) plot. The PSD indicates the signal's power content as a function of frequency [22]. The PSD does not give any direct information concerning time-acceleration history. The PSD is a statistical measurement of the motion experienced at the control point on the test sample. It defines the average acceleration of the random signal at any frequency [23]. All frequencies are excited at the same time, just as in the real world. Random vibration testing is an easy and effective way to simulate a real vibration environment.

In our random vibration test, the tracked vehicle vibration environment is simulated in the laboratory. The test procedure defined in the standard of the AECTP 400 Mechanical Environment Test [16] is implemented in our test. The gun control unit is tested separately in three-axes direction via the specified duration of the PSD profile that is illustrated in

the section named "Materiel in turret bustle rack or installed in turret" of the standard of AECTP 400 Mechanical Environment Test.

The PSD plot consists of a combination of a random broadband signal and the random narrowband signal created by the interaction of the track with the ground surfaces, road wheels, and sprockets. The test profile is shown in Figure 4-3.

Figure B-2 Tracked Vehicle Schedule Breakpoints							
Wideband Random Spectrum				Harmonic Swept Narrowbands			
Frequency, Hz	Axis, ASD Amplitude G^2/Hz			Narrowband	f_1	f_2	f_3
	V	T	L	Bandwidth, Hz	5	10	15
5	0.001	0.001	0.001	Swept BW, Hz	20 - 170	40 - 340	60 - 510
20	0.015	0.010	0.010	# Sweeps	2	2	2
510	0.015	0.010	0.010				
2000	0.001	0.001	0.001	Axis	ASD Amplitude, G^2/Hz		
				Vertical	0.30	0.20	0.10
Wideband Grms	3.56	3.03	3.03	Transverse	0.15	0.10	0.05
Total Grms	4.20	3.42	3.42	Longitudinal	0.15	0.10	0.05

Figure 4-3: Figure B-2 "Materiel in turret bustle rack or installed in turret" Test Profile

The vibration tests are carried out separately on three-axes, such as vertical, transverse, and longitudinal, indicated as X, Y, Z axis, respectively. The test setup in longitudinal, transverse, and vertical axes of direction are shown in Figure 4-4, Figure 4-5, and Figure 4-6, respectively.
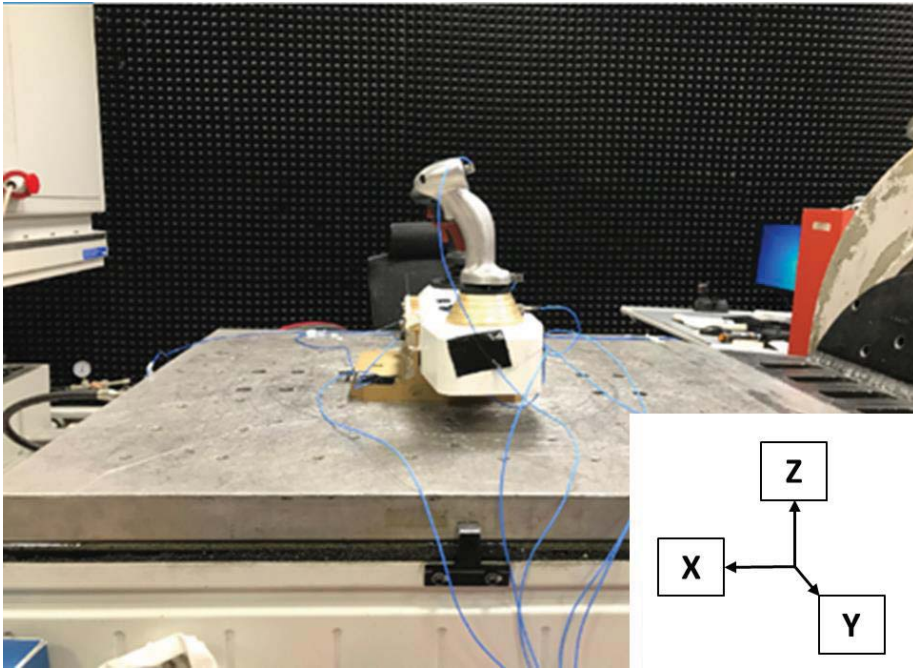
Figure 4-4: Test setup in the longitudinal axis (X-axis)
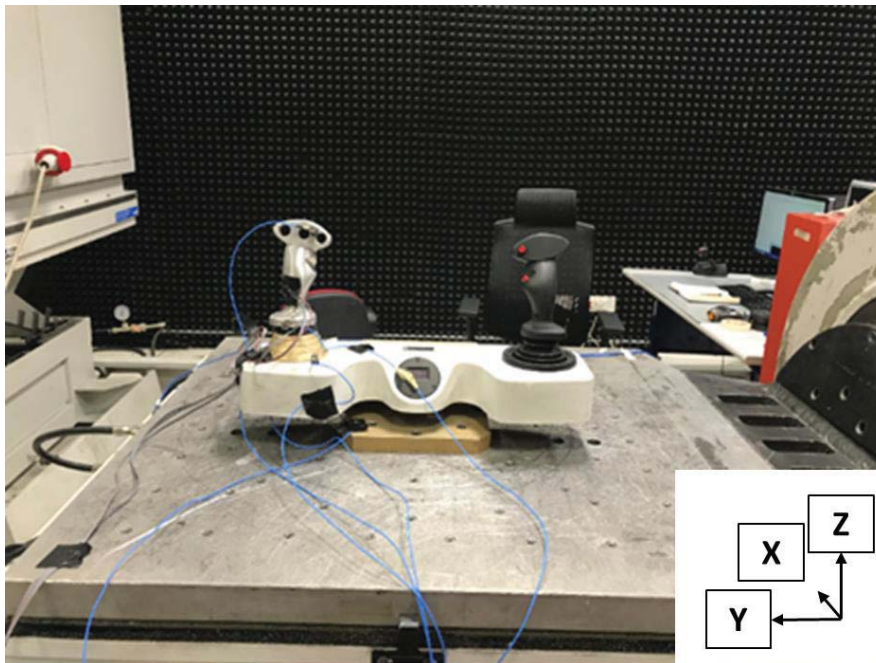
Figure 4-5: Test setup in the transverse axis (Y-axis)
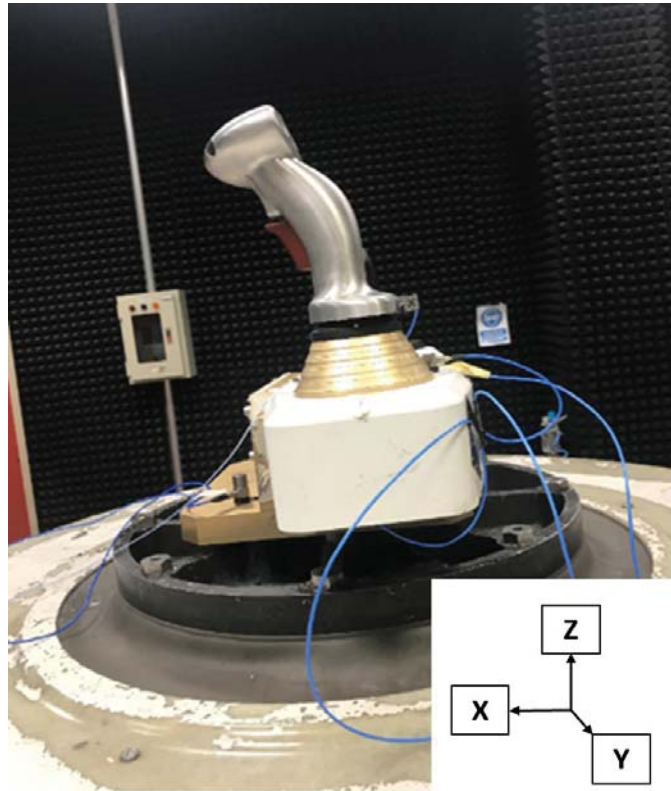
Figure 4-6: Test setup in the vertical axis (Z-axis)

4.4.1 Results of the Random Vibration Test

Firstly, the control column is exposed to random vibration in a vertical direction for 4 hours. The desired PSD profile and the output PSD profile are shown in Figure 4-7. The applied PSD profile referred to "control(f)" in Figure 4-7 is calculated with acceleration data from the control accelerometer [24]. In addition, "input2(f)" indicates the PSD of the second accelerometer data, which is located in the text fixture. "input3(f)" shows the PSD of the other accelerometer that is mounted on the control unit console. Besides, the "high-abort" and the "low-abort" lines indicate the test tolerances, which are restricted + 3 Db times of "profile(f)" from above and -3 DB times of profile from below. The graph shows that the desired PSD is applied within the specified tolerance limits. During the random vibration test in the vertical direction, no visible changes were observed.
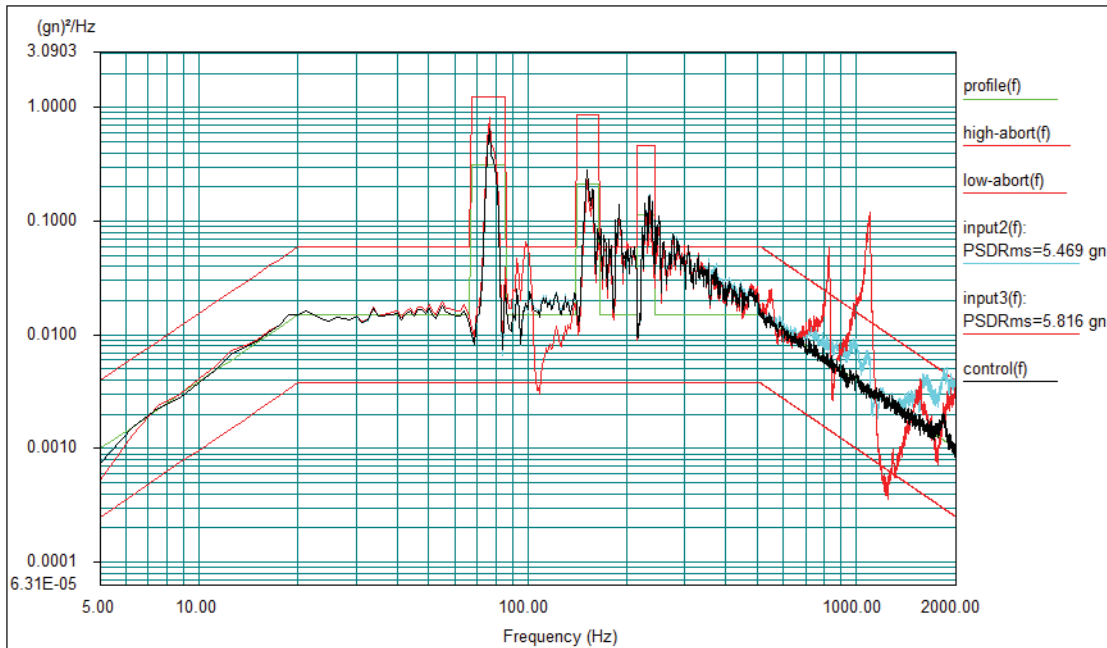
Figure 4-7: AECTP 400 Ed.3 Figure B-2 test profile in the vertical axis and output PSDs

After completing the test at the vertical axis, the gun control unit is removed from the head expander, and it is mounted in the slip table in order to perform tests in the transverse axis. The PSD input and outputs in the test of the transverse axis are presented in Figure 4-8. Neither damage nor the plastic deformation on the DUT is not observed throughout the test in the transverse axis.
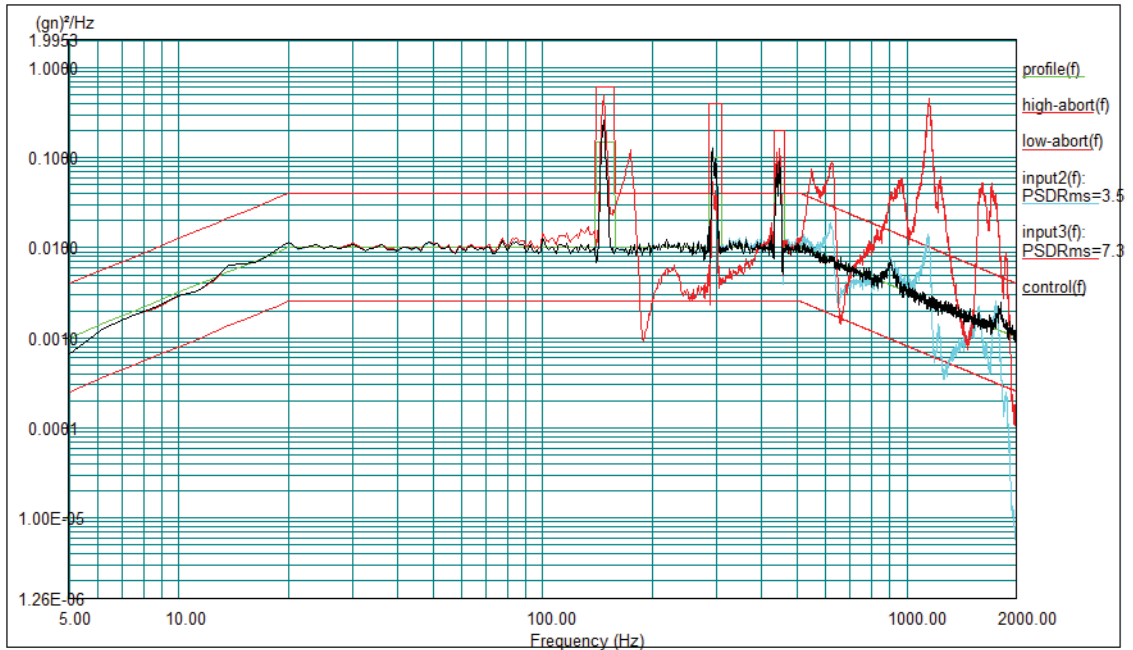
Figure 4-8: AECTP 400 Ed.3 Figure B-2 test profile in the transverse axis and output
PSDs

Finally, the test in the longitudinal axis is carried out on the slip table like the test in the transverse axis. PSD Curves in the test are shown in Figure 4-9. Just like the result of other axes, no visible deformation or crack is not detected during the test in the longitudinal axis.
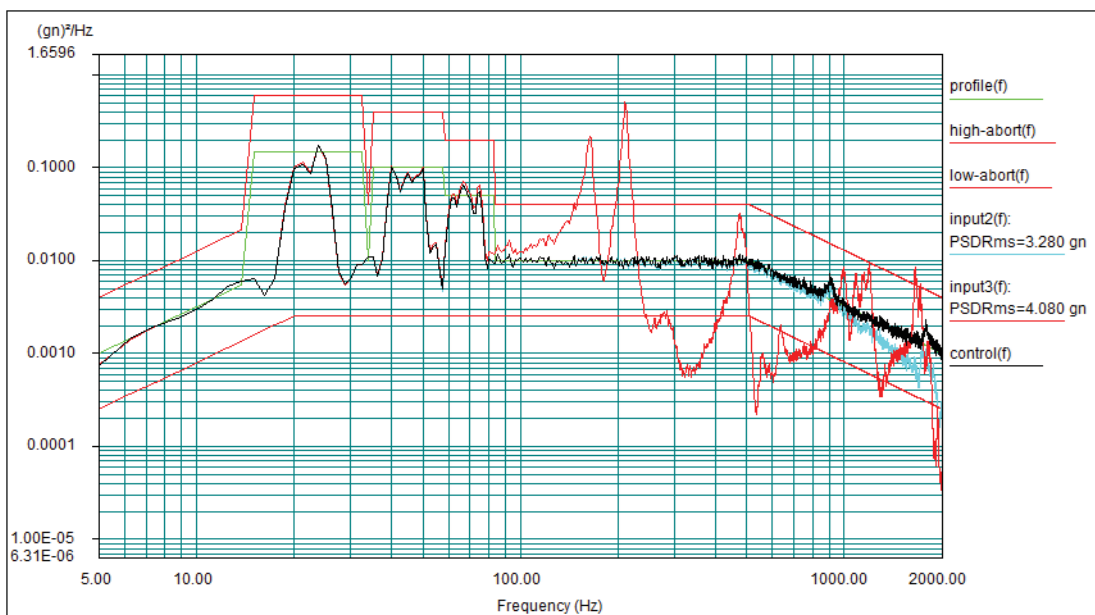
Figure 4-9: AECTP 400 Ed.3 Figure B-2 test profile in the longitudinal axis and output
PSDs

4.5 Sine Sweep test

The sine sweep test setup resembles the random vibration test setup except for accelerometers. In this setup, other output accelerometers in the random vibration test setup are removed, and output accelerometer PCB 356B21 (shown as the blue line in Figure 4-11) is added in order to observe the second natural frequency of the control column. The accelerometer is placed on the top of the surface of the control column body, as the upper part of the control column vibrates in the second mode of the control column. The schematic of the test setup is shown in Figure 4-10.
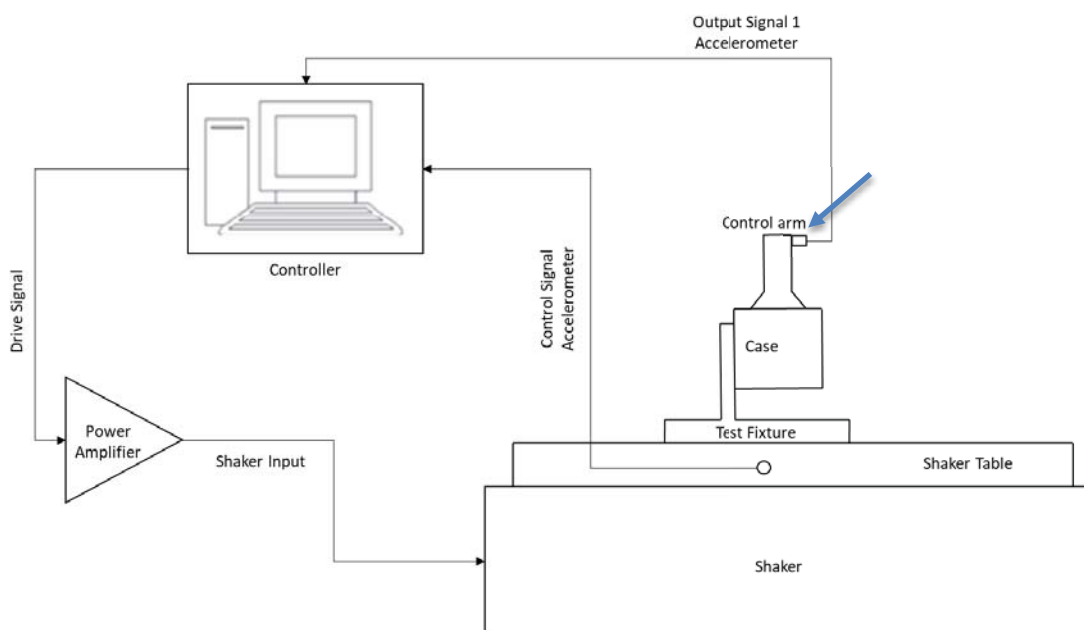
Figure 4-10: Schematic of Sine Sweep Test Setup

The sine sweep test is carried out only in the direction of the Y-axis. During the test, the frequency changes from 5 Hz to 2000 Hz at a sweep rate of 1 octave/minute. The sinusoidal vibration amplitude is set to be 1 g at each frequency. Sweep is applied only once through the test time.

The test setup is presented in Figure 4-11. The test profile is applied, which is shown in Figure 4-12. Moreover, the acceleration-time data in the Y-axis measured by the accelerometer placed on the upper part of the control column body are shown in Figure 4-13.
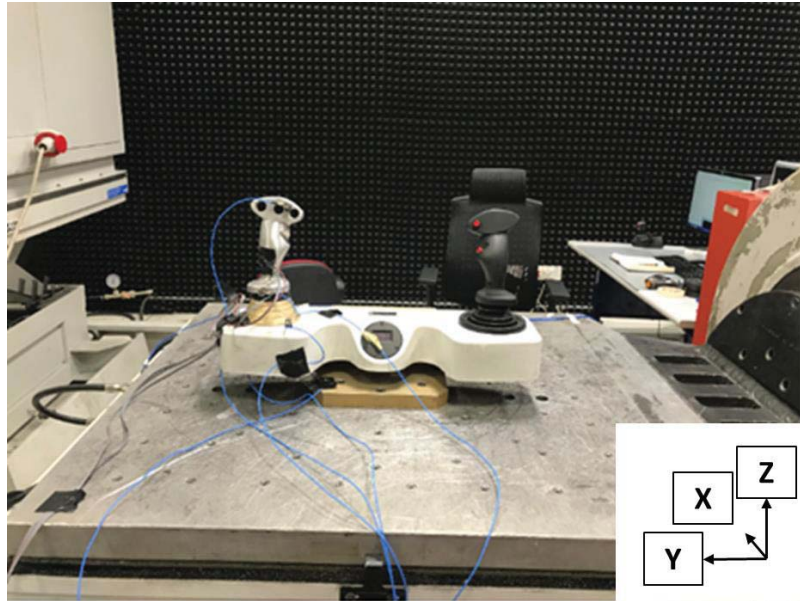
Figure 4-11: Sine Sweep Vibration Test Setup
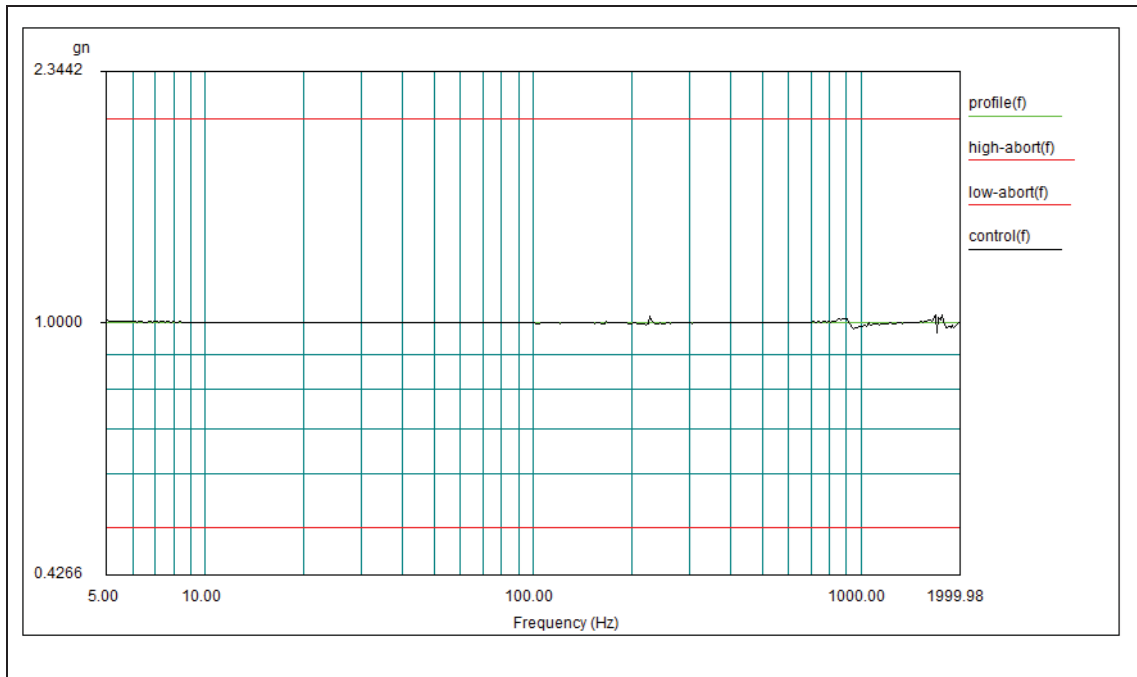
Figure 4-12: Test Profile in Y-axis
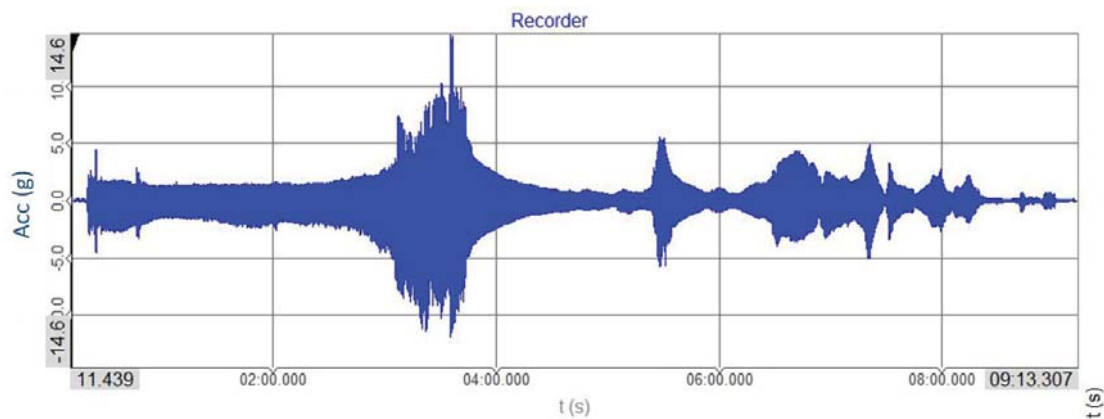
Figure 4-13: Acceleration – Time Data

The prediction of the resonance frequency of the control column is not easy in general since the real-time data does not give direct information about the frequency of the signal. In this test, the frequency analysis of the acquired data is carried out by transforming the signal from the time domain into the frequency domain with the help of FFT. The acquired signal is decomposed in the series of sinus waves, and the frequencies of each of these waves have different amplitudes.

The frequency analysis is performed by DEWEsoft software [25]. In order to obtain useful results, the settings of the FFT analysis are:

- Line resolution is directly proportional to frequency resolution. It depends on the sample rate of the data and the chosen number of FFT lines. In our case, data is picked at a rate of 20000 samples/sec, and the number of FFT lines is set to be 8192. The line resolution is calculated by dividing half of the sample rate by the number of FFT lines. In our analysis, the resolution is equal to 1.22 Hz.

- The windowing is used to mitigate the leakage effect [26] and to improve the FFT results. In our analysis, the "Hanning" window is used since it offers good frequency resolution [27].

- DC cut-off filter removes the DC or low- frequency content of the signal. In our case, the cut-off filter frequency is set to be 5 Hz.

FFT of the signal is shown in Figure 4-14. It shows that the control column oscillates in Y-axis at approximately 43 Hz. Since the response of the control column reaches its

maximum amplitude, it can be understood that the control column has the natural resonance at this frequency.
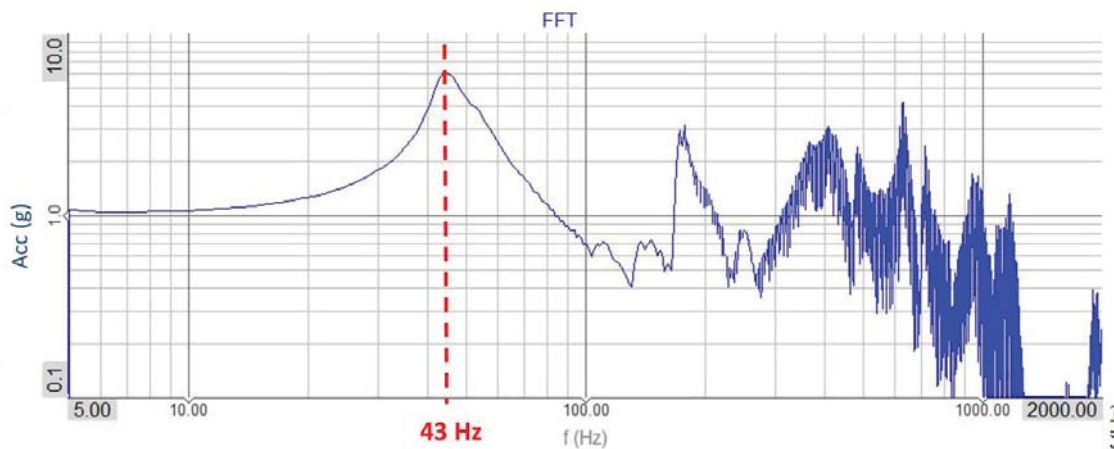
Figure 4-14: FFT graph, Y-axis, the accelerometer at the upper part of the control column

4.6 Conclusion

In order to decrease the vibration level transmitted to the control column, the isolator was added to the base of the column in Chapter 2. In this chapter, the vibration test is repeated for the gun control unit with the isolator in order to check the maintenance of the structural integrity of the control column under the tracked vehicle vibration.

The test procedure, which is illustrated in the section "Materiel in turret bustle rack or installed in turret" in AECTP 400 Mechanical Environment Test Standard, is applied during the tests. As a result of tests carried out in every three axes, it is concluded that there is no physical change in the control column. The gun control unit with the isolator is verified to be suitable for use in tracked vehicles according to the mechanical environment test standard. It can be deduced from the test results that the control column with the isolator can withstand vibration throughout its service life in the tracked vehicle environment.

In the second part of this chapter, the control column is subjected to the sine sweep test on the shaker. As a result of the test, it is observed that the control column has a natural resonance at 43 Hz. The control column vibrates in the direction of the Y-axis at this frequency. However, as described in Chapter 3, the natural frequency for the same mode

shape is calculated to be 14.0 Hz with the FEA. The difference between the results of the test and the FEA points out that the FEM is not reliable, and it needs to be improved.

In the next chapter, dynamical parameters such as natural frequencies, corresponding mode shapes, and damping ratios of the control column are obtained by experimental modal analysis methods. Thus, the dynamical behavior of the control column is identified in detail.

5. EXPERIMENTAL MODAL ANALYSIS

5.1 Introduction

In Chapter 4, the sine sweep vibration was applied to the structure via an electrodynamic shaker, as a result of the test, one of the resonance frequency of the control column whose oscillation mode in the direction of the Y-axis was determined. The natural frequency of the control column at this mode was found to be 43 Hz. The natural frequency at this mode had appeared at 14.0 Hz in the FEA of the gun control unit. The comparison shows there is a great difference between FEM and vibration test results. Therefore, experimental modal analyzes are carried out to investigate the control column dynamics in detail.

In this chapter, the dynamical behavior of the gun control unit is analyzed with the impact hammer testing method, which is one of the experimental modal analysis techniques. In the experiment, accelerometers are put on specific points on the gun control unit, and a force is applied to the control column from certain points. A data acquisition device acquires accelerations occurring on the gun control unit in response to the applied force. Data is processed in the frequency domain to obtain frequency response functions (FRF). In this way, it is determined how much reaction occurred at which point of the structure. As a result, the modal parameters such as natural frequencies, mode shapes, and damping parameters of the gun control unit are obtained by processing the FRF Sets [28, 29].

The tests are performed in two different configurations. In the first configuration, the connection bolts of the isolator are tightened with a suitable torque as in the actual configuration, and in the second configuration, the torque on the bolts is removed. Two separate impact tests were carried out for both configurations. In one of its tests, the structure was driven in the X-axis direction to precisely find the oscillation mode in the X-axis direction. In the second test, the structure was driven in the Y-axis direction to determine the oscillation mode in the direction of the Y-axis. The performed tests are listed in Table 5-1

Table 5-1: Modal Tests

Configurations	Impact Hammer Test

First Configuration: Tightened Bolt	Test 1: Driving Point 5, the direction of +X
	Test 2: Driving Point 6, the direction of +Y
Second Configuration: Loosened Bolt	Test 1: Driving Point 5, the direction of +X
	Test 2: Driving Point 6, the direction of +Y

As a result of the experimental modal analyses, dynamical parameters of the gun control unit can be obtained, and the effect of the tightening torque on the dynamics of the structure can be understood.

5.2 Test Equipment

The required equipment for a modal impact testing is listed in Table 5-2.

Table 5-2: Modal Impact Test Equipment

Equipment	Manufacturer	Type
DAQ Device	SIEMENS LMS	SCADAS
Accelerometer	PCB	356A16
Impact Hammer	PCB	086C04
Cable	PCB	034G10

The equipment is clarified briefly below.

- A data acquisition device (DAQ) is utilized to measure physical phenomena. The device incorporates the signal conditioner and the analog to digital converter (A/D). The signal conditioner process the signal from the sensor and send it to the A/D subsystem. The signal is converted into the digital domain by the A/D subsystem.

- The computer with the DAQ Software is used for signal logging and analysis. The signal processing is carried out by the Siemens Simcenter Testlab Software.

- Accelerometers convert the physical motion (vibration) into a measurable electrical signal. Accelerometers chosen for this test have the ability of measurement in three-axes.

- The cables provide signal and power transfer between the accelerometer and the DAQ device.

- The impact hammer incorporates a force transducer which is located at its tip to measure the force. Impact hammer is used with different types of material tips such as metal, plastic, rubber. The stiffness of the tip of the hammer determines the excitation bandwidth of the force input. Hard plastic or metal tips tend to excite a wider frequency range, whereas the soft tips like a rubber excite a lower frequency range [30]. The impact hammer is shown in Figure 5-1.

Figure 5-1: Impact Hammer

5.3 Test Setup

The gun control unit and its components are described in Chapter 4. Unlike the test object used in the sine sweep test, switches on the control column are mounted on the test object. The test object is shown in Figure 5-2.

Figure 5-2: Test Object

Tests are performed on the rigid test table. The test object is rigidly attached to the test table by the test fixture. The assembly is shown in Figure 5-3. The accelerometers measure the acceleration along three orthogonal axes such as X, Y, and Z. 11 accelerometers are used to mesh the structure in total. The location of the accelerometers is shown in Figure 5-4. The accelerometer is mounted with the hot glue adhesive.
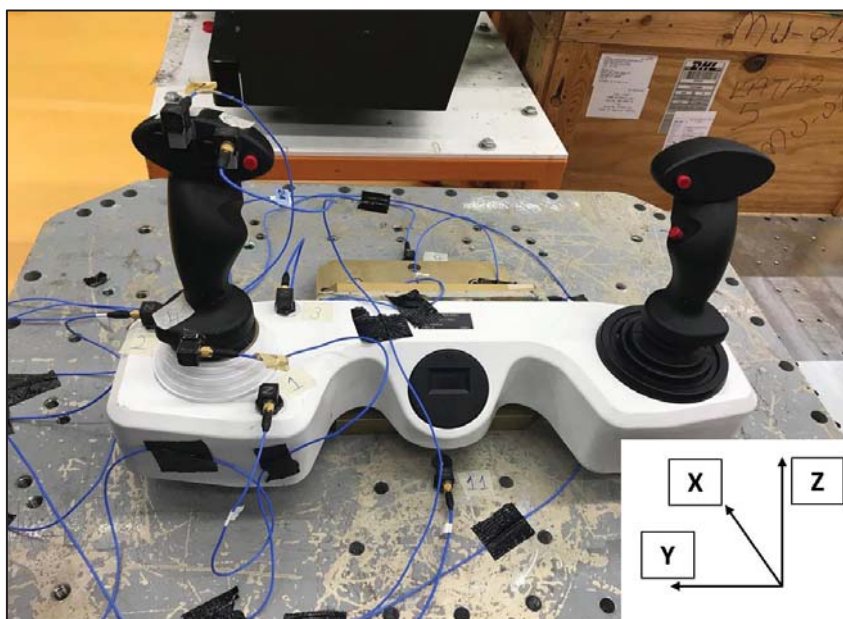
Figure 5-3: The test assembly

Figure 5-4: Accelerometers setup

The test is conducted by LMS Impact Testing Software and Siemens SCADAS DAQ. The location and the direction of accelerometers are defined on the software in order to build the modal analysis geometry. The geometry is used to show mode shapes of the structure. The geometry is shown in Figure 5-5.
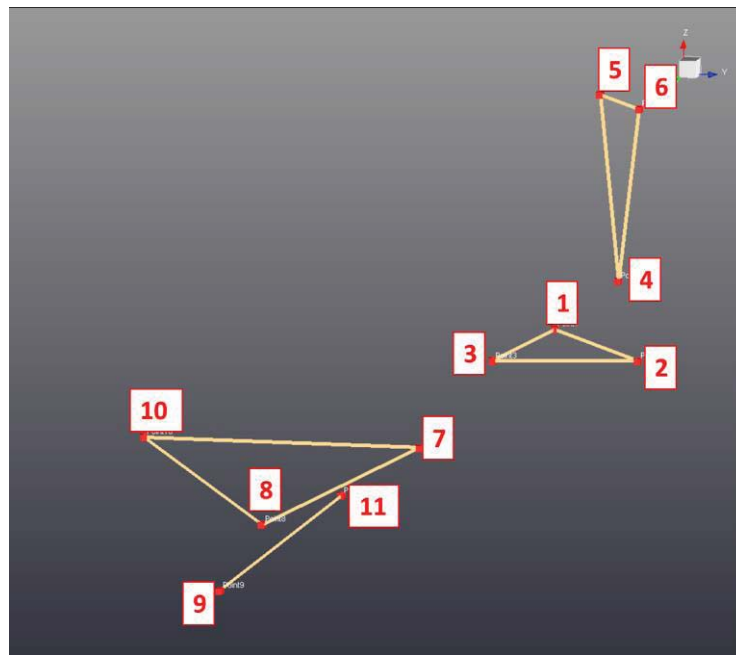
Figure 5-5: Experimental Modal Analysis Geometry

5.4 Impact Hammer Test

Two different driving point is used in the test in order to obtain the natural frequencies of the control column. In the first run, the control column is excited from the face near accelerometer 5 in the direction of +X. In the second run, the control column is excited

from the surface near accelerometer 6 in the direction of +Y. The driving points are shown in Figure 5-6.

<div align="center">a)   b)</div>
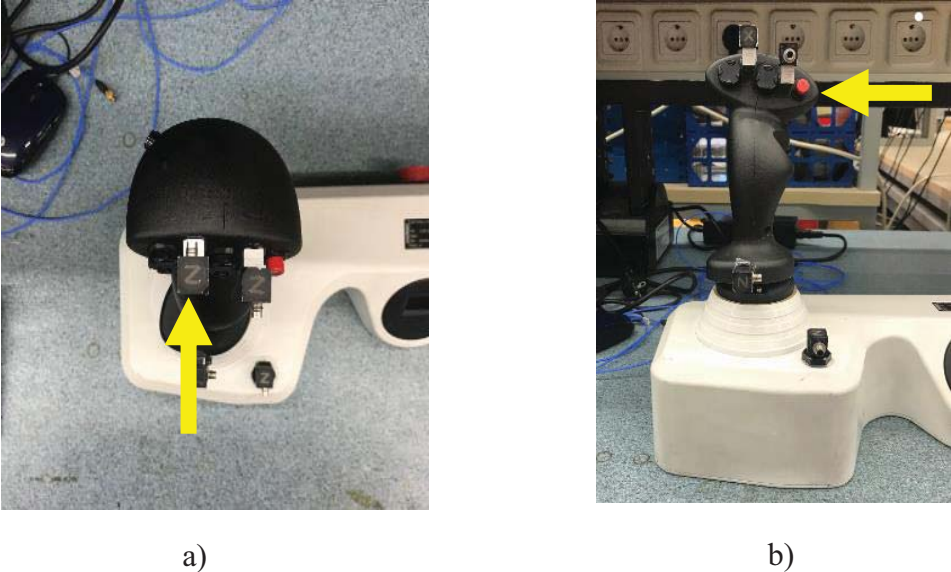
<div align="center">Figure 5-6: Driving Points: a) Run 1; b) Run 2</div>

Impact testing can be performed in two different ways, such as roving the accelerometer and roving the hammer. Moving the accelerometer has some disadvantages. Changing the location of the accelerometer alters the mass distribution of the structure. As this may cause changes in the natural frequencies of the structure, the method of roving the impact hammer is chosen.

On the LMS Simcenter Test Lab Software, the frequency resolution is set to be 0.25 Hz. The frequency range is selected as 0-256 Hz. Furthermore, the acquisition time is arranged to be 4 seconds. The exponential window is applied to the force and response data in order to minimize the effects of leakage [31]. However, the exponential window adversely affects measurement by adding artificial damping to the signal. Fortunately, modal curve fitters in Simcenter Testlab remove the artificial damping effect and provides obtaining the correct modal damping value [32].

The structure is excited 15 times with the impact hammer with a soft tip. The individual FRF is measured for each excitation. The coherence function [32], which indicates the quality of FRF, checks the repeatability of the individual FRFs. The excitations that can cause errors in the accuracy of FRF are not taken into account in the calculation. At the end of the run, by taking the average of the measured 15 FRFs, the mean FRF is obtained correctly. Since 11 accelerometers with three channels each are used, in total, 33 different

mean FRFs are calculated. FRFs are used to describe the dynamical behavior of the structure.

After the FRFs are obtained in the impact testing, experimental modal analysis is performed by using these FRFs in order to find modal parameters of the structure. Experimental modal analysis is conducted by using the Polymax Algorithm on Simcenter Testlab software.

5.5 Test Configurations

The modal impact tests are performed in two different configurations. There is only one difference between configurations. In the first test configuration, the bolts used in isolator connections are tight as it should be. A torque of 0.4 Nm is applied to the bolts with a torque wrench. The isolator structure is clamped firmly between its adjacent components with the tightened bolts. In contrast, in the second test configuration, the bolts are loosened until the tightening torque is eliminated. The loosened bolts are shown in Figure 5-7. Impact modal tests are carried out in the loosened bolt configuration to see the effect of the tightening torque on the bolts on the natural frequencies of the structure and to correlate the initial finite element model and the test model. Tightening torque on the bolts is not defined in the initial finite element model. Furthermore, no contact is defined between the isolator and the contact surfaces of its neighboring components
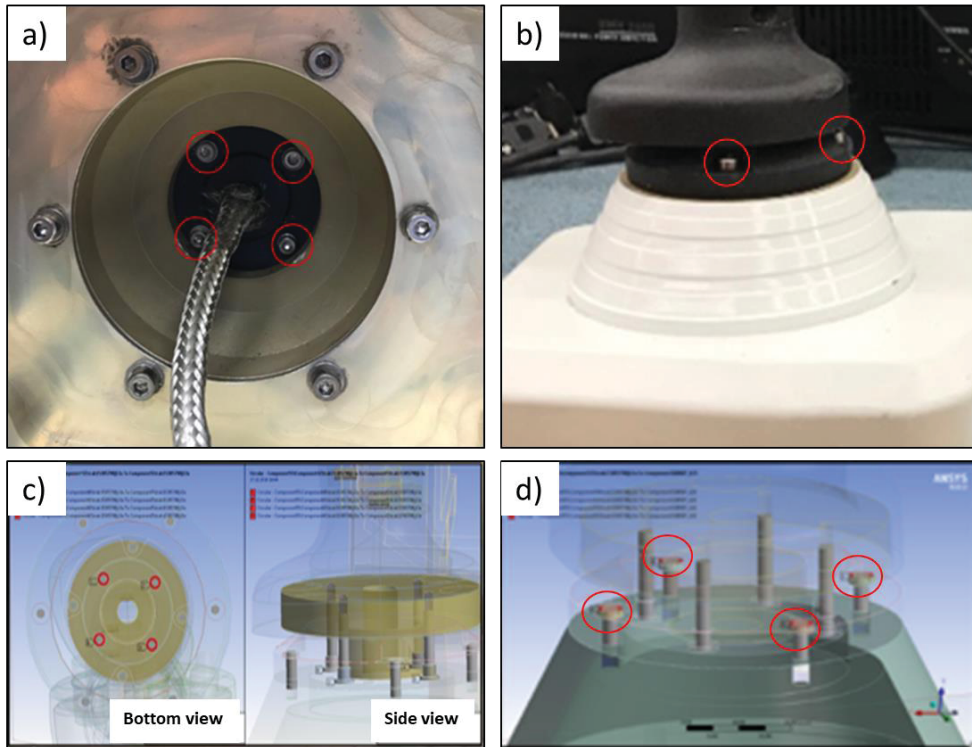
Figure 5-7: Bolts used in isolator connection: a) with the upper body; b) with the lower body; c) with the upper body in FEM; d) with the lower body in FEM

In the FEM of the control column, as described in Chapter 3, the isolator connection is provided by the beam elements. Moreover, the stress and deformations occurring on the isolator result from the tightening torque are not taken into account. Furthermore, any contact was not defined in the connection between the isolator and its adjacent body. In the second test configuration, the bolts are loosened to try to simulate the FEA model. As a result of tests, the effect of the tightening torque on the dynamic behavior of the control column can be observed, and it can be decided whether the contact model in the FEM is updated.

5.6 Analysis

FRF is a complex function that contains the amplitude and phase components. Thus, the real and imaginary terms are utilized to express this function. The frequency at which the real part of the FRF equal to zero or the imaginary part of the FRF has peak amplitude indicates the natural frequency of the structure. In addition, the width of the peak of FRF gives information about the damping ratio. The damping ratio at the interested natural

frequency can be determined by looking at 3 dB down from the peak level in the FRF curve [33].
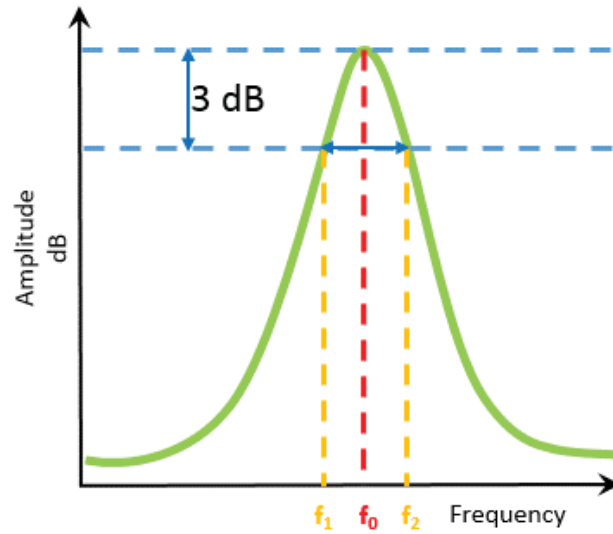
Figure 5-8: Quality factor (Q) calculation from FRF

The quality factor (Q) is found in Equation 4, where:

- f_0 is the frequency of the peak in Hz

- f_1 is a frequency value, in Hz, 3 dB down from the peak value ($f_1 < f_0$)

- f_2 is a frequency value, in Hz, 3 dB down from the peak value ($f_2 > f_0$)

$$Q = \frac{f_0}{f_2 - f_1} \tag{4}$$

Damping ratio (ζ) is obtained by equation 5.

$$\zeta = \frac{1}{2Q} \tag{5}$$

In this section, the driving points FRFs calculated by using the response from the accelerometers that are located on the upper part of the control column are presented. The natural frequencies of the control column are determined by observing the imaginary and real parts of the FRF. In addition, FRFs calculated by using the response of all accelerometers are processed by Polymax Algorithm in Simcenter TestLab software. Thus, mode shapes and damping ratios at the natural frequencies are determined.

5.6.1 Configuration 1:Tightened Bolts

5.6.1.1 Run 1, Driving Point: ACC 5, DIR: +X

In this run, the control column is excited from the surface near Accelerometer 5 in the direction of +X. The response of Accelerometer 5 in the direction of +X is used in the FRF. The imaginary and the real parts of the FRF is shown in Figure 61. As it is observed in Figure 61, the imaginary part of the FRF has a peak amplitude at 37.7 Hz. The control column has a natural resonance at this frequency value. The mode shape of the structure at this frequency is shown in Figure 5-10. The control column vibrates in X- direction at this frequency value. The damping ratio is calculated to be 8.39 percent at this natural frequency.
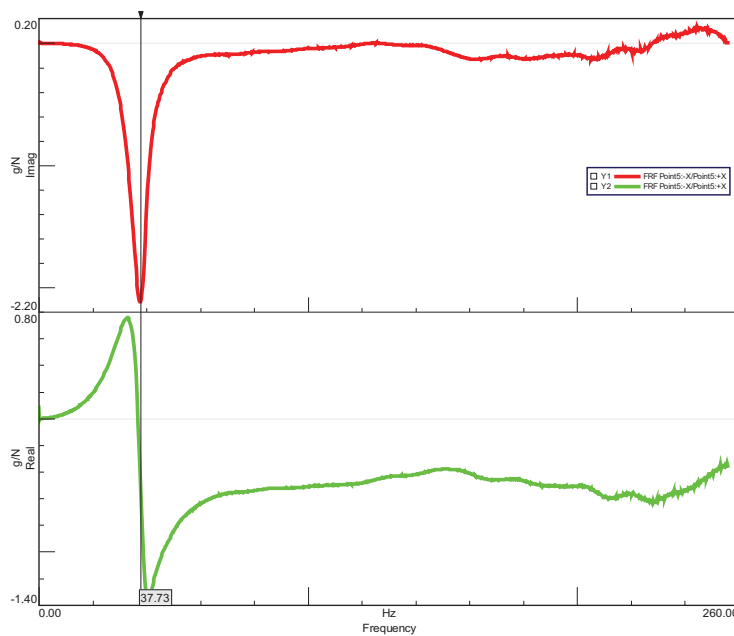
Figure 5-9: Imag and Real Parts of the FRF (Hammer: P5_+X; Acc: P5_+X)
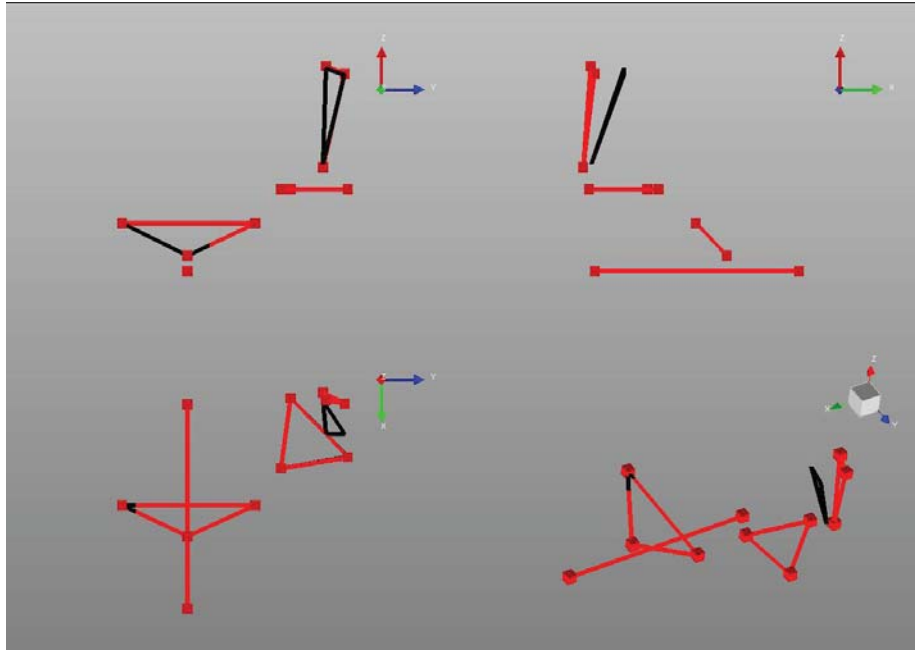
Figure 5-10: First mode shape of the control column (red line: deformed body, black line: undeformed body)

5.6.1.2 Run 2, Driving Point: ACC 6, DIR: +Y

In this run, the control column is excited from the surface next to Accelerometer 6 in the direction of +Y. The response of Accelerometer 6 in the direction of +Y is used to calculate FRF. The imaginary and the real parts of the FRF is shown in Figure 5-11. As it is observed in Figure 5-11, the imaginary part of the FRF has a peak amplitude at 39.09 Hz. The control column has a natural resonance at this frequency value. The mode shape of the structure at this frequency is shown in Figure 5-12. The control column vibrates in Y-direction at this frequency value. The damping ratio is calculated to be 4.36 percent at this natural frequency.
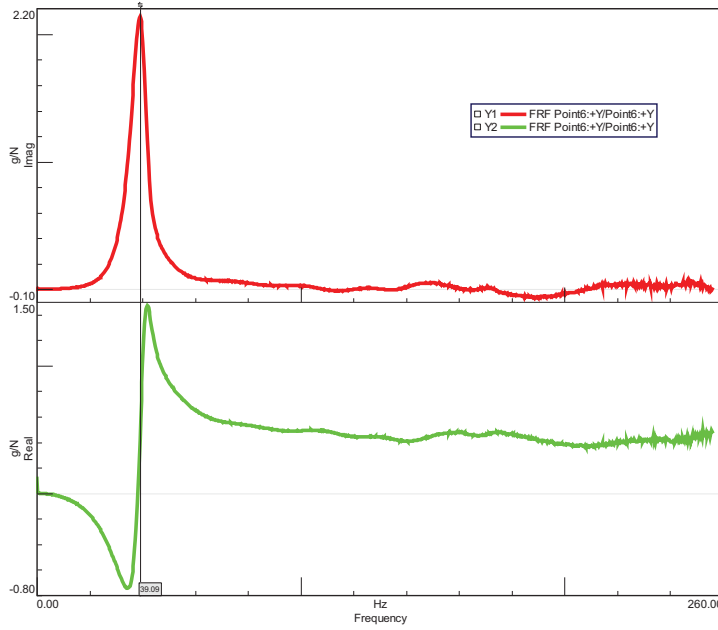
Figure 5-11: Imag and Real Parts of the FRF (Hammer: P6_+Y; Acc: P6_+Y)
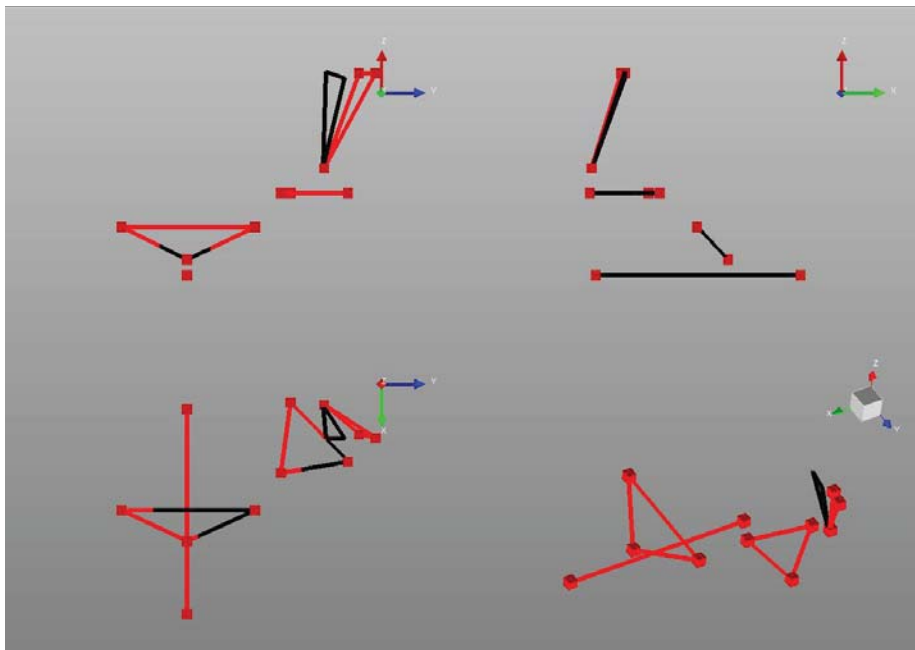
Figure 5-12: Second mode shape of the control column (red line: deformed body, black line: Undeformed body)

5.6.2 Configuration 2: Loosened Bolts

In this configuration, the bolts used in isolator connections are loosened until the tightening torque on bolts is eliminated. The impact hammer tests are then repeated for

this configuration. The driving points in the first configuration are the same as in the second configuration.

5.6.2.1 Run 1, Driving Point: ACC 5, DIR: +X

The imaginary and the real parts of the FRF is shown in Figure 5-13. The first natural frequency of the control column is 16.2 Hz. Similar to the first configuration, the control column vibrates in X- direction at this frequency value. The mode shape at first natural frequency is the same as in Configuration 1. The damping ratio is calculated to be 8.27 percent for this natural frequency.
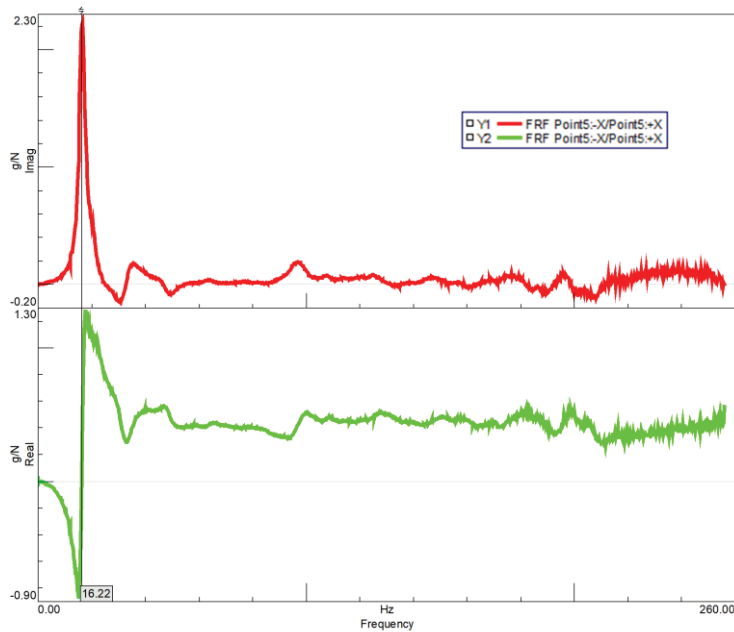
Figure 5-13: Imag and Real Parts of the FRF (Hammer: P5_+X; Acc: P5_+X) for the second configuration

5.6.2.2 Run 2, Driving Point: ACC 6, DIR: +Y

The imaginary and the real parts of the FRF is shown in Figure 5-14. The first natural frequency of the control column is 20.0 Hz. Similar to the first configuration, the control column vibrates in Y-direction at this frequency value. The mode shape at first natural frequency is the same as in Configuration 1. The damping ratio is calculated to be 4.57 percent for this natural frequency.
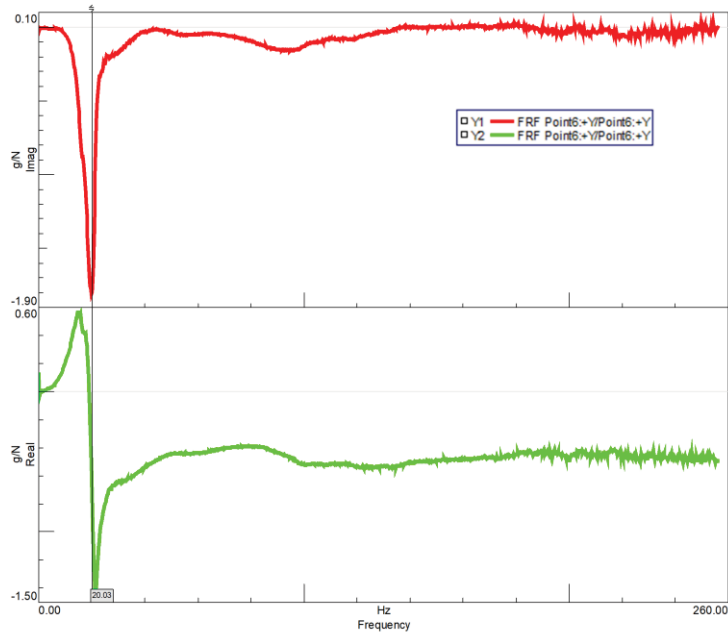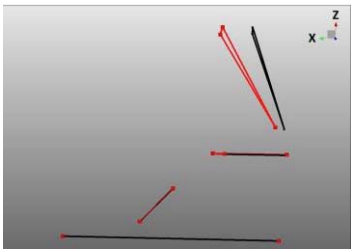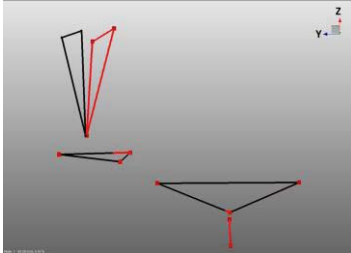
Figure 5-14: Imag and Real Parts of the FRF (Hammer: P6_+Y; Acc: P6_+Y) for the second configuration

5.7 Results

The natural frequency and damping ratio results for both configurations are summarized in Figure 5-3. As can be observed in the test results, the natural frequency values of the control column decrease almost by half when the isolator's bolts are loosened. Tightening torque on the bolts have a considerable effect on the stiffness of the control column.

Table 5-3: Impact Modal Test Results

# of modes	Tightened Bolts (Configuration 1)		Loosened Bolt (Configuration 2)		Mode Shape
	Natural Frequency (Hz)	Damping Ratio (%)	Natural Frequency (Hz)	Damping Ratio (%)	
1	37.7	8.4	16.2	8.3	
2	39.1	4.4	20.0	4.6	

The mode shapes obtained in the FEA are similar to impact hammer test results, as can be observed in Table 5-4. However, natural frequencies between the initial FEA result and the impact hammer test result are quite different from each other. The error rate for configuration 1 is around 70 percent, while it is about 30 percent for configuration 2. When tightening torque is not applied to the bolts, the natural frequencies of the structure are closer to the results of FEA. By eliminating the tightening torque on the bolts in configuration 2, the initial FEM is simulated. At the initial FEM, no preload is applied to the bolts, and no contact is defined between the isolator and its adjacent components. However, the results of the analysis are unacceptably different than those in configuration 2. These results indicate that the isolator connection type needs to be updated in the analysis model. Besides, these results show that an accurate model cannot be obtained only by updating the isolator connection type. It can be understood that other mistakes were made in modeling except for the isolator connection.

Table 5-4: Comparison of the mode shapes between FEA and impact hammer test
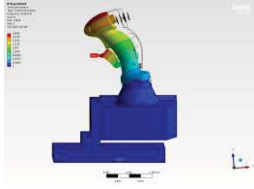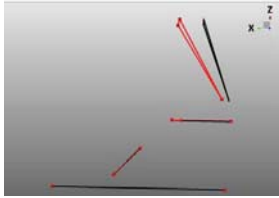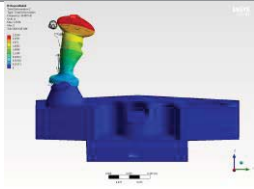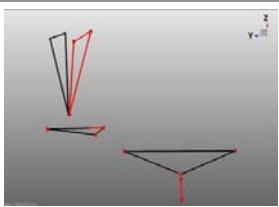
Number of Modes	Initial Finite Element Model	Impact Hammer Test (Configuration 1&2)
1		
2		

Table 5-5: Comparison of the natural frequencies between FEA and test results

# of Modes	Initial FEM-Natural Frequency	Config 1-Natural Frequency	Config 2-Natural Frequency	Error Rate (Config 1-FEM)	Error Rate (Config 2-FEM)
1	11.4 Hz	37.7 Hz	16.2 Hz	69.8 %	29.6 %
2	14.0 Hz	39.1 Hz	20.0 Hz	64.2 %	30.0 %

As mentioned in Chapter 4, in the sine sweep test, the mode that the control column oscillates in the direction of the Y-axis was observed at 43 Hz. However, the same mode is obtained at 39.1 Hz in the modal impact test. This discrepancy arises from the mass differences of the test setups. Buttons located on the control column are not mounted on the gun control unit in the sine sweep test setup. The missing mass causes the natural frequency to increase. Besides, the mass of the accelerometers located on the structure plays a significant role in the natural frequency. The number of accelerometers used in the impact test is more than the ones used in the sine sweep test. The additional mass causes the natural frequency to decrease. Therefore, the extra mass difference coming from an additional accelerometers and buttons causes the difference in natural

frequencies. In reality, the natural frequency (oscillates in the direction of the Y-axis) of the control column is between 39.1 Hz and 43 Hz.

As a result of the modal impact tests, the damping ratio at the first two modes of the control column is obtained. The lowest structural damping ratio is calculated to be 4.4 % at these natural frequencies.

5.8 Conclusion

In this chapter, the impact modal tests are performed to obtain the first and second natural frequencies of the control column, corresponding mode shapes, and the damping ratios. The impact tests are carried out for two different mounting configurations. In the first configuration, the connection bolts of the isolator are tightened with adequate torque, whereas in the second configuration, the torque on the bolts is removed. Test results show that the natural frequency values of the control column decrease almost by half when the isolator's bolts are loosened. It can be deduced from these results that the tightening torque on the bolts has a considerable effect on the dynamics of the control column.

The initial FEA result is compared with the test results. The comparison shows that the difference between the natural frequencies is around 70 percent for the first configuration, while this difference is around 30 percent for the second configuration. The outcomes from this comparison are as follows:

➢ In the first configuration, the isolator connection is made as in real usage. However, a 70 percent difference between analysis results and test results shows that the connection in the analysis model is not correct. For this reason, the isolator connection type should be updated in the finite element analysis model.

➢ The isolator connection type in the initial finite element model is simulated by removing the tightening torque in the second configuration. However, the fact that there is a 30 percent difference in natural frequencies between test and analysis results indicates that there are other erroneous modeling assumptions except for the isolator connection type.

Therefore, an accurate model cannot be obtained only by updating the isolator connection type. In addition to the isolator connection type, some boundary conditions and some material properties need to be updated in the FEM. For this reason, the tensile tests are carried out to get some mechanical properties of neoprene next chapter.

6. DETERMINATION OF NEOPRENE MATERIAL PROPERTIES

6.1 Introduction

As mentioned in Chapter 2, the neoprene isolator was added to the gun control unit in order to isolate the vibration transmitted from the platform to the control column body. In Chapter 3, the FEM of the control column with the isolator was built. Furthermore, the natural frequencies and mode shapes were calculated, and fatigue strength of the structure under the tracked vehicle vibration was obtained by the finite element method. As stated in both Chapters 4 and 5, natural frequencies obtained in the test were different than finite element results. One of the reasons for this difference is attributed to the material properties of the isolator material "Neoprene" as its Young's modulus used in the FE model was determined according to an empirical formula correlated with the durometer hardness [34]. Based on this assumption, tensile tests are carried out in order to determine the young modulus of neoprene material more accurately in this chapter.

The young modulus of the Neoprene changes according to the strain rate. Isolator has different stiffness characteristics according to the strain rate. For this reason, tensile tests are performed at different strain rates, and the young modulus of neoprene is obtained at different strain rates.

6.2 The Preparation of the Test Specimen

Tests are performed in the Polymer Laboratory in the Department of Chemistry at Hacettepe University. The BİL-PLAS company supplies neoprene sheets with the hardness of 60 Shore. Sheets have a thickness of 2 mm, and they have dimensions of 200 x 200 mm. The neoprene sheet is shown in Figure 6-1.

Figure 6-1: Neoprene Sheets

Firstly, test specimens are prepared for testing by using the hand press. The hand press is shown in Figure 6-2. The hand press extracts the test specimen from the sheet with the cutter die that is attached to the tooltip. The die determines the shape and dimension of the test specimen. In the tensile test, the test specimen has the shape of the dumb-bell. The dimension and shape of the test specimen are represented as Type 1 in the standard of ISO 37. Dimensions of dies for type 1 are presented in Figure 6-3 [35].

Figure 6-2: The hand press
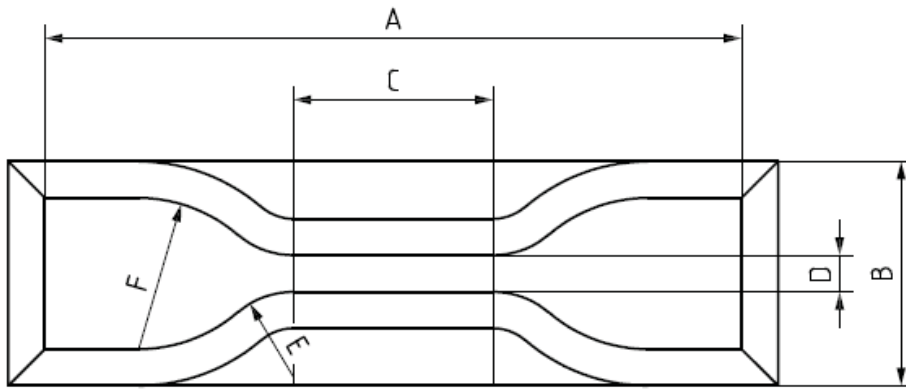
a)

Dimension		Type 1
A	Overall length (minimum)[a] (mm)	115
B	Width of ends (mm)	25 ± 1
C	Length of narrow portion (mm)	33 ± 2
D	Width of narrow portion (mm)	6,2 ± 0,2
E	Transition radius outside (mm)	14 ± 1
F	Transition radius inside (mm)	25 ± 2

b)

Figure 6-3: Dumb-bell-shaped test specimen: a) Shape b) dimensions

A sample set includes 8 test specimens that are extracted from each neoprene sheet (Figure 6-4). In total, 4 sample sets are prepared. Each set is used in tests performed with different test speeds. The tests are repeated eight times with the same test speeds. A test specimen is shown in Figure 6-5.
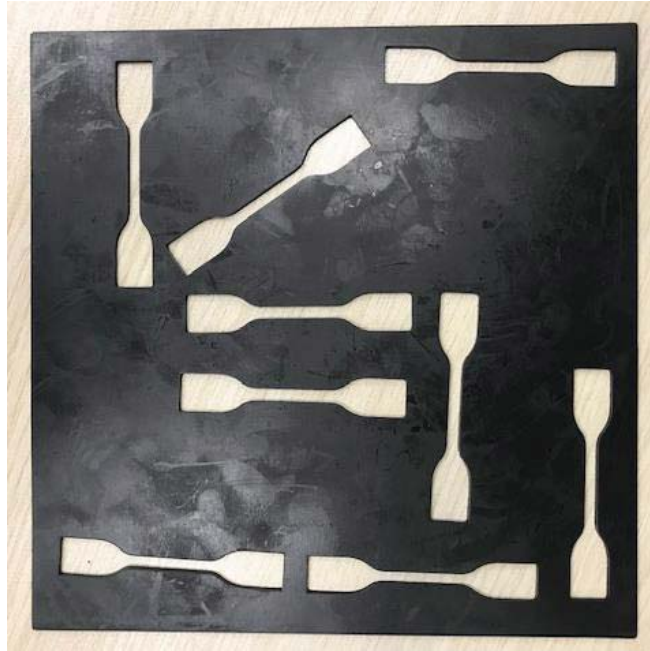
Figure 6-4: A pressed neoprene sheet

Figure 6-5: Test Specimen

6.3 Experiment Setup

The tensile tests are performed by using the ZwickRoell Z010 material testing machine. The visual of the testing machine is shown in Figure 6-6. Furthermore, an extensometer is used to measure the elongation of the specimen accurately during the test. The elongation in the gage length is measured with the long-travel type of ZwickRoell extensometer. It is shown in Figure 6-7.

Figure 6-6: ZwickRoell Z010 tensile testing machine
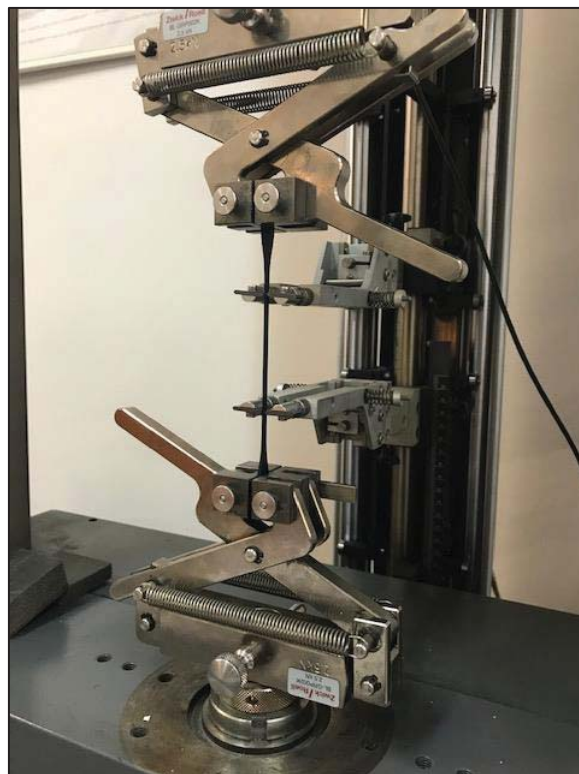
Figure 6-7: ZwickRoell long-travel extensometer

The procedure to carry out the test is as follows:

- The width and the thickness of the gauge are measured with the caliper.

- Input parameters (test name, dimensions of the gauge, preload value, test speed, etc.) are defined in the software.

- The test specimen is placed properly between the tensile grips

- Extensometer is attached to the gage length.

- Before the tensile test, preloading is done in order to remove slack.

- With the beginning test, the test specimen is elongated with the specified test speed.

- After the rupture, the test is ended.

It is estimated that the isolator gives the responses at different strain rates due to the tracked vehicle random vibration. The young modulus of neoprene material varies according to the strain rate. Isolator has different stiffness characteristics according to the strain rate. For this reason, tensile tests are performed at different strain rates, and the young modulus of neoprene is obtained at different strain rates.

Eight tests are performed at each test speed. In total, 32 measurements are taken. The information about test records is presented in Table 6-1. As observed in the table, for the third and fourth sets, the test speed in the elastic region is different than the plastic region. Since our aim is to obtain the elastic modulus, the elongation in the plastic region is not concerned for this study. Once the modulus is determined, the test speed is set to 500 mm/min to shorten the test duration.

Table 6-1: Test Schedule

Test Number	Set of Sample	Speed (at Elastic Region)	Speed (at Plastic Region)
1-8	1	100 mm/min	100 mm/min
9-16	2	500 mm/min	500 mm/min
17-24	3	20 mm/min	500 mm/min
25-32	4	1 mm/min	500 mm/min

The collected data is analyzed on the TestXpert II Software. Elasticity modulus is calculated by the slope of the strain-stress curve in the strain interval between 0.05 % and

0.25 %. The linear regression method is used in the calculation. Thanks to this method, all collected data in the strain interval are taken into account. Thus, statistically safer results are obtained [36].

6.4 Test Results

6.4.1 Test Performed at a Speed of 100 mm/min

The first eight tensile tests are carried out at a constant speed of 100 mm/min. The stress-strain diagram for each test is shown in Figure 6-8. The obtained parameters are listed in Table 6-2.
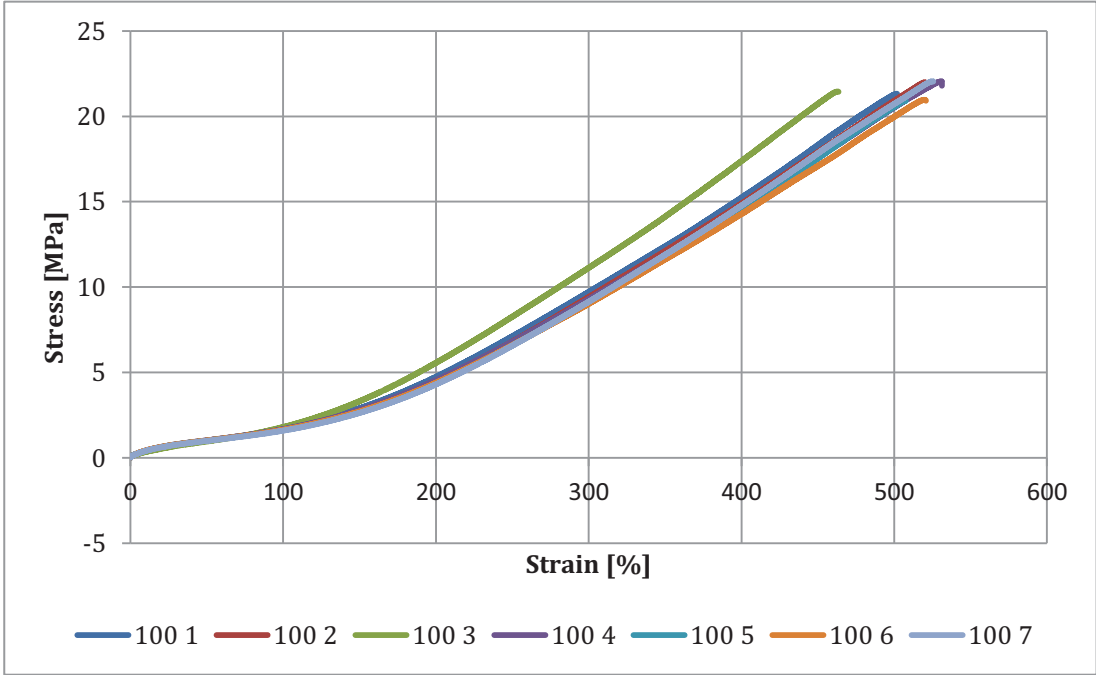
Figure 6-8: The Stress-Strain Diagram of specimens tested with a speed of 100 mm/min

Table 6-2: Result of tests at performed with a speed of 100 mm/min

# of Test	Test	Elasticity Modulus (MPa)	Tensile Strength at Break (MPa)	Strain at Break (%)
1	100 1	4.45	21.32	501.95
2	100 2	5.07	21.97	520.30
3*	100 3	3.78	21.44	463.45
4	100 4	5.31	21.79	531.25

5	100 5	4.89	20.92	507.47
6	100 6	5.34	20.92	520.70
7	100 7	5.01	22.03	525.45
8**	100 8	-	-	-

*: The test specimen is not attached to grips vertically aligned. As the misalignment creates an error, test 3 should not be considered.

**: The data is not collected in test 8.

6.4.2 Test Performed at a Speed of 500 mm/min

The tests of the number of 9-16 are performed with an elongation speed of 500 mm/min. The stress-strain diagram for each test is shown in Figure 6-9. The obtained parameters are listed in Table 6-2.
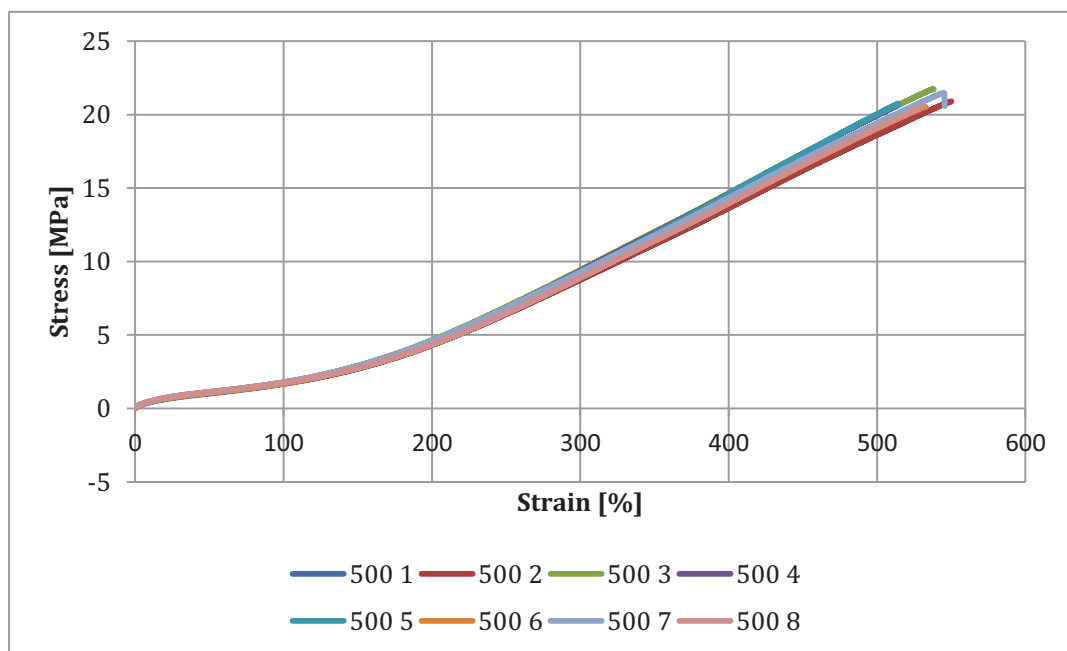
Figure 6-9: The Stress-Strain Diagram of specimens tested with a speed of 500 mm/min

Table 6-3: Result of tests at performed with a speed of 500 mm/min

# of Test	Test	Elasticity Modulus (MPa)	Tensile Strength at Break (MPa)	Strain at Break (%)

9	500 1	5.07	19.36	516.22
10	500 2	5.32	20.90	550.15
11	500 3	5.65	21.71	538.22
12	500 4	5.93	20.59	513.17
13	500 5	5.68	20.65	514.50
14	500 6	5.62	20.49	532.77
15	500 7	5.30	20.59	545.57
16	500 8	6.21	20.59	531.67

6.4.3 Test Performed at a Speed of 20 mm/min in Elastic Region

The tests from 17 to 24 begin with a speed of 20 mm/min. After obtaining the elasticity modulus, the tensile speed is increased to 500 mm/min in order to shorten the test duration. The stress-strain diagram for test specimens is shown in Figure 6-10. The parameters calculated from the diagram are presented in Table 6-4.
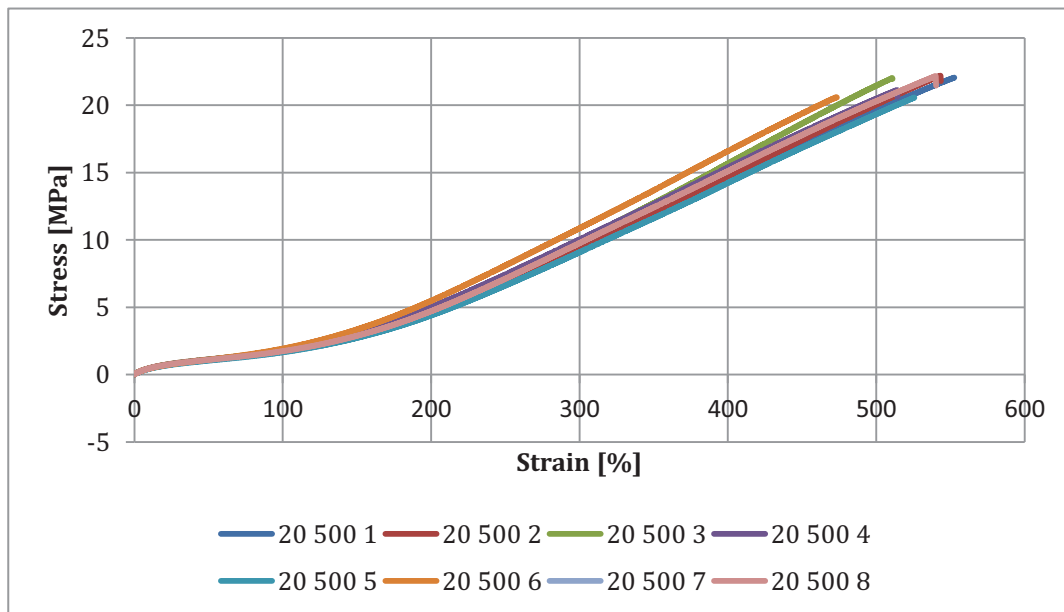
Figure 6-10: Stress-strain diagram of specimens tested with a speed 20 mm/min in the elastic region

Table 6-4: Results of tests at performed with a speed of 20 mm/min

# of Test	Test	Elasticity Modulus (MPa)	Tensile Strength at Break (MPa)	Strain at Break (%)
17	20 500 1	4.76	22.04	552.57
18	20 500 2	4.90	21.80	543.57
19	20 500 3	4.74	21.95	511.02
20	20 500 4	4.77	20.62	514.32
21	20 500 5	4.50	20.56	525.72
22	20 500 6	4.71	20.57	473.37
23	20 500 7	5.09	21.60	528.15
24	20 500 8	4.79	21.45	540.23

6.4.4 Test Performed at a Speed of 1 mm/min in Elastic Region

The tests from 25 to 32 begin with a test speed of 1 mm/min. After obtaining the elasticity modulus, the test speed is increased to 500 mm/min in order to reduce test duration. The stress-strain diagram for test specimens is shown in Figure 6-11. The obtained parameters are presented in Table 6-5.
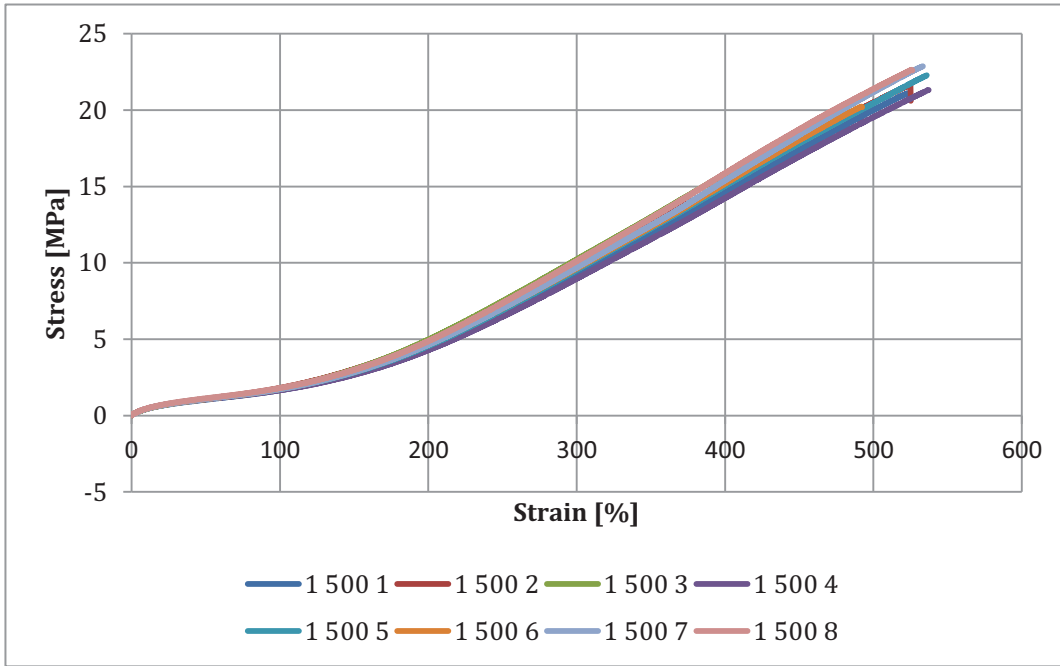
Figure 6-11: Stress-strain diagram of specimens tested with a speed of 1 mm/min in the elastic region

Table 6-5: Results of tests at performed with a speed of 1 mm/min

# of Test	Test	Elasticity Modulus (MPa)	Tensile Strength at Break (MPa)	Strain at Break (%)
25	1 500 1	3.86	21.02	523.35
26	1 500 2	4.23	20.62	525.20
27	1 500 3	4.01	21.21	499.97
28	1 500 4	4.42	21.33	537.27
29	1 500 5	4.23	22.28	536.00
30	1 500 6	3.99	20.19	492.35
31	1 500 7	4.50	22.87	533.25
32	1 500 8	4.60	22.60	526.12

6.5 Summary

In this chapter, the tensile tests of the neoprene material are performed in order to obtain the elasticity modulus of the isolator at different strain rates. The specimens are tested with different crosshead speeds, and the effect of strain rate on the elasticity modulus is observed. The average values for elasticity modulus at each test speed are presented in Table 6-6.

Table 6-6: Average values of the obtained Elasticity Modulus

Test speed in the elastic region	The average value of elasticity modulus (MPa)
1 mm/min	4.23
20 mm/min	4.78
100 mm/min	5.01
500 mm/min	5.60

As it can be observed from the table, the elasticity modulus increases proportional to the test speed. It can be deduced that the isolator shows stiffer behavior on higher deformation rates. The young modulus range of the neoprene will be used in the next chapter to update and calibrate the finite element model.

7. THE FINITE ELEMENT MODEL UPDATING

7.1 Introduction

The finite element model of the control column with the isolator was presented in Chapter 3. Then, the experimental modal analyses were performed in Chapter 5 to check whether the FEM of the gun control unit is modeled accurately. The natural frequencies obtained in the experimental modal tests were found to be quite different from the natural frequencies obtained in the FEA. As a result of the comparison, it was deduced that the FEM of the control column structure was not built accurately. Therefore, it is necessary to update the modal parameters of FEM [37].

The geometry of analysis and mesh settings of the structure, loading conditions, other settings were as presented in Chapter 3. In this updated model, the elastic modulus of neoprene, the connection types between components, and damping ratio value defined in random vibration analysis are changed.

At the beginning of this chapter, the elasticity module of the neoprene is updated with the lowest value obtained in the tensile test. Then, the isolator connection is established in different types, and modal analysis results are obtained for each connection model. The isolator connection type, which gives the closest result to the experimental modal analysis results, is chosen. Then, the type of connection between the other components of the structure is updated.

In this last part of this chapter, the finite element model is calibrated to minimize the discrepancy between the results of the experimental modal analysis and finite element analysis by changing the elasticity modulus of neoprene in a certain range. In the tests carried out in Chapter 6, it was observed that the elasticity module of the neoprene changed in the range of 4.23-5.6 MPa depending on the test speed. The exact value of the elasticity module of neoprene to be used in the analysis is unknown. Thus, the elasticity modulus is estimated to vary within the range obtained in tensile tests. Therefore, the finite element model is calibrated by changing the elasticity modulus of neoprene in a specified range. In addition, in this section, modal analysis and random vibration analysis of the calibrated FEM are performed, and fatigue damage ratios of the control column structure are calculated. Finally, calibrated finite element model results are verified by comparing with random vibration test results, and accurate FEM of the gun control unit is achieved. The update procedure is summarized in Figure 7-1.
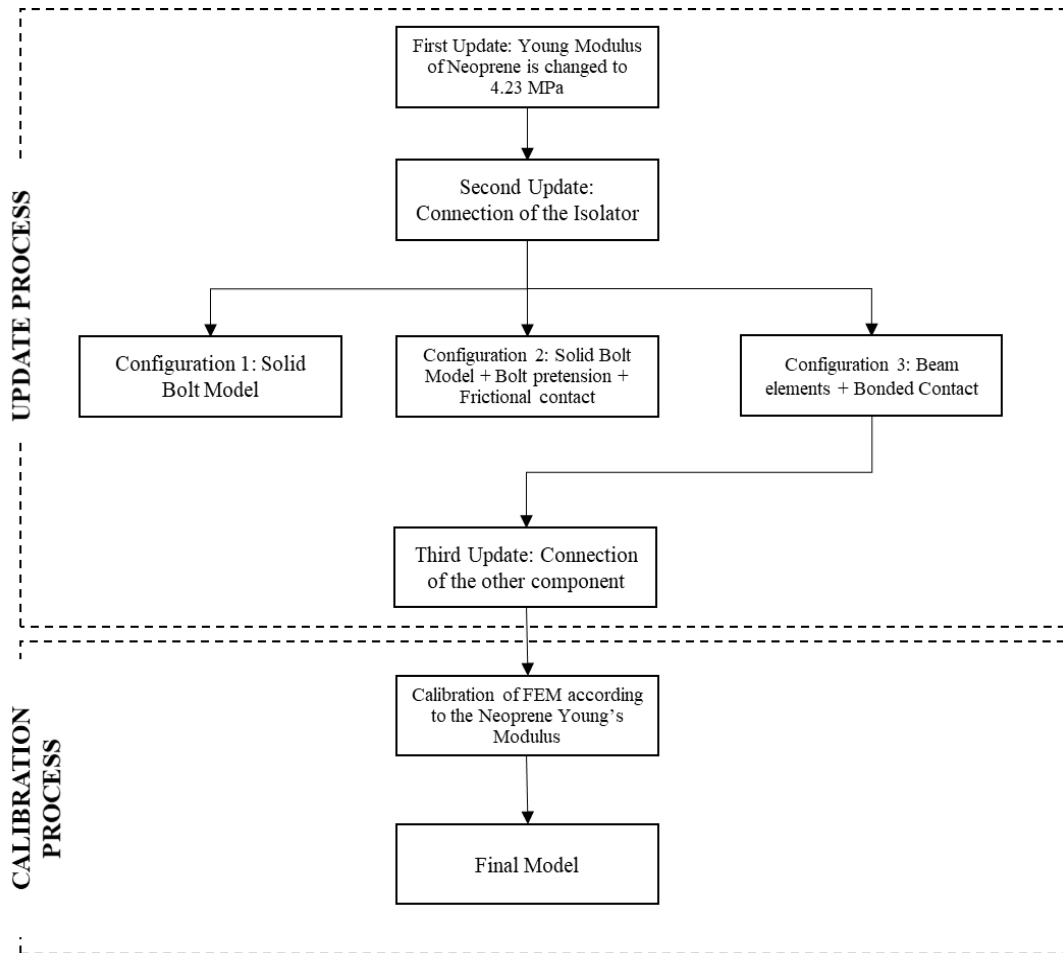
Figure 7-1: The update procedure

7.2 Material Properties of Neoprene

In the updated analysis model, all materials assigned to components were as presented in Chapter 3. Unlike the material properties in Chapter 3, the elasticity modulus of the neoprene (4.23 MPa) is updated with the average value obtained in the tensile test at the crosshead speed of 1mm/sec. As indicated in Table 7-1, the elasticity modulus of the neoprene is almost twice higher than the value used in the initial FEM, which causes the stiffness of the control column to increase. Thereby, the natural frequencies of the control column are increased. In the next analyses, until the calibration process, the neoprene elastic modulus is used as to be 4.23 MPa.

Table 7-1: Elasticity Modulus of Neoprene

	Initial FEM	Updated FEM
Elasticity of Modulus	2.06 MPa	4.23 MPa

In the experimental modal analysis in Chapter 5, the natural frequencies of the modes in which the control column structure oscillates in the direction of the X-axis and Y-axis were obtained. In the updated FEM, it is attempted to approach the natural frequencies of these modes. These mode shapes are shown in Figure 7-2. The results of FEM updated with neoprene's elasticity module and their comparison with the initial model and tests are presented in Table 7-2.

a)   b)
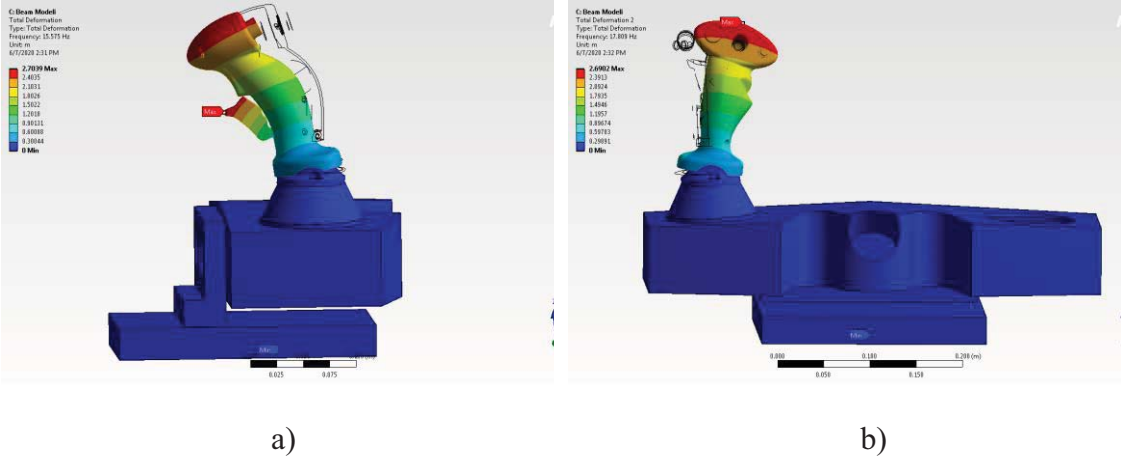
Figure 7-2: Mode Shapes: a) Oscillation in X-Axis; b) oscillation in Y-Axis

Table 7-2: Effect of the elasticity modulus of neoprene on the natural frequencies of the control column

Mode Shape	Initial FEM	Updated FEM	Test Results	The percentage difference between test and analysis
Oscillation in X-Axis	11.4 Hz	15.6 Hz	37.7 Hz	58.6 %
Oscillation in Y-Axis	14.0 Hz	17.9 Hz	39.1 Hz	54.2 %

7.3 Connection of the Isolator

Experimental modal analyses were performed for two different configurations. The first one was the tightened bolt configuration, and the second one was the loosened bolt configuration. In the first configuration, bolts used in the isolator connection was tightened until torque reaches to 0.4 Nm. Thus, the isolator was pressed between the conical base and holder, which enabled the isolator to attach to these parts properly. On

the other hand, in the second configuration, bolts were loosened until the tightening torque on the bolts is removed. As a result of the experimental modal analyses, whereas the first natural frequency of the control column was found to be 38 Hz in the first configuration, it was 16 Hz in the second configuration. This difference shows that the connection type of isolator affects the stiffness of the control column structure significantly.

In the initial FEM, the bolts used in the isolator connection were modeled by the beam elements [38], and no boundary condition was applied between the isolator and adjacent parts. As a result of the modal analysis of the initial model, the first natural frequency was found to be 11.4 Hz. A large portion of the discrepancy in the analysis and test results is thought to stem from the connection type of the isolator. The isolator connection is modeled with three different configurations.

1)   Configuration 1: Solid Bolt Model

2)   Configuration 2: Solid Bolt Model + Bolt pretension

3)   Configuration 3: Beam elements + Bonded Contact

As a result of these analyses, two natural frequencies of the control column for each configuration are obtained. These natural frequencies are compared with the results of the experimental modal analysis performed for the tightened bolt configuration. One of the configurations listed above, which has similar results to experimental modal analysis, is selected.

7.3.1   Configuration 1: Solid Bolt Model

In this configuration, bolts used in the isolator connection is prepared on the ANSYS SpaceClaim software. Beam elements used for the isolator connection in the initial FEM are suppressed. Instead of beam elements, the connection is provided by the solid bolt model. The bolt head is connected to the contact face on the isolator with the "bonded contact." Similarly, the threaded part of the bolt is connected to the bolt hole. The solid bolt model connection is presented in Figure 7-3.

a)   b)

c)   d)
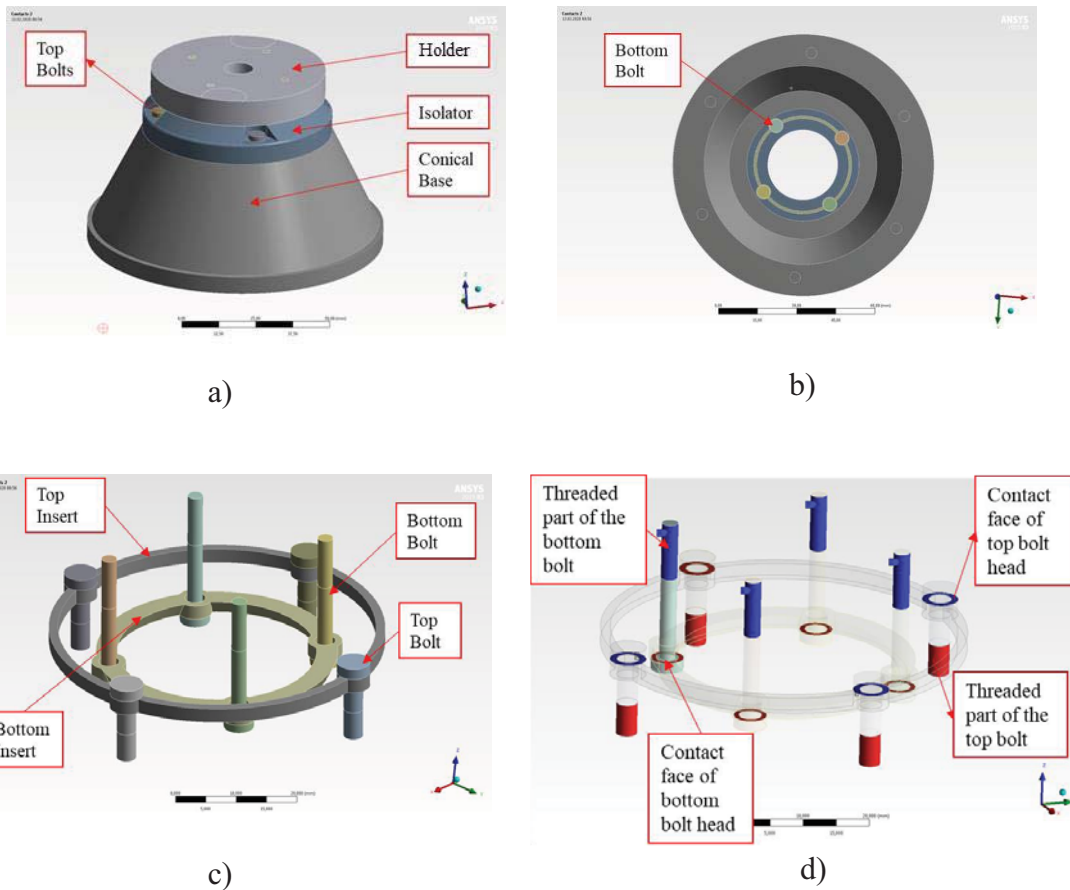
Figure 7-3: Solid Bolt Model: a) Assembly; b) bottom view; c) bolts and inserts; d) bonded contact surfaces on bolts

Two modes of the control column and their natural frequencies are presented in Table 7-3. Instead of using beam elements, using a solid bolt model causes negligible differences in the natural frequencies of the control column.

Table 7-3: Effect of solid bolt model on the natural frequencies of the control column

Mode Shape	Initial FEM + Neoprene E:4.23 MPa	Configuration 1	Test Results	The percentage difference between test and analysis
Oscillation in X-Axis	15.6 Hz	15.7 Hz	37.7 Hz	58.3 %
Oscillation in Y-Axis	17.9 Hz	18.0 Hz	39.1 Hz	54.0 %

7.3.2 Configuration 2: Solid Bolt Model + Bolt pretension

In the modal test setup, bolts used in the isolator connection were tightened until the torque reached 0.4 Nm so that the preload (also called as the pretension force) was produced on these bolts. In this configuration, the impact modal test setup is simulated with the finite element model. Two different types of analyses are conducted. Firstly, static analysis is carried out by applying the preload on the bolts. In the second analysis, modal analysis is performed in order to obtain two modes of the control column. In contrast to other FEMs, the stresses due to preloading are used as the initial condition for modal analysis. Thereby, stresses and deformations occurred in the isolator are taken into account in the modal analysis.

The tightening torque applied in the impact test setup determines the amount of pretension on the bolts. The preload is calculated by using Equation 6 [39];

$$F_p = \frac{T}{KD} \tag{6}$$

- F_p is the preload or pretension force (N)

- T is the tightening torque (Nm)

- D is the nominal diameter of the thread (m)

- K is approximately 0.2 for small to medium size bolts.

The solid bolt model prepared for the first configuration is also used in this configuration. Besides, the preload is applied to the unthreaded part of solid bolts. The preload is calculated to be 667 Nm for M3 bolts. The faces to which preload is applied are shown in Figure 7-4.
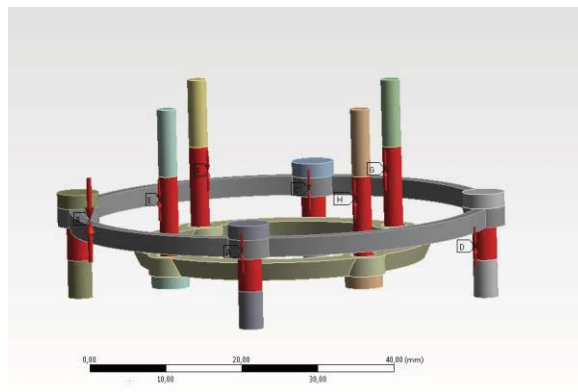
Figure 7-4: Unthreaded part of the bolts (indicated by the red color)

The frictional contact is applied in the contact surfaces, which is given in Figure 7-5 and Figure 7-6, respectively.
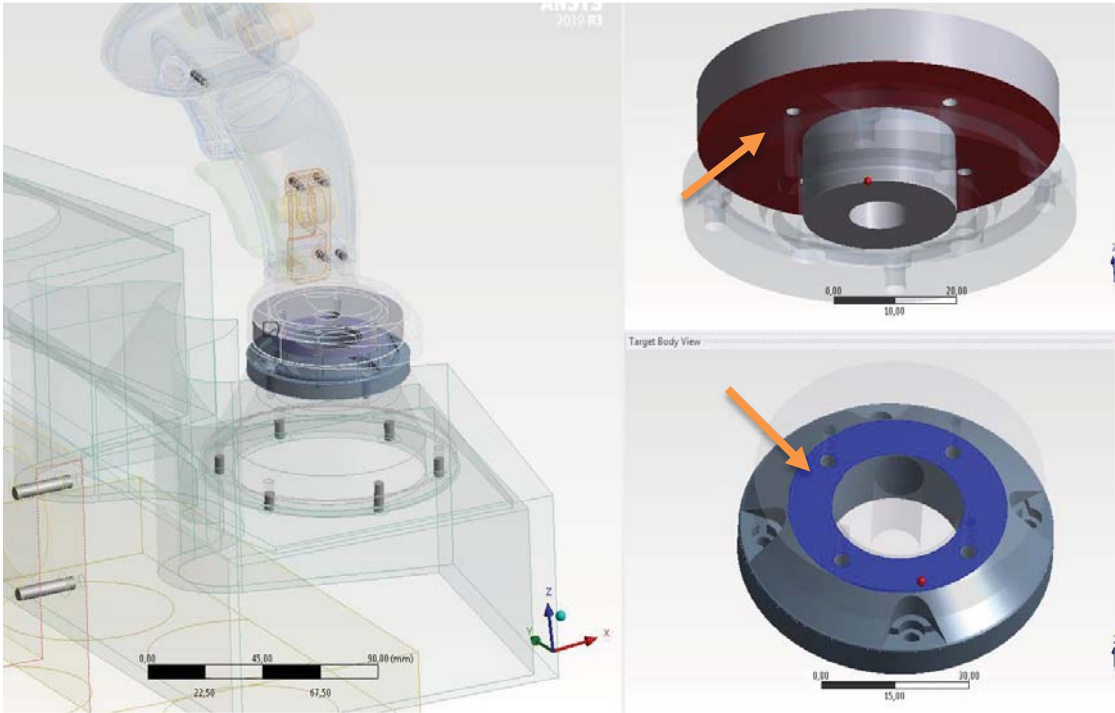
Figure 7-5: The frictional contact model is used between the isolator and the holder
(surfaces are shown by the orange arrow)
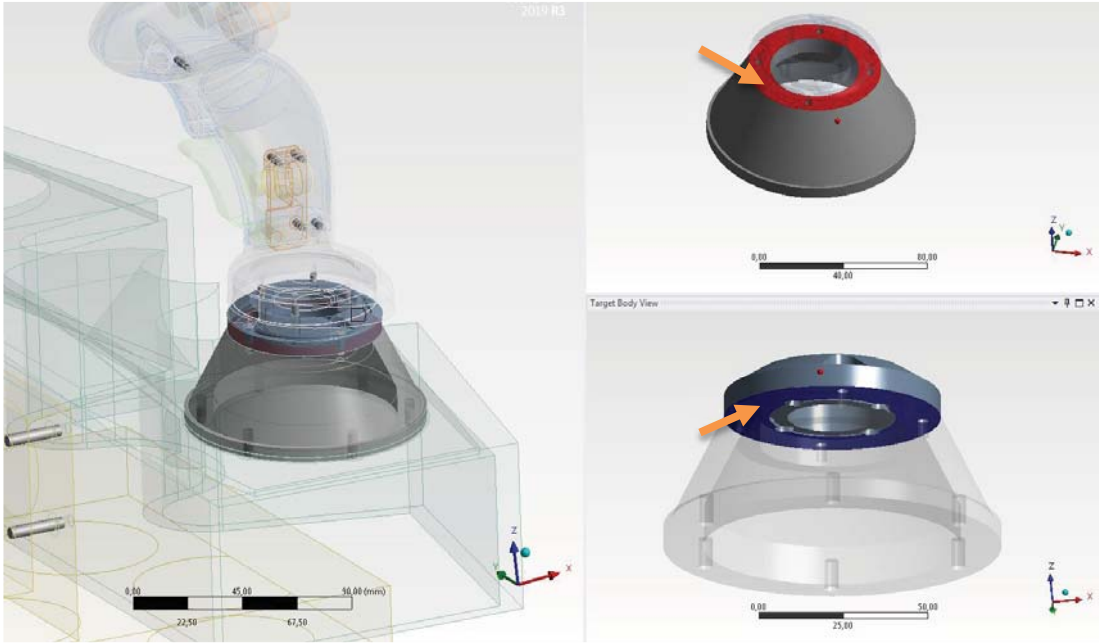
Figure 7-6: The frictional contact is applied between the isolator and the conical base

The frictional contact is a non-linear type of contact. However, in the modal analysis, the frictional contact is treated as bonded if contacts are closed. In this way, non-linear contact is made linear. Wherever there is a gap, non-linear contacts are treated as open contact [40]. When the contact status is open, contact is not taken into account during the solution.

Modal analysis results are presented in Table 7-4. The natural frequencies increase dramatically with respect to the results of the initial FEM. Since the isolator is pressed between its adjacent parts by the effect of the clamping force on the bolts, the control column gets stiffer. Furthermore, it is observed that the results of this configuration are quite similar to the results obtained in the experimental modal analysis.

Table 7-4: Comparison of natural frequencies of the initial FEM Configuration 2 and modal tests

Mode Shape	Initial FEM + Neoprene E:4.23 MPa	Configuration 2	Test Results	The percentage difference between test and analysis
Oscillation in X-Axis	15.6 Hz	33.1 Hz	37.7 Hz	12.2 %
Oscillation in Y-Axis	17.9 Hz	35.0 Hz	39.1 Hz	10.5 %

7.3.3   Configuration 3: Beam elements + Bonded Contact

This configuration is similar to the 2nd configuration in terms of the contact model. In this configuration, bonded contact is applied to the surfaces between the isolator and its adjacent parts. The bolts are modeled by using beam elements as in the initial FEM.

The beam elements used in connections of the isolator-base and isolator-holder are shown in Figure 7-7, Figure 7-8, respectively. The bonded contact surfaces between the components are shown in Figure 7-9 and Figure 7-10, respectively.
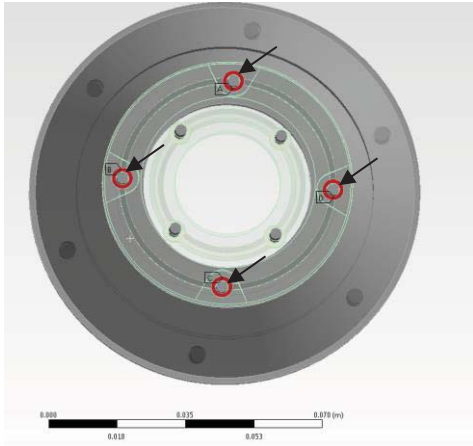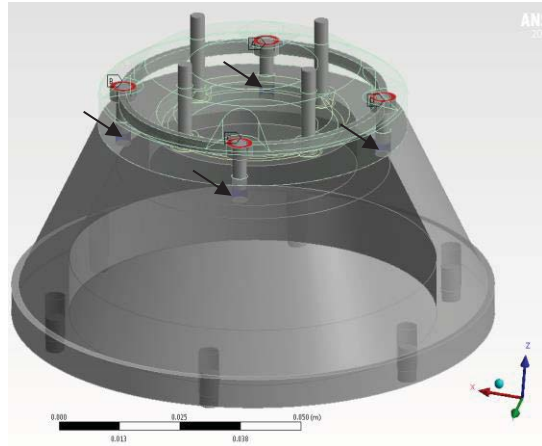
a)   b)

Figure 7-7: Beam elements in the connection of the isolator-base
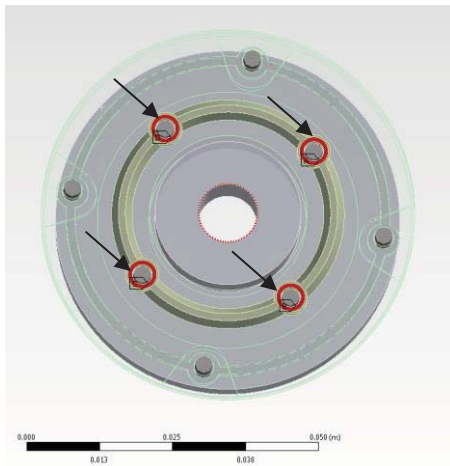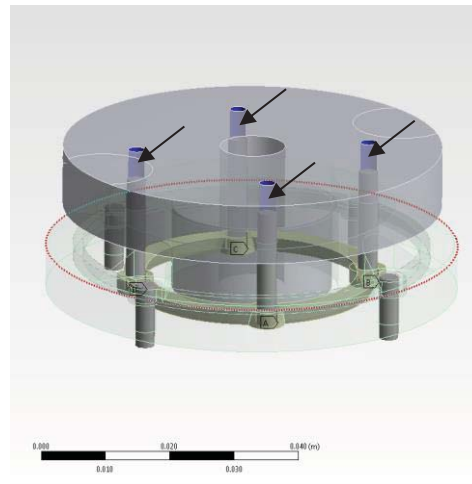
a)   b)

Figure 7-8: Beam elements in the connection of the isolator-holder
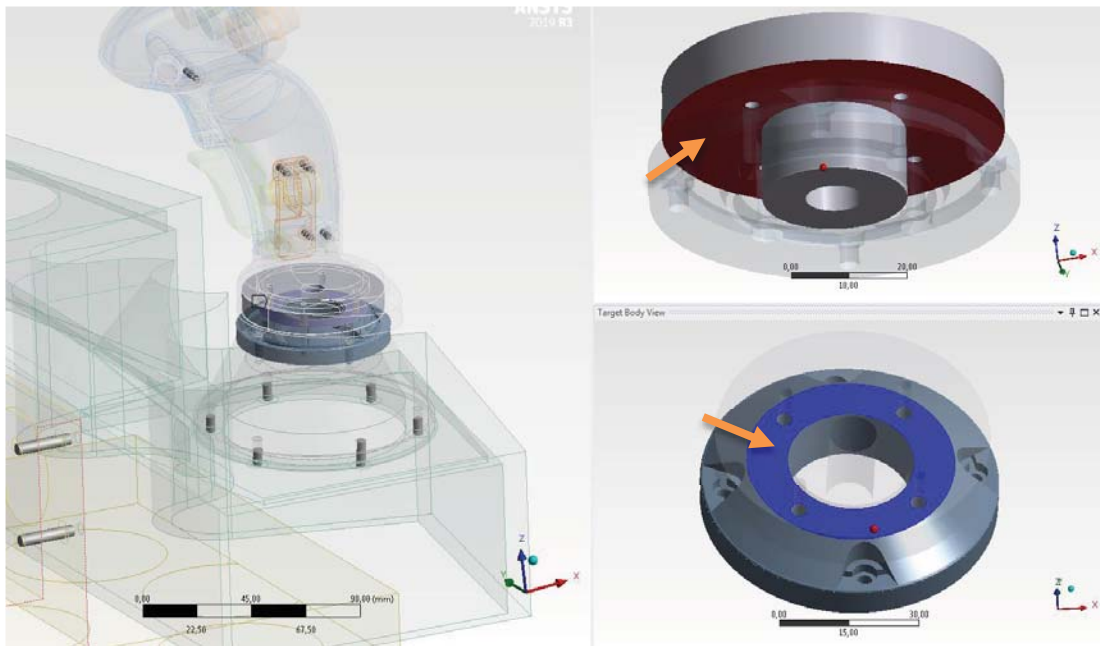
Figure 7-9: Bonded contact surfaces between the isolator and the holder
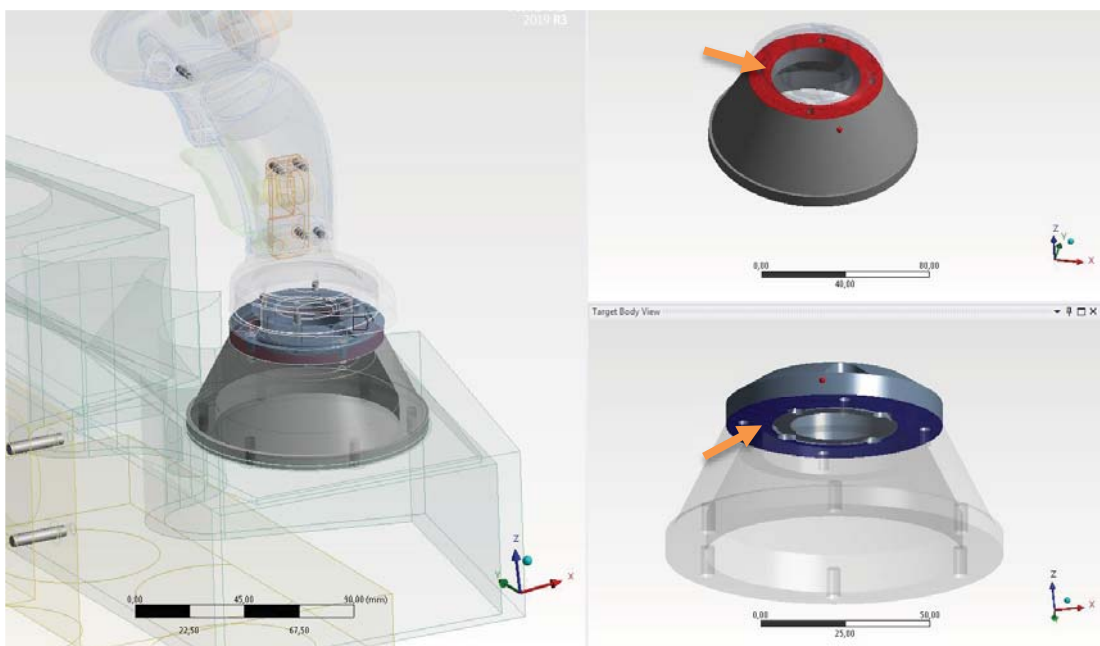
Figure 7-10: Bonded contact surfaces between the isolator and the conical base

The modal analysis results are presented in Table 7-5. The results of this configuration are compared with previous configurations. The results show that the bonded contact algorithm significantly increases the stiffness of the control column structure. The results obtained in this configuration are very similar to those obtained in the second configuration. The natural frequencies obtained in both configurations are close to the

results obtained in experimental modal analysis. In contrast, there are some differences between the analysis setup of configuration 2 and 3. While two different analyses are run, one of which is static and modal in the second configuration, only the modal analysis is solved in this configuration. Another difference is that while solid model bolts are used in the second configuration, bolts are simulated with beam elements in this configuration. Thus, the model size is significantly reduced by using fewer mesh elements. Performing the analysis in one step and reducing the size of the model provides a faster solution. Furthermore, the closest results to the test results is obtained during configuration 3. For these reasons, the beam element + bonded contact model (Configuration 3) is used for isolator connection in the final FEM. The next calibrations are performed on this model.

Table 7-5: Comparison of natural frequencies of the initial FEM Configuration 3 and modal tests

Mode Shape	Initial FEM + Neoprene E:4.23 MPa	Configuration 3	Test Results	The percentage difference between test and analysis
Oscillation in X-Axis	15.6 Hz	34.8 Hz	37.7 Hz	7.7 %
Oscillation in Y-Axis	17.9 Hz	35.3 Hz	39.1 Hz	9.7 %

7.4 Update of the Connection of the Other Components

Connection types between the components of the gun control unit are changed in the updated FEM. These changes are explained below:

- The beam element connections between the case and the test fixture are removed. Instead of this, the connection is made by means of "bonded contact." "Pressure cone" surfaces are created, and the components were connected to each other from these surfaces. The connection between the components is represented in Figure 7-11.

a)   b)
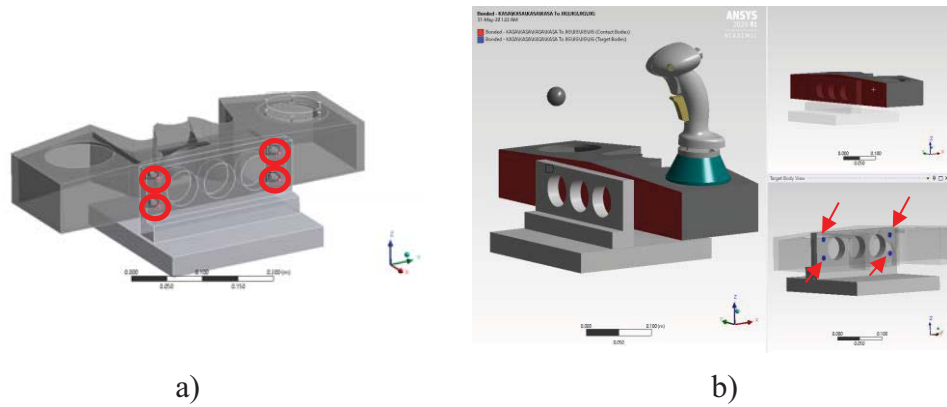
Figure 7-11: Connection between the case and the test fixture: a) with beam elements; b) with bonded contact

- Beam elements between the case and the conical base are removed. The conical base is connected to case each other from entire contact face by "bonded contact."

a)   b)
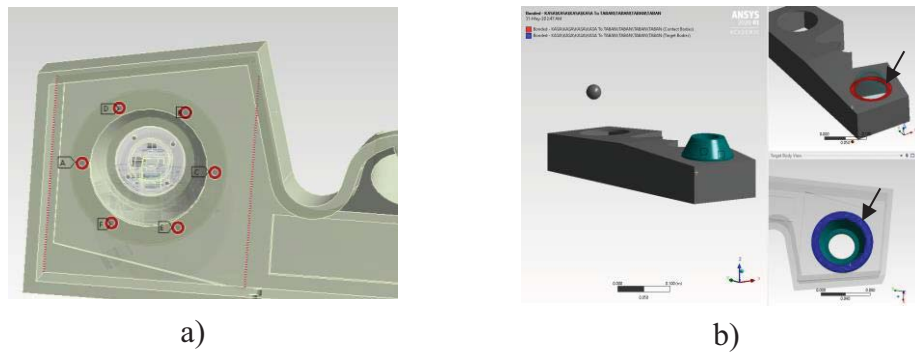
Figure 7-12: Connection between the case and the conical base: a) with beam elements; b) with bonded contact

- In the initial FEM, the right and left body of the control column was connected by two different beam elements. In this update, except for the beam element connection, the structures are connected to each other via bonded contact from the contact surfaces. Thus, the stiffness of the structure is increased slightly. The contact surfaces are shown in Figure 7-13.
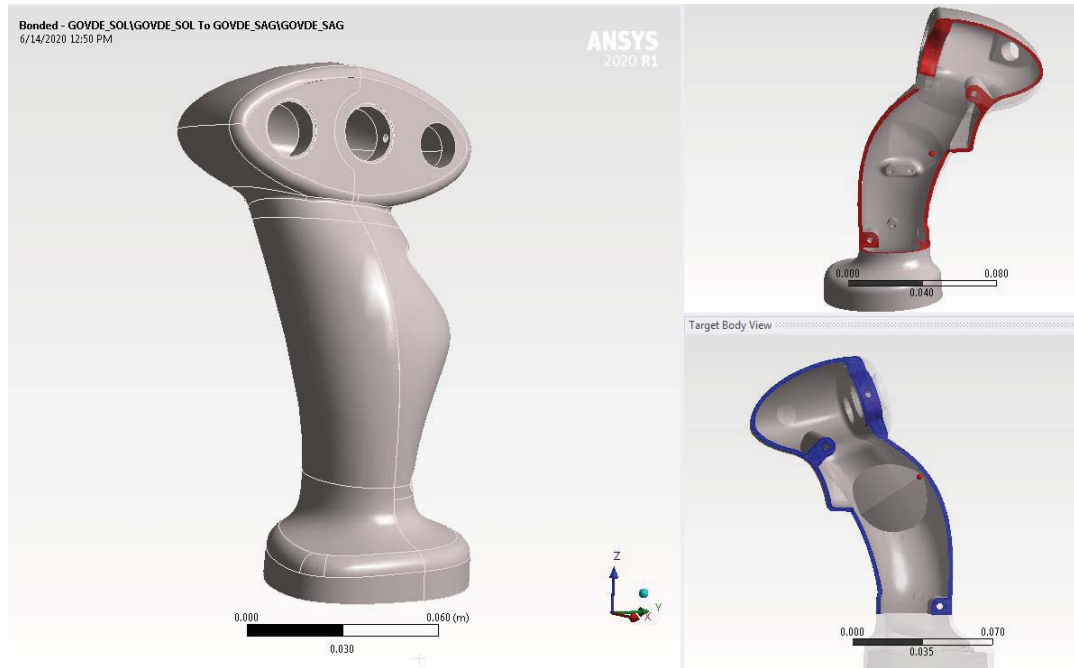
Figure 7-13: The contact surfaces between the left and right bodies of the control column (shown by blue and red colored)

- In the initial FEM model, the left body of the control column and the trigger holder was connected to each other with three different beam elements. In this update process, in addition to the beam element connection, the structures are connected to each other with bonded contact. Contact surfaces are shown in Figure 7-14.
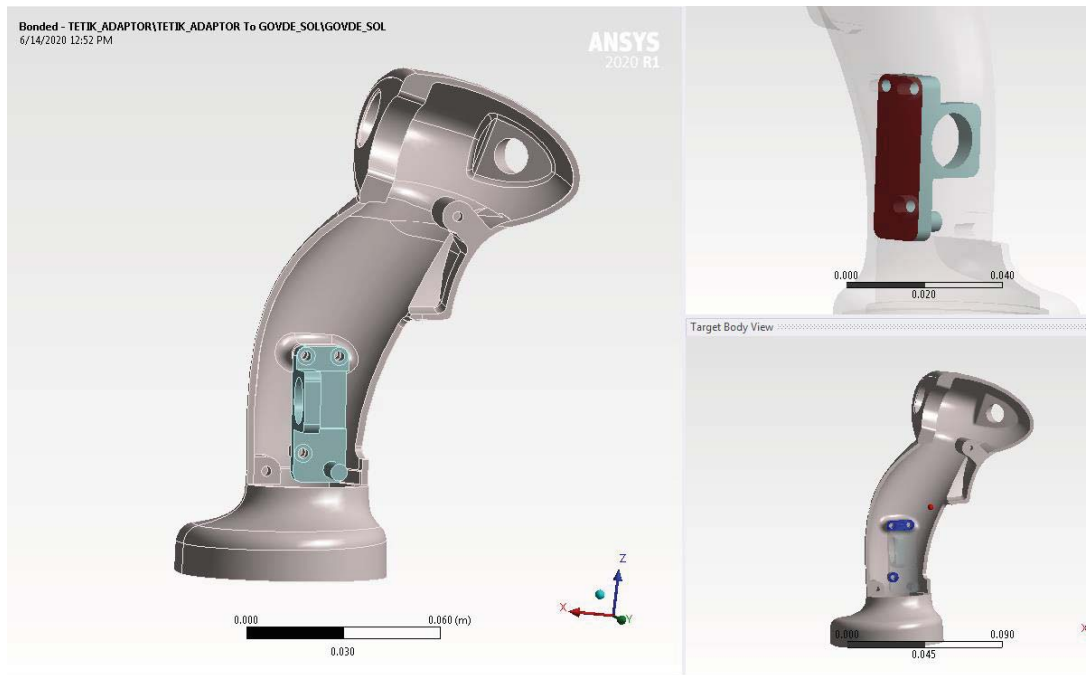
Figure 7-14: The contact surfaces between the trigger holder and left body of the control column (shown by blue and red colored)

Thus, bonded contact is applied to all contact surfaces in the model. Thanks to bonded contact, all degrees of freedom of the surfaces is restricted. In summary, the changes made up to this point can be listed as follows:

- Neoprene's elasticity modulus is changed to be 4.23 MPa.

- Apart from beam elements, the isolator is fixed to the adapter and conical base by bonded contact.

- Bonded contact is applied to all contact surfaces.

The effect of all these changes on the natural frequencies of the control column is presented in Table 7-6. The natural frequencies obtained as a result of the changes in the FEM are close to the experimental modal analysis results. Thanks to changes in the FEM, the biggest error percentage observed in natural frequencies is reduced from 69.8 percent to 6.9 percent. The error in the updated model is thought to be due to the stiffness of the isolator structure. Therefore, the model is calibrated by changing the elasticity modulus of the neoprene.

Table 7-6: Results of the updated model

Mode Shape	Natural Frequencies of the Control Column (Hz)			The percentage difference between test and analysis	
	Initial FEM	Updated Model	Test Results	Initial FEM	Updated Model
Oscillation in X- Axis	11.4	35.5	37.7	69.8 %	5.8 %
Oscillation in Y-Axis	14.0	36.4	39.1	64.1 %	6.9 %

7.5 Calibration of FEM according to the Neoprene Young's Modulus

The stiffness of the isolator structure significantly affects the dynamics of the control column structure. The stiffness of the material of the isolator varies according to preload, tensile speed, and rate of loading. Indeed, in the tensile tests mentioned in Chapter 5, it was observed that neoprene has different elasticity modulus values under different tensile test speeds. In the modal tests, the exact value of the elasticity modulus value of the isolator material is not known, but it is estimated to be within the elasticity module range obtained in the material tests.

At the start of the update process of the FEM, the elasticity modulus for neoprene was chosen as 4.23 MPa. This value had obtained in the material test that is performed at 1 mm/sec tensile test speed. Then, the boundary conditions such as type of connection were updated in the FEM. After all, the natural frequencies of this model were calculated to compare with experimental modal analysis results. As a result of the comparison, the maximum discrepancy ratio between the natural frequencies for the same modes was found to be 6.9 percent. Since this error rate is thought to arise from the elasticity module value of the neoprene material, the elasticity module of the neoprene is defined as a variable parameter in the calibration process. The eight different modal analyses are run by changing the elasticity module of neoprene within the range of 4.23-5.2 MPa. The natural frequency values of the modes of interest are calculated for different elasticity modules of neoprene. The results are presented in Table 7-7. In Table 7, terms of f1 and

f2 represent the natural frequencies of the modes. These modes express the oscillation of the control column in the x-axis and y-axis, respectively. Also, the terms of "e1" and "e2" indicate the amount of error percentage respect to experimental modal analysis results. The results show that using the young modulus values obtained from the tensile tests did not change the results significantly. It can be concluded that the natural frequencies are not very sensitive to the young modulus of neoprene obtained by various test speeds. When the elasticity modulus is taken as 4.9 MPa, it is observed in Table 7 that the maximum error rate expressed as a term of "e max" is equal to 0.64 percent. The discrepancy of results of FEA and experimental modal analysis is reduced below 1% in consequence of the calibration process. Hence, this value is used in the final analysis model.
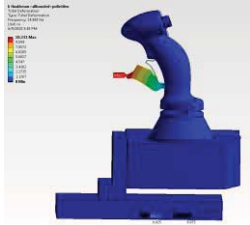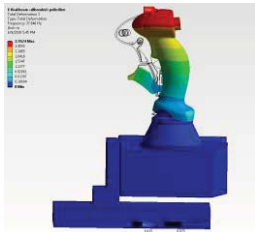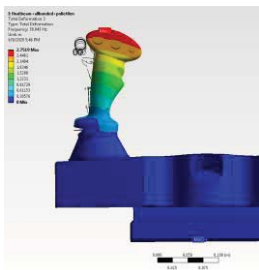
Table 7-7: The results of the parametric analyses

E (MPa)	f1 (Hz)	f2 (Hz)	e1	e2	e max
4.23	35.49	36.40	5.85%	6.91%	6.91%
4.4	36.11	37.04	4.22%	5.28%	5.28%
4.6	36.81	37.77	2.35%	3.39%	3.39%
4.8	37.51	38.49	0.51%	1.55%	1.55%
4.9	37.85	38.85	0.39%	0.64%	0.64%
5	38.19	39.20	1.29%	0.25%	1.29%
5.1	38.52	39.55	2.18%	1.14%	2.18%
5.2	38.85	39.89	3.05%	2.02%	3.05%

7.6 Results of the Final Analysis Model

The modal analysis results (first three modes) of the calibrated FEM are presented in Table 7-8 with comparison with the experimental results. According to the experimental results, the error was decreased to 0.64%.

Table 7-8: Modal analysis results of the calibrated FEM

# of Modes	Natural Frequency	Mode Shape Definition	Mode Shapes	Experimental Modal Analysis	Error Rate
1*	25.0 Hz	Mode of the trigger spring		-	-
2	37.8 Hz	Oscillation of the control column in the direction of X-axis (longitudinal)		37.7 Hz	0.39 %
3	38.8 Hz	Oscillation of the control column in the direction of Y-axis (transverse)		39.1 Hz	0.64 %

*: The first mode occurred at 25.0 Hz comes from the trigger spring constant (1500 N/m), and it is the local mode of the trigger and does not depend on the dynamic of the control column.

In the modal analysis, in total, 115 modes are calculated within the range of 0-3001 Hz. All modes are used in random vibration analyses in order to calculate fatigue damage on the control column. As in the initial analysis, random vibration analyses are performed using the modal superposition method.

In the calibrated FEM, the constant damping ratio used in random vibration analysis is updated. In the initial random vibration analysis, the constant damping ratio was taken as 2 %. In experimental modal analyses mentioned in Chapter 6, the minimum damping ratio

for modes of interest was found to be 4.5 percent. Based on the results obtained in experimental modal analysis, the constant damping ratio is adjusted as to be 4.5 percent.

Under the same loading conditions, random vibration analysis is repeated for the calibrated FEM, and fatigue damages occurred in the control column body is obtained. The maximum fatigue damage ratios in the direction of 3-axes are shown in Figure 7-15, Figure 7-16, Figure 7-17, respectively. Fatigue damage ratios occurring in the structure in consequence of random vibrations are below "1" for each direction of the three-axis. This result shows that the control column model with the isolator is not damaged under the applied vibration load. It was revealed in the vibration tests mentioned in Chapter 4 that the control column structure maintains its structural integrity throughout the life of the tracked vehicle. As a result, the vibration test results of the control column structure verify the fatigue damage results of the calibrated FEM.
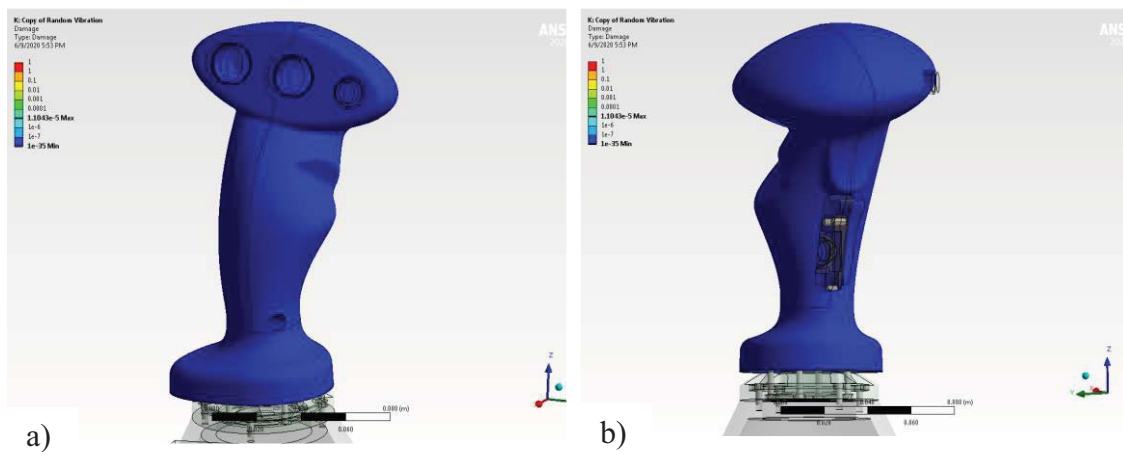
Figure 7-15: Fatigue damage results of the random vibration analysis performed in the direction of X-axis: a) front view, b) the rear view of the control column
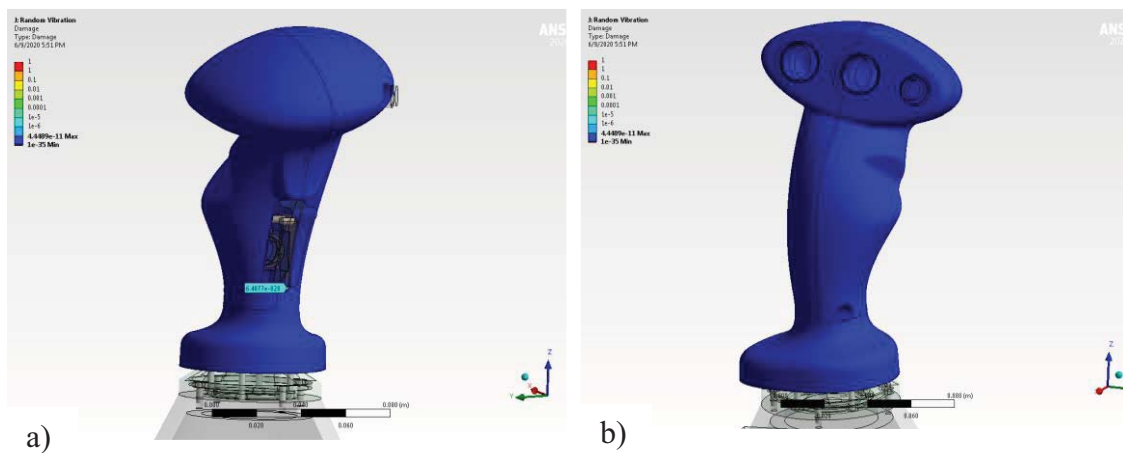
Figure 7-16: Fatigue damage results of the random vibration analysis performed in the direction of Y-axis: a) front view, b) the rear view of the control column

a)   b)
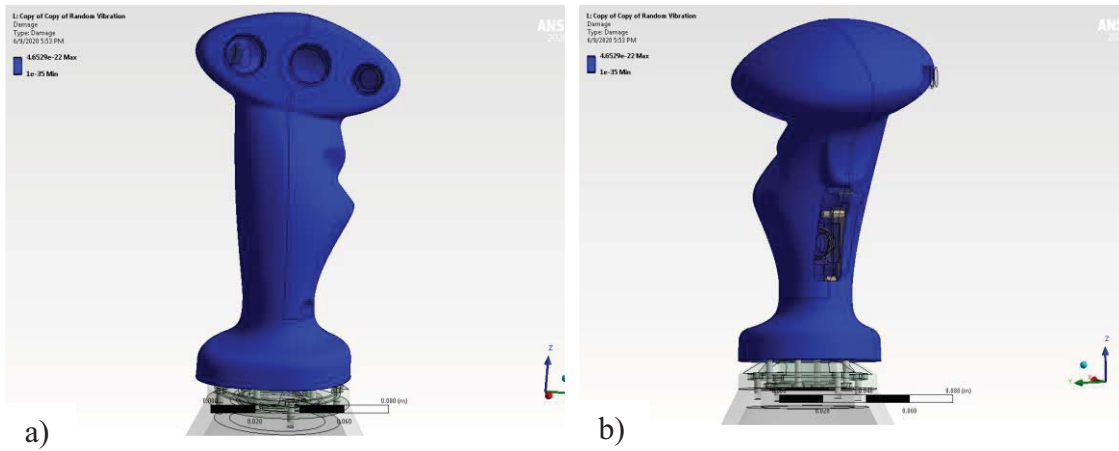
Figure 7-17: Fatigue damage results of the random vibration analysis performed in the direction of Z-axis: a) front view, b) the rear view of the control column

7.6 Conclusion

In this chapter, in order to minimize the inconsistency between analysis and test results, the boundary conditions of the finite element model and the elasticity module of the neoprene material are updated.

Initially, the lowest Young's modulus obtained from the tests were implemented instead of the literature value used in the initial FEM. This update increased the first natural frequency considerably, and much closer results were obtained compared to the tests.

Then, the different types of contacts are studied for the isolator connection in the FEM, and the results of the modal analysis performed for different configurations are compared. As a result of the comparison, bonded contact is applied to the contact surfaces between the isolator and its adjacent components. Furthermore, the isolator bolts are modeled as beam elements. As a result of this update, the difference between the natural frequencies obtained in the test and analysis fell below 10%. Then, bonded contact is applied to all contact surfaces in the structure. As a result of this update, this difference is reduced to 6.9%.

In the calibration process, the elasticity module of the neoprene is changed in a certain range. In this way, the model is calibrated according to the results of experimental modal

analysis. Thus, the discrepancy in modal analysis and test results is reduced to less than 1% for the modes of interest.

Finally, the random vibration analyses are performed for the calibrated FEA model to observe the strength of the control column structure under tracked vehicle vibration. In the final FEM, the damping ratio value is taken from the experimental modal analysis results instead of the value used in the initial FEM. Since the increase in constant damping ratio decreases the transmitted vibration to the structure, the fatigue damage ratio occurring in the structure is reduced. As a result of the random vibration analysis of the final FEM, it can be concluded that the control column structure is not damaged under the tracked vehicle vibration as in the vibration test results.

The results of the calibrated FEM are validated with experimental modal analysis and vibration test results. Henceforth, an accurate FEM is achieved.

8. GENERAL CONCLUSION

8.1 Summary

A remote-controlled weapon system can be used in various ground platforms. The weapon system and its sub-units are exposed to the vibration that comes from the platform. The weapon system and its sub-units are expected to be resistant to vibration throughout its life. One of the sub-units of this system is the gun control unit that contains two control columns that are fixed and moving. In this thesis, the problem is that one of the control column, fixed one, is damaged due to the vibration transmitted from a tracked vehicle platform. The control column is broken from the part of the base due to the load of the accelerated tracked vehicle random vibration during the shaker test. This thesis is aimed to obtain a control column that will preserve its structural integrity after vibration test and to develop a finite element model of the weapon control unit validated with experimental modal analysis results.

The thesis consists of two main parts. In the first part of this thesis, the fatigue failure occurring in the fixed control column is prevented. At first, the gun control unit is modeled by the finite element method. The shaker test is simulated in the finite element environment, and fatigue damage is also observed with the result of the finite element analysis. In this part of the thesis, an absorber is designed and added to the structure. An absorber material, which is also called an isolator, made of neoprene, is assembled under the damaged part of the control column to prevent fatigue failure. Subsequently, the finite element model of the gun control unit with an isolator is built, and the analysis is repeated. As a result of this analysis, it is estimated that the isolator can prevent fatigue damage in the control column. The gun control unit with the isolator is manufactured, and the accelerated tracked vehicle vibration is applied to the prototype by using the shaker. The prototype is successfully completed the vibration test without any damage. Hence, the gun control unit is obtained that preserves the structural integrity under armored tracked vehicle vibration.

In addition, a sine sweep vibration test is applied to the gun control unit during the shaker test, and one of the resonance frequencies of the control column is obtained. The tests showed different resonance frequencies compared to the ones obtained by finite element analysis. Thus, it was decided to enhance the finite element analysis.

In the second part of the thesis, the finite element model is updated to minimize the discrepancy between the natural frequencies obtained in the test and analysis. Initially, experimental modal analysis is performed, and control column dynamical behavior is explained. In the experimental modal analysis, the impact hammer and accelerometers are used to measure the dynamic response of the control column. Natural frequencies, corresponding mode shapes, and damping ratios are obtained via these tests. Then tensile tests are conducted to determine the elasticity modulus of the isolator's material. According to the outcomes of the tests, boundary conditions and material parameters of the finite element model are updated. Then the finite element analysis is calibrated with the result of the experimental modal analysis with parametric analyses. Finally, the analysis results of the calibrated finite element model are verified by the experimental modal analysis and random vibration test results.

In conclusion, the fatigue damage occurring in the gun control unit is prevented by utilizing an elastomer isolator, and a reliable finite element model of the gun control unit is developed, which is verified with the vibration tests.

8.2 Key Findings and Outcomes

The outcomes and the key findings in the scope of the thesis as follows:

- Neoprene plays a significant role in minimizing fatigue damage in the control column structure. Neoprene has a large energy absorption capacity compared to metals, which enables to keep the vibrations transmitted from the platform to the structure at the minimum.

- The fatigue damage occurring in the control column is correctly estimated with the Steinberg algorithm used in ANSYS Software's fatigue tool.

- The need for the physical prototype of the control column in the design process is minimized by utilizing the finite element method.

- Since neoprene has lower stiffness than Aluminum, the isolator causes in the natural frequencies of the control column structure to decrease.

- The tightening torque on the isolator connection bolts significantly increases the stiffness of the control column.

- Neoprene material tends to exhibit stiffer behavior in higher deformation rates.

- The effects of the types of connection of the isolator on the natural frequencies are as follows;

  ➢ Modeling the bolts with the beam elements or solid bolt causes a negligible difference in modal analysis results.

  ➢ Applying preload to the bolts in the isolator connection gives similar results regarding natural frequencies compared to the isolator connection with only bonded contact. However, preloading the bolts requires more computational time.

- Providing connections with both bonded contact and beam elements results in more accurate in modal analysis.

- Natural frequencies of the structure are not very sensitive to the Young modulus of neoprene obtained by various test speeds. Using Young modulus values obtained from the tensile tests does not change the natural frequencies of the gun control unit significantly.

8.3 Potential Future Study

Given the findings of the study, the following research is proposed as a future study:

The effect of geometric changes in the isolator on the fatigue damage and natural frequencies can be investigated. The inner and outer diameters, the height of the absorbent material can be used as variable parameters (Figure 8-1).
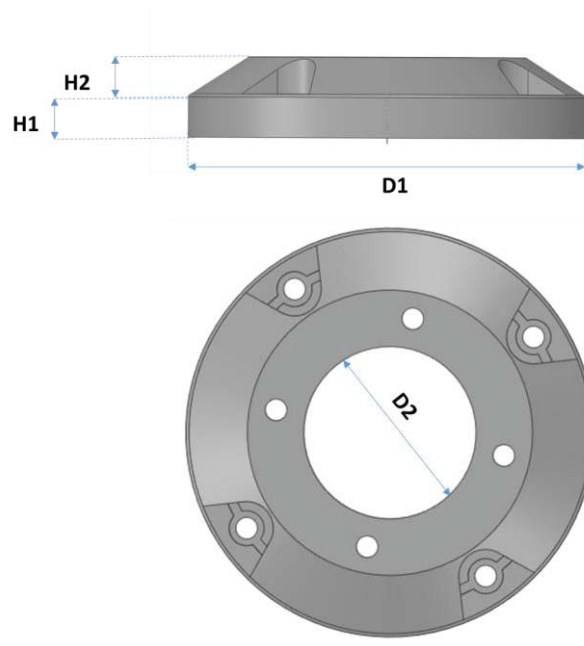
Figure 8-1: Parameters for the sensitivity analysis

9. REFERENCES

1. *SST-Remote Controlled Weapon Systems*, in *I001 / 04-2017*, ASELSAN, Editor. 2017.
2. Anonymous. *Isolator Selection Guide*. 16.10.2020]; Available from: https://novibration.com/isolator-selection-guide/.
3. Alrashdan;, A., A. Alsumait;, and O.S. Es-Said, *Material Selection of an Elastomer Capable of Absorbing Vibrations Actuated by a 4D Movie Theater.* Journal of Failure Analysis and Prevention, 2017. **17**.
4. Frankovich, D., *The Basics of Vibration Isolation Using Elastomeric Materials.* Aearo Technologies LLC: Indianapolis, Indiana.
5. Limited, G.D., *Cambridge Engineering Selector (CES EduPack)*. 2011: Cambridge, UK.
6. Ardic, H., *Design and Modeling Elastomeric Vibration Isolators Using Finite Element Method*. 2013.
7. Anonymous, *Workbence - Mechanical Introduction 12.0 Vibration Analysis*. 2009, ANSYS, Inc.
8. Anonymous, *Harmonic Analysis*, in *ANSYS Training Manual*. 2005.
9. Morgan, K., *Shock & Vibration using ANSYS Mechanical*. 2015.
10. Tao, S., B. Chen, and X.-J. Fan, *Structural Fatigue Life Prediction Based on ANSYS Random Vibration Analysis*. 2016.
11. Steinberg, D.S., *Vibration Analysis for Electronic Equipment*. 2000: John Wiley & Sons Inc.
12. Kumar, S.M., *Analyzing Random Vibration Fatigue*, in *ANSYS Advantage*. 2008, ANSYS India.
13. Navuri, K., et al., *Random Vibration Analysis of Mechanical Hardware of Flight Data Recorder* Asian Research Publishing Network, 2016. **11**.
14. Aykan, M., *Vibration Fatigue Analysis of Equipments used in Aerospace*. 2005, Middle East Technical University,: Ankara.
15. Lin, J., *Frequency Domain Fatigue in Mechanical at 18.0*. 2018, ANSYS UK.
16. Organization, N.A.T., *Mechanical Environmental Tests AECTP 400*. 2006.
17. Defense, U.D.o., *Environmental Engineering Considerations and Laboratory Tests*, in *METHOD 514.6 ANNEX A*. 2008.
18. Browell;, R., *Calculating and Displaying Fatigue Results*, A. Hancq, Editor. 2006, ANSYS Inc.
19. Gent, A.N., *On the relation between indentation hardness and Young's modulus.* Institution of Rubber Industry -- Transactions, 1958: p. 46-57.
20. Anonymous. *FFT Spectral Analysis*. [cited 2020 9 August 2020]; Available from: https://training.dewesoft.com/online/course/fft-spectral-analysis.
21. Mihaylov, B., *Brüel & Kjær Vibration Test Systems (VTS).* NDT Days, 2018. **1**(2).
22. Anonymous. *What is a Power Spectral Density (PSD)*. Community Article 2019 16.08.2020]; Available from: https://community.sw.siemens.com/s/article/what-is-a-power-spectral-density-psd.

23. Baren, J.V., *What is Random Vibration Testing?*, in *Sound & Vibration*. 2012, Vibration Research Corporation: Jenison, Michigan. p. 12.
24. Anonymous. *Random RMS Calculator Tutorial.* 09 August 2020]; Available from: https://vibrationresearch.com/resources/random-rms-calculator/.
25. Dewesoft, *Dewesoft X3 User Manual*, Dewesoft, Editor. 2019.
26. Mila, T. *Windows and Spectral Leakage*. 2019 09 August 2020]; Available from: https://community.sw.siemens.com/s/article/windows-and-spectral-leakage.
27. Avitabile, P., *Modal Testing A Practitioner's Guide*. 2018: John Wiley & Sons Ltd : The Society for Experimental Mechanics.
28. Avitabile, P., *Modal Testing - A Practitioner's Guide*. 2018: JohnWiley & Sons Ltd.
29. Zhao Liu, et al., *Comparison of Finite Element and Experimental Modal Analysis of Multi-Joint Flexible Robotic Arm*, in *2017 International Conference on Mechanical, System and Control Engineering*. 2017.
30. Tony L. schmitz, K.S.S., *Mechanical Vibrations Modeling and Measurement*. 2012, New York, NY 10013, USA: Springer Science+Business Media.
31. Anonymous. *Window Types: Hanning, Flattop, Uniform, Tukey, and Exponential*. Community Article 2019 16.08.2020]; Available from: https://community.sw.siemens.com/s/article/window-types-hanning-flattop-uniform-tukey-and-exponential.
32. Anonymous. *Simcenter Testlab Impact Testing*. Community Article 16.08.2020]; Available from: https://community.sw.siemens.com/s/article/simcenter-testlab-impact-testing.
33. Anonymous. *How to calculate damping from a FRF?* Community Article 2019 09 August 2020]; Available from: https://community.sw.siemens.com/s/article/how-to-calculate-damping-from-a-frf.
34. Larson, K., *Can You Estimate Modulus From Durometer Hardness for Silicones?* Dow White Paper.
35. Standardization, T.I.O.f., *ISO 37 Rubber, vulcanized or thermoplastic-Determination of the tensile stress-strain properties*. 2012, ISO.
36. Fahrenholz, H., *Determination of Tensile Properties*. 2018, Zwick Roell.
37. Guy Banwell, et al., *Using experimental modal analysis to validate a finite element model of a tennis racket*, in *9th Conference of the International Sports Engineering Association (ISEA)*. 2012, Elsevier Ltd.
38. Jandric, D. *An overview of methods for modelling bolts in ANSYS V15*. in *2014 ANSYS Regional Conference*. 2014. Chicago.
39. Mahesh P. Mestry, K.H.M., Ashish Pawar, *Pre-Stressed Modal Analysis of Composite Bolted Structure.* JETIR, 2018. **5**(7).
40. Anonymous. *Pre-Stressed Modal Analysis Linked to Nonlinear Static Analysis in Ansys® Mechanical (Workbench) V14.0*. Simutrain 09 August 2020]; Available from: https://www.simutechgroup.com/tips-and-tricks/fea-articles/160-fea-tips-tricks-ansys-14-pre-stressed-modal-analysis-nonlinear-static-analysis.